72-16,895

RILEY, Jr., James Joseph, 1944-
COMPUTER SIMULATIONS OF TURBULENT DISPERSION.

The Johns Hopkins University, Ph.D., 1971
Engineering Mechanics

University Microfilms, A XEROX Company, Ann Arbor, Michigan

THIS DISSERTATION HAS BEEN MICROFILMED EXACTLY AS RECEIVED

Reproduced with permission of the copyright owner. Further reproduction prohibited without permission.

COMPUTER SIMULATIONS OF TURBULENT DISPERSION

by

James J. Riley

A dissertation submitted to The Johns Hopkins University in conformity with the requirements for the degree of Doctor of Philosophy.

Baltimore, Maryland

June, 1971

Reproduced with permission of the copyright owner. Further reproduction prohibited without permission.

PLEASE NOTE:

Some pages may have

indistinct print.

Filmed as received.

University Microfilms, A Xerox Education Company

Reproduced with permission of the copyright owner. Further reproduction prohibited without permission.

ABSTRACT

The dispersion of fluid material points and of small, spherical particles on both homogeneous turbulent shear flows and isotropic turbulence is studied by numerical simulation of the flow fields.

The method is to set up a mathematical model of the random Eulerian field, and to compute dispersion on this field. The Eulerian field is chosen of the isochoric form:

$$\underset{\sim}{u}(\underset{\sim}{x},t) = \underset{\sim}{U}(\underset{\sim}{x}) + \sum_{n=1}^{N} T(\xi_n, t_n)\, \frac{\underset{\sim}{k}_n}{k_n} \times \left\{ \underset{\sim}{\alpha}_n \cos(\underset{\sim}{k}_n \cdot \underset{\sim}{x}) + \underset{\sim}{\beta}_n \sin(\underset{\sim}{k}_n \cdot \underset{\sim}{x}) \right\}$$

where $\underset{\sim}{U}(\underset{\sim}{x})$ is the mean velocity, $t_n = t - t_{o_n}$ where t_{o_n} is the random initial time of energy "transfer" into the nth mode, $T(\cdot,\cdot)$ is chosen to model the energy gain and loss of the various modes, and $\underset{\sim}{\alpha}_n$, $\underset{\sim}{\beta}_n$, $\underset{\sim}{k}_n$ are random variates from suitably selected probability distributions, chosen so that $\underset{\sim}{u}(\underset{\sim}{x},t)$ will have statistical properties similar to those of the flow field under investigation. The non-linear terms in the Navier-Stokes are only indirectly modeled through the distribution of the $\underset{\sim}{k}_n$ and by the function $T(\cdot,\cdot)$; there is no interaction among the different wave number vectors.

"Ensembles" of realizations are analyzed. One group employs the "response" equations

$$\frac{d}{dt}\underset{\sim}{x} = \underset{\sim}{u}(\underset{\sim}{x},t) \quad , \quad \underset{\sim}{x}(t_o) = \underset{\sim}{x}_o$$

Reproduced with permission of the copyright owner. Further reproduction prohibited without permission.

(the fluid material point case), and another employs

$$\frac{d^2\underline{x}}{dt^2} + \alpha\left\{\frac{d\underline{x}}{dt} - \underline{u}(\underline{x},t)\right\} = g + K\frac{d}{dt}\underline{u}(\underline{x},t);\ \underline{x}(t_0)=\underline{x}_0,\ \left.\frac{d\underline{x}}{dt}\right|_{t_0} = \underline{u}(\underline{x}_0,t_0),$$

the small "sluggish particle case. The equations are integrated numerically.

"Ensemble" averages are taken for various quantities of interest. Various phenomena, such as (i) Lagrangian one-point diffusion (especially the shear flow results), (ii) the deviation from Lagrangian diffusion of small particles for α^{-1} small, (iii) the effect of gravity on the diffusion of small particles, and (iv) the "direct inertial effect" and the "crossing trajectories effect" of small particles are examined.

Attempts made to simulate the turbulence as two-dimensional led to Eulerian properties qualitatively different from those measured in homogeneous shear flow, so three-dimensional simulation was preferred.

Reproduced with permission of the copyright owner. Further reproduction prohibited without permission.

ACKNOWLEDGEMENTS

It is my pleasure to thank my adviser, Professor Stanley Corrsin, for his advice, criticisms, and timely suggestions during the course of this investigation. I would also like to thank Professor William Schwarz, who consented to perform the duties of second reader.

K. Smith and A. Kacala of the JHU Computing Center, J. Hastings and R. Jenne of the NCAR Computing Center, and Mike Karweit were helpful at various stages of the computing.

I would like to thank Mrs. Jean McFeely and Mrs. Jane Zee for helping type the manuscript, and Mrs. Virginia Pradick for drawing many of the figures.

This work was supported by the Office of Naval Research (Contract No. N000-14-67A-0163-0005), the Atomic Energy Commission (Contract No. AT-30-1-4045), and the National Science Foundation (Contract No. GK-10268).

Acknowledgement is made to the National Center for Atmospheric Research, which is sponsored by the National Science Foundation, for use of its Control Data 6600 computer.

Reproduced with permission of the copyright owner. Further reproduction prohibited without permission.

TABLE OF CONTENTS

ABSTRACT

ACKNOWLEDGEMENTS

LIST OF FIGURES

I. INTRODUCTION

A. Objective 1
B. Definition of the Problem 1
C. Brief Review of Some Pertinent Previous Work 7

II. APPLICATION OF NUMERICAL SIMULATION TO TURBULENT DISPERSION

A. Rationale 17
B. Some General Aspects of Numerical Simulation 20
C. Application to Turbulent Dispersion 21

III. DESCRIPTION OF THE VELOCITY FIELDS

A. Mathematical Background 25
1. Introduction
2. Two-Dimensional Flows
3. Three-Dimensional Flows
4. Some Identifications for the Model Field
B. The Shear Flow Model 38
1. Conditions to Be Satisfied by the Model
2. Selection of the Statistical Properties of the α_n and β_n.
3. Time Development of the Model Flow
4. Choice of the Statistical Properties of the k_n.
C. The Isotropic Turbulence Model 60

IV. A DISCUSSION OF THE EQUATIONS OF MOTION FOR "SMALL" SPHERICAL PARTICLES

A. Introduction 62
B. Development of a Force Balance 62
C. Some Special Cases 75
D. Summary 77

Reproduced with permission of the copyright owner. Further reproduction prohibited without permission.

V. EULERIAN FIELD SIMULATION RESULTS

A. Determination of the Parameters 78
1. Homogeneous, Stationary Shear Flow
2. Stationary, Isotropic Flow
B. Simulation Results 89
1. Homogeneous, Stationary Shear Flow
2. Stationary, Isotropic Flow

VI. FLUID PARTICLE AND "ALIEN" PARTICLE DISPERSION

A. Simulation Results of Fluid Particle Dispersion on the Homogeneous, Stationary Shear Flow 113
1. Introduction
2. Statistical Properties of the Displacement Covariance Tensor
3. Isoprobability Contours
4. Statistical Properties of the Lagrangian Velocity Autocorrelation Coefficients
5. Turbulent Diffusivities
6. Simulation of Plume Dispersion Experiments
B. Simulation Results for Fluid Particle and "Alien" Particle Dispersion on a Stationary Isotropic Field 159
1. Fluid Particle Results
2. "Alien" Particle Results
a. Introduction
b. A Typical Case
c. Effect of Varying the Alien Particle Inverse Relaxation Time
d. The Effect of Varying the Effective Gravity Force: The "Fallout Problem"

VII. SUMMARY AND SOME CONCLUSIONS 191

APPENDIX

A. Random Number Generation 195
B. Random Sampling and Error Analyses 201
C. Numerical Integration Procedure 208

BIBLIOGRAPHY

VITA

Reproduced with permission of the copyright owner. Further reproduction prohibited without permission.

LIST OF SOME FIGURES

No.	Caption	Page
13	Eulerian velocity autocorrelation coefficients, computed at a point of zero mean velocity, for the homogeneous shear flow.	92
14	The Eulerian velocity time cross-correlation coefficient, computed at a point of zero mean velocity, for the homogeneous shear flow.	94
15	Spatial autocorrelations of the Eulerian fluctuation velocity in the direction of the mean flow (u_1').	95
16	Spatial autocorrelations of the Eulerian fluctuation velocity in the direction of the mean velocity gradient (u_2').	96
17	Spatial autocorrelations of the Eulerian fluctuation velocity in the direction normal to both the mean velocity and mean velocity gradient (u_3').	97
18	Eulerian velocity spatial cross-correlation along the direction of the mean velocity (r_1).	98
19	Eulerian velocity spatial cross-correlation along the direction of the mean velocity gradient (r_2).	99
20	Eulerian velocity spatial cross-correlation along the direction normal to both the mean velocity and mean velocity gradient (r_3).	100
21	Spatial autocorrelation functions along the streamwise direction (r_1) for a series of values of r_2.	102
22	Spatial isocorrelation contours in the plane of the mean velocity (r_1) and mean velocity gradient (r_2). R_{11}	104
23	Spatial isocorrelation contours in the plane of the mean velocity (r_1) and mean velocity gradient (r_2). R_{22}	105
24	Spatial isocorrelation contours in the plane of the mean velocity (r_1) and mean velocity gradient (r_2). R_{33}	106
25	Spatial isocorrelation contours in the plane of the mean velocity (r_1) and mean velocity gradient (r_2). R_{12}	107
26	Spatial isocorrelation contours in the plane of the mean velocity (r_1) and mean velocity gradient (r_2). R_{21}	108

Reproduced with permission of the copyright owner. Further reproduction prohibited without permission.

No.	Caption	Page
27	Eulerian velocity time autocorrelation coefficients for the isotropic model flow.	109
28	The Karman-Howarth f and g functions for the isotropic model flow.	111
30	Dispersion in the direction of the mean velocity gradient, and normal to both the mean velocity and the mean velocity gradient.	117
31	Lagrangian dispersion in the direction of the mean velocity.	119
32	The fluid particle cross-covariance function $\langle I_1 I_2 \rangle$ for the shear flow simulations.	121
33	A log-log plot of the covariance function $\langle I_1 I_2 \rangle$	122
34	The fluid particle cross-correlation coefficient for the shear flow simulations.	124
35	The angle of the major principal axis of the dispersion tensor in the x_1x_2 plane for the shear flow simulations.	126
36	The probability distribution of $\mathcal{R}_\beta(t)$, t = 3.0.	130
37	The probability distribution of $\mathcal{R}_\beta(t)$, t = 6.0.	131
38	Contours of constant displacement probability in the x_1x_2 plane, for "short" and "moderate" times.	132
39	Contours of constant displacement probability in the x_1x_2 plane, for "moderate" to "long" times.	133
40	Fluid particle velocity autocorrelation coefficients for the shear flow simulations.	136
41	A comparison of a one-point Eulerian time autocorrelation coefficient and a fluid particle velocity autocorrelation for the shear flow simulations.	137
42	A comparison of the normalized one-point Eulerian time cross-correlation and the normalized fluid particle velocity cross-correlation for the shear flow simualtions.	139
43	The turbulent diffusivities $\mathcal{K}_{21}(t)$ and $\mathcal{K}_{33}(t)$ computed from the shear flow simulations.	146
44	The turbulent diffusivity $\mathcal{K}_{11}(t)$ computed from the shear flow simulations using equation (47).	147

Reproduced with permission of the copyright owner. Further reproduction prohibited without permission.

No.	Caption	Page
45	The turbulent diffusivity $K_{12}(t) + K_{21}(t)$ computed from the simulations.	148
47	The displacement probability densities $f_1(x_2; D)$ and $f_{\Delta_2}(x_2; D/U_0)$ for U_0 = 10.0 and D = 6.0.	154
48	The displacement probability densities $f_1(x_2; D)$ and $f_{\Delta_2}(x_2; D/U_0)$ for U_0 = 10.0 and D = 12.0.	155
49	The displacement probability densities $f_1(x_2; D)$ and $f_{\Delta_2}(x_2; D/U_0)$ for U_0 = 10.0 and D = 18.0.	156
50	Fluid particle velocity autocorrelation coefficients for the isotropic flow simulations.	161
51	A comparison of the one-point Eulerian autocorrelation coefficient $R_{f_{11}}(\xi_2, t)$ and the fluid particle velocity autocorrelation coefficient $R_{f_{11}}(t)$ for the isotropic flow simulations.	162
52	Fluid particle dispersion for the isotropic model flow.	164
53	A comparison of the autocorrelation coefficients of the particle velocity, of the velocity of the fluid in the vicinity of the particle, and of the relative velocity, for a typical "sluggish" particle (α = 5.0, β = 0.0, κ = 0.0).	167
54	A typical plot (α = 5.0, β = 0.0, κ = 0.0) of the cross-correlation coefficient between the particle velocity and the velocity of surrounding fluid.	172
55	The alien particle velocity autocorrelation coefficient for various values of α (with β = 0.0, κ = 0.0).	173
56	The autocorrelation coefficient of the velocity of the fluid surrounding the alien particle for various values of α (with β = 0.0, κ = 0.0).	175
57	The autocorrelation coefficient of the relative velocity of the alien particle and the surrounding fluid for various values of α (with β = 0.0, κ = 0.0).	177
58	The mean fallout velocity of alien particles for the cases α = 5.0, β = -4.0 and α = 5.0, β = -25.0.	179
59	The autocorrelation coefficient of the velocity of the fluid surrounding the alien particle for various values of β with α = 5.0.	181

Reproduced with permission of the copyright owner. Further reproduction prohibited without permission.

No.	Caption	Page
60	The alien particle velocity autocorrelation coefficient for various values of β with α = 5.0.	183
61	A comparison of the simulation results for $R_{u_{11}}(\xi)$, $R_{u_{22}}(\xi)$, and $R_{u_{33}}(\xi)$ (for α = 5.0, β = -25.0) with the hypothesis expressed by equations (111), (112), and (113).	187
62	The alien particle velocity autocorrelation coefficients for the case α = 5.0 and β = -25.0.	188

Reproduced with permission of the copyright owner. Further reproduction prohibited without permission.

I. INTRODUCTION

A. Objective

An important result of fluid motion is the transport both of the fluid itself and also of quantities embedded or suspended in it, such as heat, dust, chemical contaminants, silt, or sand. It is well known that the average transport of such quantities is greatly enhanced if the fluid motion is turbulent. (For example, see Hinze 1959, chapter 5.) This is a result of the convection of these quantities by the irregular motion of the fluid, a phenomenon usually termed turbulent diffusion. (When the turbulent diffusion originates from a relatively local source (e.g., a point or line source), it is usually termed turbulent dispersion.) The object of the present research is to investigate the feasibility and the results of numerically simulating turbulent diffusion.

B. Definition of the Problem

The problem of turbulent diffusion can be defined in a number of ways, depending on the quantity dispersed, the thermodynamic state of the fluid, the boundary or initial conditions, the objectives of the investigator, and so on. A somewhat restricted mathematical statement of the problem is the following: find the joint statistical properties of the random fields $\{ \underset{\sim}{u}(\underset{\sim}{x},t), p(\underset{\sim}{x},t), \theta(\underset{\sim}{x},t) \}$ satisfying

$$\frac{\partial}{\partial t}\underset{\sim}{u} + (\underset{\sim}{u}\cdot\nabla)\underset{\sim}{u} = -\frac{1}{\rho}\nabla p + \nu\nabla^2\underset{\sim}{u} \qquad (1)$$

Reproduced with permission of the copyright owner. Further reproduction prohibited without permission.

$$\nabla \cdot \underset{\sim}{u} = 0 \tag{2}$$

$$\frac{\partial}{\partial t}\theta + (\underset{\sim}{u} \cdot \nabla)\theta = \kappa \nabla^2 \theta \tag{3}$$

and appropriate initial and boundary conditions. Here $\underset{\sim}{u}$ is the turbulent velocity, p the static pressure, θ the quantity diffused, ρ the (constant) fluid density, ν the (constant) kinematic viscosity, and κ the (constant) diffusivity of θ. This system is valid in several different circumstances, and for several different interpretations of θ. (Bird, Stewart, and Lightfoot 1964 list most of the situations in which these equations are valid.) The two most common are when θ is interpreted as temperature, in which case (3) is a simplification of the equation of internal energy balance, and when θ is interpreted as the concentration of a chemical contaminant.

The equations imply that the density ρ and kinematic viscosity ν are constants, independent of θ. (These are good approximations for "small" temperature or concentration fluctuations.) Thus equations (1) and (2) are mathematically independent of θ, and the turbulent dynamics problem is separable from the turbulent diffusion problem. This is not the case in the general statement of the problem, where the density and viscosity are functions of θ, so that the velocity field is influenced by the θ field, and vice-versa. In this case, the equations are of more

Reproduced with permission of the copyright owner. Further reproduction prohibited without permission.

general form, are mathematically interdependent, and must be solved simultaneously.

The problem as stated can be further simplified. For since the turbulent transport is much more effective than the molecular transport (in almost all known cases the ratio of the thermal diffusivity to the "turbulent diffusivity" is very small[1]), and since from a fundamental point of view we are interested in the diffusion by the turbulence alone -- not complicated by molecular diffusion -- the molecular diffusion term in equation (3) can be neglected. Also since the turbulent dynamics problem is independent of the turbulent diffusion problem for the case stated, the diffusion problem is often defined in the following much simpler form: given the random Eulerian velocity field $\{ \underset{\sim}{u}(\underset{\sim}{x},t) \}$, defined in some statistical sense and satisfying the Navier-Stokes equations and appropriate initial and boundary conditions, find the joint statistical properties of $\{\theta(\underset{\sim}{x},t), \underset{\sim}{u}(\underset{\sim}{x},t)\}$ satisfying

$$\frac{\partial}{\partial t}\theta + (\underset{\sim}{u}\cdot\nabla)\theta = 0 \quad , \quad \theta(\underset{\sim}{x},t_0) = f(\underset{\sim}{x}) . \tag{4}$$

---

[1] See chapter VI section A.5 for a discussion of "turbulent diffusivities", where in particular it is pointed out that the concept of turbulent diffusivities is wrong in principle, although often useful in practice.

Reproduced with permission of the copyright owner. Further reproduction prohibited without permission.

This equation is more easily and naturally studied using the Lagrangian description of the motion (see Corrsin, 1961). Defining $\underset{\sim}{X}(\underset{\sim}{a},t)$ as the position at time t of the fluid particle which was at $\underset{\sim}{a}$ at time t_0, and

$$\Theta(\underset{\sim}{a},t) = \theta\left[\underset{\sim}{X}(\underset{\sim}{a},t),t\right] \tag{5}$$

as the Lagrangian quantity corresponding to the Eulerian quantity θ, then Θ satisfies

$$\frac{\partial}{\partial t}\Theta = 0 \;, \quad \Theta(\underset{\sim}{a},t_0) = f(\underset{\sim}{a}) . \tag{6}$$

To see this, differentiate (5) with respect to time, holding $\underset{\sim}{a}$ fixed, and apply equation (6):

$$\frac{\partial}{\partial t}\Theta = \left\{ \frac{\partial \theta}{\partial t} + \left(\frac{\partial \underset{\sim}{X}}{\partial t}\cdot\nabla\right)\theta \right\}_{\underset{\sim}{x}=\underset{\sim}{X}(\underset{\sim}{a},t)} = 0 . \tag{7}$$

Transforming (7) from the Lagrangian to the Eulerian frame gives equation (4).

Equation (6) is easily integrated to give

$$\Theta(\underset{\sim}{a},t) = \Theta(\underset{\sim}{a},t_0) = f(\underset{\sim}{a})$$

so that Θ is constant following a fluid particle. Hence our primary

Reproduced with permission of the copyright owner. Further reproduction prohibited without permission.

concern is the trajectory of the fluid particles. For if we know Θ initially, (say $\Theta(\underset{\sim}{a},t_0) = f(\underset{\sim}{a})$), and know the trajectories of the fluid particles $\underset{\sim}{X}(\underset{\sim}{a},t)$, then we can compute $\Theta(\underset{\sim}{x},t)$.

Since the fluid particle trajectories are the primary interest, the problem is redefined in terms of $\underset{\sim}{X}$. Given the random velocity field $\{\underset{\sim}{u}(\underset{\sim}{x},t)\}$, defined in some statistical sense and satisfying the Navier-Stokes equations and appropriate initial and boundary conditions, compute the statistical properties of $\{\underset{\sim}{X}(\underset{\sim}{a},t), \underset{\sim}{u}[\underset{\sim}{X}(\underset{\sim}{a},t),t]\}$ satisfying

$$\frac{\partial}{\partial t}\underset{\sim}{X}(\underset{\sim}{a},t) = \underset{\sim}{u}\left[\underset{\sim}{X}(\underset{\sim}{a},t),t\right], \quad \underset{\sim}{X}(\underset{\sim}{a},t_0) = \underset{\sim}{a}. \tag{8}$$

These are the ordinary differential equations for the trajectories $\underset{\sim}{X}$, given the velocity $\underset{\sim}{u}(\underset{\sim}{x},t)$. The equations are also the "characteristic equations" for the partial differential equation (4) [see, for example, Courant and Hilbert 1953].

It will be shown in chapter IV that the motion of "small" particles on a turbulent field can be approximately described by the equation

$$\frac{\partial^2}{\partial t^2}\underset{\sim}{Y}(\underset{\sim}{b},t) + \alpha\left\{\frac{\partial}{\partial t}\underset{\sim}{Y}(\underset{\sim}{b},t) - \underset{\sim}{u}\left[\underset{\sim}{Y}(\underset{\sim}{b},t),t\right]\right\} = \underset{\sim}{g} + \kappa\frac{\partial}{\partial t}\underset{\sim}{u}\left[\underset{\sim}{Y}(\underset{\sim}{b},t),t\right] \tag{9}$$

where $\alpha = \frac{9\nu}{r^2(2\frac{\rho'}{\rho}+1)}$, $\underset{\sim}{g} = -\underset{\sim}{g}\frac{(\frac{\rho'}{\rho}-1)}{(\frac{\rho'}{\rho}+\frac{1}{2})}$, $\kappa = \frac{3}{(2\frac{\rho'}{\rho}+1)}$, and ν is the kinematic viscosity of the fluid, r the particle radius, ρ' the density of the particle, ρ the density of the fluid, and $\underset{\sim}{g}$ the gravity

Reproduced with permission of the copyright owner. Further reproduction prohibited without permission.

vector. α^{-1} is the relaxation time of the particle, and $\underline{Y}$ the position vector. This differential equation may be expressed in the integral form:

$$\underline{Y}(\underline{b},t) = \underline{b} + \frac{1}{\alpha}(1-e^{-\alpha t})\left[\frac{\partial \underline{Y}}{\partial t}\Big|_{t_0} - \kappa \underline{u}(\underline{b},t_0) - \frac{g}{\beta\alpha}\right] + \frac{g}{\beta}\frac{t}{\alpha}$$

$$+ \int_{t_0}^{t} \underline{u}\left[\underline{Y}(\underline{b},t'),t'\right]\left\{1+(\kappa-1)e^{-\alpha(t-t')}\right\} dt' . \qquad (10)$$

As $\rho' \to \rho$, then $\kappa \to 1$ and $\frac{g}{\beta} \to 0$, so that if $\frac{\partial \underline{Y}}{\partial t}\Big|_{t_0} = \underline{u}(\underline{b},t_0)$, then equation (10) reduces to

$$\underline{Y}(\underline{b},t) = \underline{b} + \int_{t_0}^{t} \underline{u}\left[\underline{Y}(\underline{b},t'),t'\right] dt' , \qquad (11)$$

which is the integral expression for the fluid point, equation (8). Also for $\rho \neq \rho'$, equation (11) is the non-uniform limit of equation (10) as $\alpha \to \infty$. So fluid particle dispersion can be included in this more general system of equations.

With all of the preceding discussion in mind, we will take the following as the definition of the problem under investigation. Given the random velocity field $\{\underline{u}(\underline{x},t)\}$, defined in some statistical sense and satisfying the Navier-Stokes equations and appropriate initial and boundary conditions, compute statistical properties of $\{\underline{Y}(\underline{b},t), \frac{\partial}{\partial t}\underline{Y}(\underline{b},t), \underline{u}[\underline{Y}(\underline{b},t),t]\}$ satisfying

Reproduced with permission of the copyright owner. Further reproduction prohibited without permission.

$$\frac{\partial^2}{\partial t^2}\underset{\sim}{Y}(\underset{\sim}{b},t) + \alpha\left\{\frac{\partial}{\partial t}\underset{\sim}{Y}(\underset{\sim}{b},t) - \underset{\sim}{u}\left[\underset{\sim}{Y}(\underset{\sim}{b},t),t\right]\right\} = \frac{g}{\rho} + \kappa\frac{\partial}{\partial t}\underset{\sim}{u}\left[\underset{\sim}{Y}(\underset{\sim}{b},t),t\right]$$

$$\underset{\sim}{Y}(\underset{\sim}{b},t_o) = \underset{\sim}{b} \quad , \quad \left.\frac{\partial \underset{\sim}{Y}}{\partial t}\right|_{t_o} = \underset{\sim}{u}(\underset{\sim}{b},t_o). \tag{12}$$

C. Brief Review of Some Pertinent Previous Work

The investigation of turbulent dispersion, both theoretically and experimentally, has kept more or less abreast of turbulence dynamics studies. Some of the results of past investigations, pertinent to the present work, will be discussed here. The reader is referred to excellent reviews of the subject by Batchelor and Townsend (1956), Hinze (1959), and Corrsin (1961) for broader and more in depth coverage and for more extensive references on the subject.

Taylor (1921) developed the first fundamentally correct theory of turbulent dispersion (which he labelled "Diffusion by Continuous Movements" to contrast it with the theories of diffusion by discontinuous movement used to describe Brownian motion). His theory employs equation (8), using the Lagrangian velocity $\underset{\sim}{U}(\underset{\sim}{a},t) \equiv \underset{\sim}{u}\left[\underset{\sim}{X}(\underset{\sim}{a},t),t\right]$. Thus

$$\frac{\partial}{\partial t}\underset{\sim}{X}(\underset{\sim}{a},t) = \underset{\sim}{U}(\underset{\sim}{a},t) \quad , \quad \underset{\sim}{X}(\underset{\sim}{a},t_o) = \underset{\sim}{a}. \tag{13}$$

He assumed in effect an isotropic, stationary (Lagrangian) flow with zero

Reproduced with permission of the copyright owner. Further reproduction prohibited without permission.

mean. Integrating a component of equation (13) gives:

$$X_1(\underline{a},t) = a_1 + \int_{t_0}^{t} U_1(\underline{a},t')\,dt'. \tag{14}$$

Taking $a_1 = 0$, multiplying (14) by twice (13), and averaging gives:

$$\frac{d}{dt}\langle X_1^2(\underline{a},t)\rangle = 2\langle U_1^2(\underline{a},t)\rangle \int_{t_0}^{t} R_{F_{11}}(t')\,dt', \tag{15}$$

where $R_{F_{11}}(\tau) = \dfrac{\langle U_1(\underline{a},t)U_1(\underline{a},t+\tau)\rangle}{\langle U_1^2(\underline{a},t)\rangle}$ is the Lagrangian velocity auto-correlation coefficient. Integrating equation (15) with respect to t , using integration by parts, gives, finally:

$$\langle X_1^2(\underline{a},t)\rangle = 2\langle U_1^2(\underline{a},t)\rangle \int_{0}^{(t-t_0)} [(t-t_0)-\tau]\, R_{F_{11}}(\tau)\,d\tau. \tag{16}$$

(This particular form of Taylor's result is due to Kampe de Feriet (1939).) In this manner, we can obtain various moments of $\underset{\sim}{X}$ from those of $\underset{\sim}{U}$.

The following limiting expressions are obtained from equation (16):

(i) for "small" times, since the velocity field is assumed stationary (and continuous), $R_{F_{11}}(\tau) = R_{F_{11}}(-\tau) = 1 + O(\tau^2)$, so

$$\langle X_1^2(\underline{a},t)\rangle = \langle U_1^2(\underline{a},t)\rangle (t-t_0)^2 + O[(t-t_0)^4]; \tag{17}$$

(ii) for times t such that $\int_0^{t-t_0} R_{F_{11}}(\tau)\,d\tau \doteq \int_0^{\infty} R_{F_{11}}(\tau)\,d\tau \equiv T_{F_{11}}$, say,

Reproduced with permission of the copyright owner. Further reproduction prohibited without permission.

the Lagrangian velocity integral time scale, then

$$\langle X_i^2(a,t)\rangle \doteq 2\langle U_i^2(a,t)\rangle (t-t_0) T_{F_{ii}} . \qquad (18)$$

The limiting expression (18) is also characteristic of Brownian motion, which is defined by the condition that

time interval of interest $>>$ the integral time scale of the random velocity following a material point.

This is a main distinction between turbulent and molecular diffusion, for in turbulent diffusion we are often interested in times such that

time interval of interest $\lesssim$ time scale of the velocity autocorrelation.

Taylor's analysis has been extended to homogeneous, non-isotropic flows (Batchelor 1949), and to homogeneous, self-similarly decaying flows (Townsend 1954). It has also been expressed in terms of the Lagrangian frequency spectrum, the Fourier transform of $R_{F_{ii}}$ (Batchelor 1949 and Kampe de Feriet 1939).

Corrsin (1953) has further extended this to a homogeneous, stationary shear flow, defined in the Eulerian frame by:

$$\underset{\sim}{u}(\underset{\sim}{x},t) = \underset{\sim}{U}(\underset{\sim}{x}) + \underset{\sim}{u}'(\underset{\sim}{x},t) , \qquad (19)$$

Reproduced with permission of the copyright owner. Further reproduction prohibited without permission.

where $\langle \underset{\sim}{u}(\underset{\sim}{x},t)\rangle = \underset{\sim}{U}(\underset{\sim}{x}) = \left(\frac{dU}{dx_2}\right) x_2 \, \underset{\sim}{i}_1 \quad , \quad \left(\frac{dU_i}{dx_2}\right)$

being a constant. He defined a Lagrangian velocity by

$$\underset{\sim}{u}(\underset{\sim}{a},t) = \underset{\sim}{u}\left[\underset{\sim}{X}(\underset{\sim}{a},t),t\right] = \left(\frac{dU}{dx_2}\right) X_2(\underset{\sim}{a},t)\,\underset{\sim}{i}_1 + \underset{\sim}{u}'\left[\underset{\sim}{X}(\underset{\sim}{a},t),t\right] = \left(\frac{dU_i}{dx_2}\right) X_2(\underset{\sim}{a},t)\,\underset{\sim}{i}_1 + \underset{\sim}{U}'(\underset{\sim}{a},t) \tag{20}$$

(note that $\underset{\sim}{U}'$ is not a simple turbulent Lagrangian velocity fluctuation) and using the method of Taylor, obtained:

$$\langle X_1^2(\underset{\sim}{a},t)\rangle = \left(\frac{dU}{dx_2}\right)^2 \langle U_2'^2(\underset{\sim}{a},t)\rangle \left\{ \frac{2t^3}{3}\int_0^t R_{f_{22}}(\tau)\,d\tau - t^2 \int_0^t \tau R_{f_{22}}(\tau)\,d\tau + \int_0^t \frac{\tau^3}{3} R_{f_{22}}(\tau)\,d\tau \right\}$$

$$+ \left(\frac{dU}{dx_2}\right) \langle U_1'(\underset{\sim}{a},t) U_2'(\underset{\sim}{a},t)\rangle \left\{ \int_0^t (t-\tau)^2 \left[R_{f_{12}}(\tau) + R_{f_{21}}(\tau)\right] d\tau + 2\int_0^t \tau (t-\tau) R_{f_{12}}(\tau)\,d\tau \right\}$$

$$+ 2\langle U_1'^2(\underset{\sim}{a},t)\rangle \int_0^t (t-\tau) R_{f_{11}}(\tau)\,d\tau \tag{21}$$

$$\langle X_1(\underset{\sim}{a},t) X_2(\underset{\sim}{a},t)\rangle = \left(\frac{dU}{dx_2}\right) \langle U_2'^2(\underset{\sim}{a},t)\rangle \int_0^t R_{f_{22}}(\tau)\,d\tau$$

$$+ \langle U_1'(\underset{\sim}{a},t)\, U_2'(\underset{\sim}{a},t)\rangle \int_0^t (t-\tau)\left[R_{f_{12}}(\tau) + R_{f_{21}}(\tau)\right] d\tau \tag{22}$$

$$\langle X_2^2(\underset{\sim}{a},t)\rangle = 2\int_0^t (t-\tau) R_{f_{22}}(\tau)\,d\tau \cdot \langle U_2'^2(\underset{\sim}{a},t)\rangle \tag{23}$$

where $R_{f_{ij}} = \dfrac{\langle U_i'(\underset{\sim}{a},t)\, U_j'(\underset{\sim}{a},t+\tau)\rangle}{\langle U_i'(\underset{\sim}{a},t) U_j'(\underset{\sim}{a},t)\rangle}$, and the process is also assumed homogeneous and stationary. (These results are a slight extension of Corrsin's, since they do not require the turbulent

Reproduced with permission of the copyright owner. Further reproduction prohibited without permission.

velocity fluctuations to be isotropic).

The "short" time results of equations (21) to (23) are similar to those of equation (16), but for "long" times,

$$\langle X_1^2(a,t)\rangle \sim \frac{2}{3}\left(\frac{dU}{dx_2}\right)^2 t^3 T_{F_{22}} \langle U_2'^2(a,t)\rangle \tag{24}$$

$$\langle X_1(a,t)X_2(a,t)\rangle \sim \left(\frac{dU}{dx_2}\right) t^2 T_{F_{22}} \langle U_2'^2(a,t)\rangle. \tag{25}$$

These expressions indicate the significance the role the added mean velocity plays in enhancing the dispersion process, and reflect the interaction of the turbulent dispersion along the mean velocity gradient and the shearing by the mean velocity gradient.

From a Lagrangian point of view then, some significant results have been achieved. However, because the dynamic equations are much easier to handle in the Eulerian frame, and because almost all experimental data (in particular, velocity data) are taken in the Eulerian frame, the usefulness of these Lagrangian results is greatly limited unless the Lagrangian velocity statistics can be related to Eulerian velocity statistics.

Some limited success has been achieved by Lumley (1961) in investigating this "Euler-Lagrangian" problem, who was able to

Reproduced with permission of the copyright owner. Further reproduction prohibited without permission.

arrive at the following conclusions:

(i) by expanding the Lagrangian velocity in a time series in terms of the Eulerian velocity field, i.e.,

$$\underset{\sim}{U}(\underset{\sim}{a},t) = \sum_{n=0}^{\infty} \frac{t^n}{n!} \left\{ \left[\frac{\partial}{\partial t} + \underset{\sim}{u}(\underset{\sim}{x},t) \cdot \nabla \right]^n \underset{\sim}{u}(\underset{\sim}{x},t) \right\}_{\substack{x=a \\ t=0}}$$

he was able to conclude that

(a) Eulerian homogeneity $\Rightarrow$ Lagrangian homogeneity,

(b) Eulerian isotropy $\Rightarrow$ Lagrangian isotropy;

(ii) for a homogeneous, incompressible fluid, the one-point Lagrangian velocity probability density equals the one-point Eulerian velocity density;

(iii) if the Eulerian field is both homogeneous and stationary, the Lagrangian velocity autocorrelation $\langle U_i(a,t)\, U_j(a,t+\tau) \rangle$ is a function of τ only.

Corrsin has shown, using "inertial range" expressions for velocity spectra* and dimensional reasoning, that the Lagrangian integral time scale T_L is roughly equal to the Eulerian integral time scale, and that $\langle U^2 \rangle T_L$ is roughly equal to the Eulerian space

* first proposed by Inoue in 1951 for the Lagrangian case

Reproduced with permission of the copyright owner. Further reproduction prohibited without permission.

integral scale. He also suggested (1959a) that $\underset{\sim}{X}(\underset{\sim}{a},t)$ and $\underset{\sim}{y}(\underset{\sim}{x},t)$ become statistically independent for large diffusion times which results in the relation

$$\langle u_i(\underset{\sim}{a},t)\, u_j(\underset{\sim}{a},t)\rangle = \int_{\underset{\sim}{x}} \langle u_i(\underset{\sim}{a},0)\, u_j(\underset{\sim}{x}',t)\rangle\, p_{\underset{\sim}{X}}(\underset{\sim}{x}';\underset{\sim}{a},t)\, d\underset{\sim}{x}', \qquad (26)$$

where $p_{\underset{\sim}{X}}(\underset{\sim}{x};\underset{\sim}{a},t)$ is the probability density of $\underset{\sim}{X}(\underset{\sim}{a},t)$.

Many ad hoc theories have been applied to the turbulent diffusion problem. A prominent example is Robert's (1961) application of the "direct interaction approximation" (DIA), which was first formulated by Kraichnan (1959) for the turbulence dynamics problem. For homogeneous stationary flows with zero mean, Roberts obtained

$$\frac{\partial}{\partial t} p_{\underset{\sim}{X}}(\underset{\sim}{x},t) = \frac{\partial^2}{\partial x_i \partial x_j} \int_0^t dt' \int_{\underset{\sim}{x}} d\underset{\sim}{x}' \langle u_i(\underset{\sim}{x}'',t'')\, u_j(\underset{\sim}{x}''-\underset{\sim}{x}',t''-t')\rangle\, p_{\underset{\sim}{X}}(\underset{\sim}{x}',t')\, p_{\underset{\sim}{X}}(\underset{\sim}{x}-\underset{\sim}{x}',t-t') \qquad (27)$$

where $p_{\underset{\sim}{X}}(\underset{\sim}{x}-\underset{\sim}{a},t) = p_{\underset{\sim}{X}}(\underset{\sim}{x};\underset{\sim}{a},t)$ is the probability density of the displacement $\underset{\sim}{X}(\underset{\sim}{a},t)$. This equation exhibits many of the properties expected of an equation for $p_{\underset{\sim}{X}}$, in particular "non-localness" in space and time. It is interesting to note that one result of this DIA application is Corrsin's conjecture, equation (26). Roberts also investigated the statistics of the relative diffusion of two fluid particles.

Reproduced with permission of the copyright owner. Further reproduction prohibited without permission.

In the field of "alien" particle dispersion, Tchen Chan-Mou (1947) contributed a derivation of the equations of motion of the particle (although his application of the equations appears to be in error (Corrsin and Lumley 1956)). Lumley (1957) clarified the problem with a rigorous mathematical statement of it, as well as a more rigorous mathematical derivation of the equations of motion of the particle. He included a general method for solving the problem (which involves integration in function space, which in general is not now within the capabilities of modern mathematical analysis), and discussed several particular aspects of the topic.

Yudine (1959) approached the problem from a physically intuitive basis. He introduced the concepts of the "inertial" effect, by which "sluggish" particles do not follow completely the high frequency fluctuations of the turbulent medium, and the "crossing trajectories" effect, by which the "sluggish" particles cross the trajectories of the fluid particles.

In investigating the problem of "heavy" particles, rapidly falling out because of gravity, Yudine (1959), Csanady (1963) and others have suggested a hypothesis (analogous to Taylor's hypothesis made in interpreting time correlations at a fixed point as spatial cor-

Reproduced with permission of the copyright owner. Further reproduction prohibited without permission.

relations) which determined the particle velocity covariance in terms of the Eulerian spatial velocity covariance. Their results indicated considerable reduction of the dispersion when the particle was falling out.

Friedlander (1957) obtained expressions for mean square relative velocity between the particle and fluid and for the eddy diffusion coefficient, both in terms of the correlation coefficient of the velocity of the fluid in the neighborhood of the particles.

Several "Lagrangian" experiments have been performed in isotropic flows, starting with Simmons (reported in Taylor 1935), then Schubauer (1935), Uberoi and Corrsin (1953), Townsend (1954), Mickelsen (1955), and Shlien (1971) among others. They consist of "tagging" fluid particles, usually with heat or some other contaminant, and then measuring the statistics of $\underset{\sim}{\mathcal{I}}$ by measuring the mean statistics of the contaminant downstream from the tagging position. There are two main difficulties in this approach. The first arises in attempting to eliminate the effect of molecular diffusion, which is not easily separated from the turbulent dispersion (see, for example, Corrsin 1959b and Saffman 1961). Second, Lagrangian velocity statistics are nearly impossible to obtain, because: (1) it is difficult to follow the trajectories of the contaminants and so obtain their velocities at

Reproduced with permission of the copyright owner. Further reproduction prohibited without permission.

different points in time; and (2) obtaining velocity statistics from those of $\underline{X}$ involves such questionable techniques as double differentiation of experimental curves (e.g. using the time derivatives of equation (15)).

In spite of these difficulties some important conclusions have been established. Primary among these is that, for nearly isotropic homogeneous turbulence, the Lagrangian displacement probability density $f_{\underline{X}}$ is approximately Gaussian for all times. This result implies that only $\langle X_i X_j \rangle$ is then needed to define $f_{\underline{X}}$. However, because of the difficulties mentioned, reliable results do not exist even on the Lagrangian velocity correlation function. And only recently (Shlien 1971 using the Eulerian data of Comte-Bellot and Corrsin 1971) have the relative values of the Lagrangian and Eulerian time microscales been fairly accurately determined.

The same techniques have been employed in the mean shear regions of jets (Hinze and van der Hegge Zijnen 1951, and Uberoi and Corrsin 1953), and in boundary layers (Skramstad and Schubauer 1938), where "small" time results have agreed with "small" time predictions of Hinze and van der Hegge Zijnen (1951).

More recently, techniques have been developed to measure the position (and infer velocity) of small spheres carefully injected into

Reproduced with permission of the copyright owner. Further reproduction prohibited without permission.

homogeneous, turbulent wind tunnel flows. Kennedy (1965) first succeeded in achieving these measurements, but his results seem to be in doubt because of (1) erroneous Eulerian turbulence level measurements; (2) double-differentiation of $\langle I^2 \rangle$ curves to obtain R_f ; and (3) too few realizations sampled. Snyder (1969) performed experiments similar to Kennedy's, but was able to infer Lagrangian velocities as well as to increase the number of realizations sampled. He concluded that the velocity autocorrelations decrease faster for denser particles than for fluid points. His measurements of velocity autocorrelations for the very small, fast responding particles (the ratio of the particle response time to the Eulerian integral time scale approaching zero) appears to be one of the first reliable sets of "Lagrangian" velocity autocorrelation measurements in isotropic flow.

II. APPLICATION OF NUMERICAL SIMULATION TO TURBULENT DISPERSION

A. Rationale

In both theoretical and experimental turbulent diffusion, the investigator is confronted with inherent difficulties, several of which have already been mentioned.

For example, expressing θ and y in terms of their mean and fluctuating components,

Reproduced with permission of the copyright owner. Further reproduction prohibited without permission.

$$\theta(\underline{x},t) = \langle\theta(\underline{x},t)\rangle + \theta'(\underline{x},t)$$

$$\underline{u}(\underline{x},t) = \langle\underline{u}(\underline{x},t)\rangle + \underline{u}'(\underline{x},t) \ ,$$

substituting these expressions into equation I.4, and averaging results in

$$\left[\frac{\partial}{\partial t} + \langle\underline{u}(\underline{x},t)\rangle \cdot \nabla\right]\langle\theta(\underline{x},t)\rangle = -\nabla \cdot \langle\underline{u}'(\underline{x},t)\theta'(\underline{x},t)\rangle . \tag{1}$$

This is one equation in four unknowns,

$$\langle\theta(\underline{x},t)\rangle, \langle u_i'(\underline{x},t)\,\theta'(\underline{x},t)\rangle \qquad (i = 1,2,3) .$$

To close this set of equations, equations for $\langle u_i'\theta'\rangle$ are needed. However, equations for $\langle u_i'\,\theta'\rangle$ contain higher order averages of u_i' and θ', and so on with the equations for higher moments. A continuation of the process leads to an infinite set of equations, the number of equations being always fewer than the number of unknowns. This is another example of the "closure problem", although in this case it arises, not because of the non-linearity of the equations involved (as in turbulence dynamics), but because of the

Reproduced with permission of the copyright owner. Further reproduction prohibited without permission.

random coefficients $u_i(x,t)$ in the $(u \cdot \nabla)\theta$ term. In electrical engineering such a system is sometimes described as "parametrically driven".

So, viewed in the Eulerian frame, the problem of turbulent dispersion possesses some of the basic difficulties characteristic of turbulence itself.

It has been mentioned that solving the problem from a Lagrangian point of view (as stated just before and including equation (I. 12)) involves performing an integration in function space, a task which the tools of mathematical analysis do not yet permit. Thus from either the Lagrangian or Eulerian points of view, theoretical analyses of the problem are at an impasse, and so theoretical attempts are mostly limited to the investigation of results of ad hoc hypotheses, and to computing "short" time, "long" time, and "small" scale results.

The experimentalist approaching the problem must have sufficient data describing the Eulerian field, and must find adequate fluid tracers — small particles, balloons, heat, etc. — which do not affect the velocity field appreciably, whose position and velocity are easily detectable, which are cheap and easy to produce, etc. As has been mentioned, as a result of the inherent difficulties in this approach, few reliable results exist even on so basic a function as the velocity

Reproduced with permission of the copyright owner. Further reproduction prohibited without permission.

Filmed as received

without page(s) 20 .

UNIVERSITY MICROFILMS.

Reproduced with permission of the copyright owner. Further reproduction prohibited without permission.

study of deterministic mathematical problems by "simulating a stochastic process whose moments, density function, or cumulative distribution function satisfy the functional relationships or the solution requirements of the deterministic problem" (Naylor et al, 1966); and (2) the study of stochastic processes themselves. It is this latter variety of Monte Carlo analysis that is employed in this investigation.

C. Application to Turbulent Dispersion

The manner in which this method is used to simulate dispersion is described briefly in what follows. The random, three-dimensional Eulerian velocity field is limited to isochoric form, and represented in Fourier series:

$$\underset{\sim}{u}(\underset{\sim}{x},t) = \underset{\sim}{U}(\underset{\sim}{x}) + \sum_{n=1}^{N} T(\underset{\sim}{k}_n, t_n) \frac{\underset{\sim}{k}_n}{k_n} \times \left\{ \underset{\sim}{\alpha}_n \cos(\underset{\sim}{k}_n \cdot \underset{\sim}{x}) + \underset{\sim}{\beta}_n \sin(\underset{\sim}{k}_n \cdot \underset{\sim}{x}) \right\} \qquad (2)$$

where $\underset{\sim}{U}(\underset{\sim}{x})$ is the mean velocity. The deterministic function $T(\cdot,\cdot)$ is chosen to model the energy gain and loss in the various Fourier modes $\underset{\sim}{k}_n$, and $t_n = t - t_{0_n}$, where t_{0_n} is the random "initial" time at which energy is injected into the nth mode. The vectors $\underset{\sim}{\alpha}_n$, $\underset{\sim}{\beta}_n$, and $\underset{\sim}{k}_n$ are random variables defined by probability distributions selected so that $\{\underset{\sim}{u}(\underset{\sim}{x},t)\}$ will have statistical

Reproduced with permission of the copyright owner. Further reproduction prohibited without permission.

properties similar to those measured in a real Eulerian turbulent flow, like the flow field under investigation. [The non-linear terms in the Navier-Stokes equations are only indirectly modeled through the distribution of the K_n and by the function $TC(\cdot,\cdot)$; there is no interaction among the different wave number modes.]

"Ensembles" of realizations are analyzed, and ensemble averages are taken. In each realization, values for ζ_{0_n} , α_n , β_n , K_n are generated digitally using "pseudo random" techniques (see Appendix A), and equations (I. 8) -- or (I. 12) depending on the problem under consideration -- are integrated numerically using Hamming's fourth-order modified predictor corrector method (see Appendix C). The output of each realization is stored on magnetic tape, so that after all the realizations have been completed, various Lagrangian statistical quantities can be computed by "ensemble" averaging.

So the Eulerian field under investigation is modeled, and corresponding Lagrangian statistics computed, thus providing a method of solution to the problem as defined.

Variations of this approach to the dispersion problem have been used in several instances in the past. Patterson and Corrsin (1966) were perhaps the first to employ computer simulation in the investigation of turbulent dispersion. They studied a class of one-dimensional random walks (first investigated by Lumley and Corrsin 1959) in which

Reproduced with permission of the copyright owner. Further reproduction prohibited without permission.

probabilities were assigned, not to the walking particle (as is done in the classical random walk problem), but to the binary Eulerian field on which the particles moved. They generated "ensembles" of random binary fields on $(\underset{\sim}{x},t)$ grids, then allowed "fluid material particles" to wander across the grids according to the actual velocities in each realization. Ensemble averages using the position and velocity of the dispersing particles gave Lagrangian statistics, while ensemble averages taken over the original binary fields gave Eulerian space-time statistics.

More recently Kraichnan (1970) and Deardorff and Peskin (1970) have employed computer simulation to investigate dispersion. Deardorff (1970) had previously modeled three-dimensional turbulent dynamics by direct numerical integration of the primitive equations of motion for the case of turbulent, plane Poiseuille flow at very large Reynolds numbers. Spatial subgrid scale effects were simulated with eddy coefficients proportional to the local velocity deformation rate. Subsequently Deardorff and Peskin (1970) "marked and followed" particles in the mean shear region of this flow field, using Euler's method of numerical integration. After 480 particles were followed, "ensemble" averages were taken to obtain various Lagrangian properties.

The method selected in this project to model the Eulerian flow is a modification of Kraichnan's. His fields were realized in the form:

Reproduced with permission of the copyright owner. Further reproduction prohibited without permission.

$$\underset{\sim}{u}(\underset{\sim}{x},t) = \sum_{n=1}^{N} \underset{\sim}{\kappa}_n \times \left\{ \underset{\sim}{\zeta}_n \cos(\underset{\sim}{\kappa}_n \cdot \underset{\sim}{x} + \omega_n t) + \underset{\sim}{\xi}_n \sin(\underset{\sim}{\kappa}_n \cdot \underset{\sim}{x} + \omega_n t) \right\} \quad (3)$$

where the vectors $\underset{\sim}{\kappa}_n$, $\underset{\sim}{\zeta}_n$, $\underset{\sim}{\xi}_n$ and the scalar ω_n were random variates from distributions chosen so that $\underset{\sim}{u}$ was stationary and isotropic. (The differences between the present method and Kraichnan's, as well as reasons for these differences, are presented and expanded upon in chapter III.) The present method of performing and analyzing the "ensembles" of realizations is also similar to Kraichnan's.

The purpose of Kraichnan's numerical experiment was to compare the results of the exact calculation (from the simulation) with those of his "direct-interaction approximation" (DIA) applied to the model. The functions computed by the DIA agreed well with those computed from the simulation, except for two dimensional frozen (i.e., time independent) Eulerian fields, where strong "trapping" effects were found.

Reproduced with permission of the copyright owner. Further reproduction prohibited without permission.

III. DESCRIPTION OF THE VELOCITY FIELDS

A. Mathematical Background

1. Introduction

As mentioned in chapter II, the velocity fluctuation fields used in this study are expressible in the general form (see equation (II.2))

$$\underset{\sim}{u}'(\underset{\sim}{x},t) = \sum_{n=1}^{N} \frac{\underset{\sim}{\kappa}_n}{\kappa_n} \times \left\{ \underset{\sim}{a}_n(\underset{\sim}{\kappa}_n,t)\cos(\underset{\sim}{\kappa}_n\cdot\underset{\sim}{x}) + \underset{\sim}{b}_n(\underset{\sim}{\kappa}_n,t)\sin(\underset{\sim}{\kappa}_n\cdot\underset{\sim}{x}) \right\} \quad (1)$$

This is intended to model random, isochoric fields of the (Fourier-Steltjes) form

$$\underset{\sim}{u}(\underset{\sim}{x},t) = \int_{\underset{\sim}{\kappa}} \frac{\underset{\sim}{\kappa}}{\kappa} \times \left\{ d\underset{\sim}{A}(\underset{\sim}{\kappa},t)\cos(\underset{\sim}{\kappa}\cdot\underset{\sim}{x}) + d\underset{\sim}{B}(\underset{\sim}{\kappa},t)\sin(\underset{\sim}{\kappa}\cdot\underset{\sim}{x}) \right\} \quad (2)$$

Since we shall be dealing extensively with the statistical properties of these fields, and since they are expressed in unconventional form, it is helpful (i) to compute the conventional energy spectral tensor $\Phi_{ij}(\underset{\sim}{\kappa},t)$, defined by Batchelor, (1953)

$$\Phi_{ij}(\underset{\sim}{\kappa},t) = \left(\frac{1}{2\pi}\right)^3 \int_{\underset{\sim}{r}} \langle u_i(\underset{\sim}{x},t)u_j(\underset{\sim}{x}+\underset{\sim}{r},t)\rangle e^{-i\underset{\sim}{\kappa}\cdot\underset{\sim}{r}}\, d\underset{\sim}{r}, \quad (3)$$

in terms of the statistical properties of $d\underset{\sim}{A}$ and $d\underset{\sim}{B}$; and (ii) to determine the statistical properties of the various random quantities in the model (e.g. $t_{0_n}, \alpha_n, \beta_n, \underset{\sim}{\kappa}_n$) in terms of the statistical properties of $d\underset{\sim}{A}$ and $d\underset{\sim}{B}$. This will be done for the case of an isotropic field.

Reproduced with permission of the copyright owner. Further reproduction prohibited without permission.

Assume that $\underset{\sim}{v}(\underset{\sim}{x},t)$ is a statistically homogeneous function of $\underset{\sim}{x}$, and consider its expression in Fourier-Stieltjes form (omitting the time dependence in the notation):

$$\underset{\sim}{v}(\underset{\sim}{x}) = \int_{\underset{\sim}{k}} e^{i\underset{\sim}{k}\cdot\underset{\sim}{x}}\, d\underset{\sim}{z}(\underset{\sim}{k}), \tag{4}$$

where, because of the reality of $\underset{\sim}{v}$, $d\underset{\sim}{z}(\underset{\sim}{k}) = d\underset{\sim}{z}^{*}(-\underset{\sim}{k})$. ($\underset{\sim}{V}^{*}$ denotes the complex conjugate of $\underset{\sim}{V}$.) So the real $(d\underset{\sim}{z}_R)$ and the imaginary $(d\underset{\sim}{z}_I)$ components of $d\underset{\sim}{z}$ satisfy

$$d\underset{\sim}{z}_R(\underset{\sim}{k}) = d\underset{\sim}{z}_R(-\underset{\sim}{k}), \tag{5}$$

$$d\underset{\sim}{z}_I(\underset{\sim}{k}) = -\,d\underset{\sim}{z}_I(-\underset{\sim}{k}). \tag{6}$$

With $e^{i\underset{\sim}{k}\cdot\underset{\sim}{x}} = \cos(\underset{\sim}{k}\cdot\underset{\sim}{x}) + i\sin(\underset{\sim}{k}\cdot\underset{\sim}{x})$, equation (4) can be written as

$$\underset{\sim}{v}(\underset{\sim}{x}) = \int_{\underset{\sim}{k}} \left\{ \left[d\underset{\sim}{z}_R \cos(\underset{\sim}{k}\cdot\underset{\sim}{x}) - d\underset{\sim}{z}_I \sin(\underset{\sim}{k}\cdot\underset{\sim}{x}) \right] + i\left[d\underset{\sim}{z}_R \sin(\underset{\sim}{k}\cdot\underset{\sim}{x}) + d\underset{\sim}{z}_I \cos(\underset{\sim}{k}\cdot\underset{\sim}{x}) \right] \right\} \tag{7}$$

Because of (5) and (6), the second bracketed term in the integrand of (7) is an odd function of $\underset{\sim}{k}$, and thus integrates to zero, so that

$$\underset{\sim}{v}(\underset{\sim}{x}) = \int_{\underset{\sim}{k}} \left[d\underset{\sim}{z}_R \cos(\underset{\sim}{k}\cdot\underset{\sim}{x}) - d\underset{\sim}{z}_I \sin(\underset{\sim}{k}\cdot\underset{\sim}{x}) \right]. \tag{8}$$

Hence, comparing (8) and (2), the conventional Fourier components can be (uniquely) defined in terms of $d\underset{\sim}{A}$ and $d\underset{\sim}{B}$ by

Reproduced with permission of the copyright owner. Further reproduction prohibited without permission.

$$d\underset{\sim}{Z}_R(\underset{\sim}{k}) = \frac{k}{k} \times d\underset{\sim}{A}(\underset{\sim}{k}) \tag{9}$$

$$-d\underset{\sim}{Z}_I(\underset{\sim}{k}) = \frac{k}{k} \times d\underset{\sim}{B}(\underset{\sim}{k}) \tag{10}$$

However, given $(d\underset{\sim}{Z}_R, d\underset{\sim}{Z}_I)$, one cannot uniquely compute $(d\underset{\sim}{A}, d\underset{\sim}{B})$. This can be seen from examining the magnitude of equation (9),

$$|d\underset{\sim}{Z}_R| = \sin(\underset{\sim}{k}, d\underset{\sim}{A})\, |d\underset{\sim}{A}|,$$

where $\sin(\underset{\sim}{k}, d\underset{\sim}{A})$ is the sine of the angle between $\underset{\sim}{k}$ and $d\underset{\sim}{A}$. It is obvious from this expression that, given $|d\underset{\sim}{Z}_R|$, an infinity of $d\underset{\sim}{A}$'s could be found to satisfy the expression.

Next, define:

$$\Psi_{ij}^{AA}(\underset{\sim}{k}) = \lim_{d\underset{\sim}{k}\to\underset{\sim}{0}} \frac{\langle dA_i(\underset{\sim}{k})\, dA_j(\underset{\sim}{k})\rangle}{dk_1\, dk_2\, dk_3} \tag{11}$$

$$\Psi_{ij}^{AB}(\underset{\sim}{k}) = \lim_{d\underset{\sim}{k}\to\underset{\sim}{0}} \frac{\langle dA_i(\underset{\sim}{k})\, dB_j(\underset{\sim}{k})\rangle}{dk_1\, dk_2\, dk_3} \tag{12}$$

$$\Psi_{ij}^{BB}(\underset{\sim}{k}) = \lim_{d\underset{\sim}{k}\to\underset{\sim}{0}} \frac{\langle dB_i(\underset{\sim}{k})\, dB_j(\underset{\sim}{k})\rangle}{dk_1\, dk_2\, dk_3} \tag{13}$$

(The limits exist, since $\lim_{d\underset{\sim}{k}\to\underset{\sim}{0}} \frac{\langle dZ_i(\underset{\sim}{k}) dZ_j^*(\underset{\sim}{k})\rangle}{dk_1\, dk_2\, dk_3}$ is known to exist. (Batchelor 1953)) Assuming the statistical orthogonality of the $d\underset{\sim}{A}$'s and $d\underset{\sim}{B}$'s for different values of $\underset{\sim}{k}$, and using the cartesian component form of the cross product

Reproduced with permission of the copyright owner. Further reproduction prohibited without permission.

$[(\underset{\sim}{a}\times\underset{\sim}{b})_i = \varepsilon_{ijk}\, a_j\, b_k$, where ε_{ijk} is the "alternating unit tensor"], we find

$$\langle v_i(\underset{\sim}{x})\, v_j(\underset{\sim}{x}+\underset{\sim}{r})\rangle = \int_{\underset{\sim}{k}} \varepsilon_{isn}\,\varepsilon_{jpq}\,\frac{k_n k_p}{k^2}\left\{\left[\Psi^{AA}_{mq}\cos(\underset{\sim}{k}\cdot\underset{\sim}{x})\cos[\underset{\sim}{k}\cdot(\underset{\sim}{x}+\underset{\sim}{r})\right]\right.$$

$$+\Psi^{BB}_{mq}\sin(\underset{\sim}{k}\cdot\underset{\sim}{x})\sin[\underset{\sim}{k}\cdot(\underset{\sim}{x}+\underset{\sim}{r})]\Big] + \Big[\Psi^{AB}_{mq}\cos(\underset{\sim}{k}\cdot\underset{\sim}{x})\sin[\underset{\sim}{k}\cdot(\underset{\sim}{x}+\underset{\sim}{r})]$$

$$\left.+\Psi^{BA}_{mq}\sin(\underset{\sim}{k}\cdot\underset{\sim}{x})\cos[\underset{\sim}{k}\cdot(\underset{\sim}{x}+\underset{\sim}{r})]\right]\Big\}\, d\underset{\sim}{k} \,. \tag{14}$$

A condition sufficient to insure that $\langle v_i(\underset{\sim}{x})\, v_j(\underset{\sim}{x}+\underset{\sim}{r})\rangle$ is independent of $\underset{\sim}{x}$, is:

$$\Psi^{AA}_{mq} = \Psi^{BB}_{mq} \equiv u_{mq} \,, \tag{15}$$

$$\Psi^{AB}_{mq} = -\Psi^{BA}_{mq} \equiv \sigma_{mq} \,. \tag{16}$$

Using equations (11), (12), and (13), $\Psi^{AA}_{mq} = \Psi^{AA}_{qm}$, and $\Psi^{AB}_{mq} = \Psi^{BA}_{qm}$, so

$$u_{mq} = u_{qm} \,, \tag{17}$$

$$\sigma_{mq} = -\sigma_{qm} \,. \tag{18}$$

Using (15) and (16), equation (14) reduces to:

$$\langle v_i(\underset{\sim}{x})\, v_j(\underset{\sim}{x}+\underset{\sim}{r})\rangle = \int_{\underset{\sim}{k}} \varepsilon_{isn}\,\varepsilon_{jpq}\,\frac{k_n k_p}{k^2}\left\{u_{mq}\cos(\underset{\sim}{k}\cdot\underset{\sim}{r}) + \sigma_{mq}\sin(\underset{\sim}{k}\cdot\underset{\sim}{r})\right\} d\underset{\sim}{k} \,. \tag{19}$$

By means of the tensor identity

Reproduced with permission of the copyright owner. Further reproduction prohibited without permission.

$$\varepsilon_{ism}\varepsilon_{jpq} = \delta_{ij}\delta_{sp}\delta_{mq} + \delta_{ip}\delta_{sq}\delta_{mj} + \delta_{iq}\delta_{sj}\delta_{mp} - \delta_{ij}\delta_{sq}\delta_{mp} - \delta_{ip}\delta_{sj}\delta_{mq} - \delta_{iq}\delta_{sp}\delta_{mj} ,$$

equation (19) can be put into the form

$$\langle v_i(\underline{x})v_j(\underline{x}+\underline{r})\rangle = \int_{\underline{k}} \Big\{ \Big[\delta_{ij}u_{mm} + \frac{k_m k_i}{k^2}u_{jm} + \frac{k_i k_m}{k^2}u_{mj} - \delta_{ij}\frac{k_k k_m}{k^2}u_{km}$$

$$- \frac{k_i k_j}{k^2}u_{mm} - u_{ij}\Big]\cos(\underline{k}\cdot\underline{r}) + \Big[\frac{k_i k_m}{k^2}v_{jm} + \frac{k_j k_m}{k^2}v_{mi} + v_{ij}\Big]\sin(\underline{k}\cdot\underline{r})\Big\} d\underline{k} . \quad (20)$$

2. Two-Dimensional Flows.

For <u>two-dimensional flows</u> [say in the (x_1, x_2) plane], it is sufficient to take $d\underline{A} = (0, 0, dA)$, $d\underline{\beta} = (0, 0, d\beta)$, and $\underline{k} = (\kappa_1, \kappa_2, 0)$, so that with (11), (12), (13), (17), and (18)

$$u_{mn}(\underline{k}) = \begin{cases} \phi(\underline{k}), \text{ say, for } m=n=3 \\ 0 \text{ otherwise} \end{cases} \quad (21)$$

$$v_{mn}(\underline{k}) = 0 \quad \text{any } m,n. \quad (22)$$

Thus, with $R_{ij}(\underline{r}) = \langle v_i(\underline{x})v_j(\underline{x}+\underline{r})\rangle$:

$$\tfrac{1}{2}R_{ii}(\underline{r}) = \tfrac{1}{2}\int_{\underline{k}} \phi(\underline{k})\cos(\underline{k}\cdot\underline{r})\, d\underline{k} \quad (23)$$

$$R_{11}(\underline{r}) = \int_{\underline{k}} {}^{k_2^2}\!/_{k^2} \cdot \phi(\underline{k})\cos(\underline{k}\cdot\underline{r})\, d\underline{k} \quad (24)$$

Reproduced with permission of the copyright owner. Further reproduction prohibited without permission.

$$R_{12}(\underline{r}) = R_{21}(\underline{r}) = -\int_{\underline{k}} \frac{k_1 k_2}{k^2}\, \phi(\underline{k}) \cos(\underline{k}\cdot\underline{r})\, d\underline{k} \tag{25}$$

$$R_{22}(\underline{r}) = \int_{\underline{k}} \frac{k_1^2}{k^2}\, \phi(\underline{k}) \cos(\underline{k}\cdot\underline{r})\, d\underline{k}. \tag{26}$$

Two things are noteworthy. First, using (21) and the trace of the transform of (3),

$$\phi(\underline{k}) \equiv \lim_{d\underline{k}\to 0} \frac{\langle dA_3(\underline{k})\, dA_3(\underline{k})\rangle}{dk_1\, dk_2\, dk_3} = \Phi_{ii}(\underline{k}), \tag{27}$$

the trace of the energy spectrum tensor.

Second, in attempting to model a three-dimensional shear flow with $\frac{dU_1}{dx_2} > 0$, we would want the model flow to meet two (experimentally observed (for example, see Champagne, Harris, and Corrsin 1970, and Graham, Harris, and Corrsin 1971)) requirements. The first is that $R_{12}(\underline{0}) < 0$ (implying that energy is transferred from the mean flow to the turbulence since the term $\frac{dU_1}{dx_2}\langle u_1 u_2\rangle$, representing the rate of production of turbulent kinetic energy from the mean flow kinetic energy, is positive). Secondly, the spatial isocorrelation contours of R_{11} should be of the form shown in figure 1 (from Graham, Harris, and Corrsin 1971). If R_{11} is of this general form then according to (24) $\phi(\underline{k})$ will have constant contour curves qualitatively like those in figure 2.

Reproduced with permission of the copyright owner. Further reproduction prohibited without permission.

Reproduced with permission of the copyright owner. Further reproduction prohibited without permission.

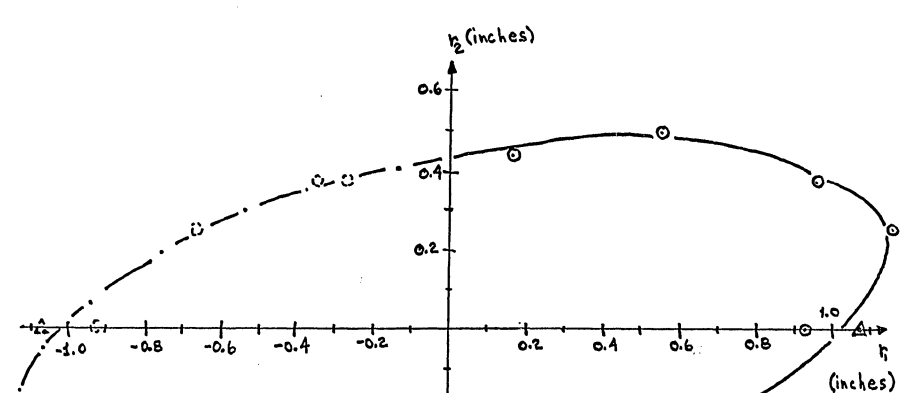

Figure 1. Spatial isocorrelation contour [$\mathcal{R}_{11}(r_1, r_2, 0, 0)$] in the plane of the mean velocity (r_1) and the mean velocity gradient (r_2) from Graham et al (1971).

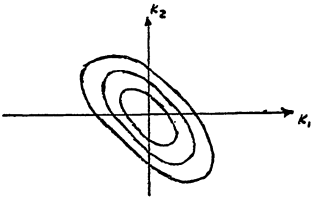

Figure 2

Consequently, $\int_{\underline{k}} \frac{k_1 k_2}{k^2} \phi(\underline{k})\, d\underline{k} < 0$ because the second and fourth quadrants (where $k_1 k_2 < 0$) will be weighted more than the first and third (where $k_1 k_2 > 0$). Thus, from (25) $R_{12}(\underline{r}) > 0$.

So it appears that in the two-dimensional case, the two requirements are incompatible. This fact may be related to the well known two-dimensional phenomenon whereby energy flows from smaller eddies to larger eddies (see, for example, Fjörtoft 1953, Kraichnan 1967, Batchelor 1969, and Lilly 1969) which is the opposite of what generally occurs in three-dimensional turbulent shear flows.

3. Three-Dimensional Flows

For three dimensional flows, equation (20) gives:

$$\tfrac{1}{2} R_{ii}(\underline{r}) = \tfrac{1}{2} \int_{\underline{k}} \left(u_{mn} - \frac{k_n k_m}{k^2} u_{sm} \right) \cos(\underline{k}\cdot\underline{r})\, d\underline{k} \qquad (28)$$

$$R_{11}(\underline{r}) = \int_{\underline{k}} \left(\frac{k_3^2}{k^2} u_{22} + \frac{k_2^2}{k^2} u_{33} - 2 \frac{k_2 k_3}{k^2} u_{23} \right) \cos(\underline{k}\cdot\underline{r})\, d\underline{k} \qquad (29)$$

Reproduced with permission of the copyright owner. Further reproduction prohibited without permission.

$$R_{12}(\underset{\sim}{r}) = R_{21}(-\underset{\sim}{r}) = -\int_{\underset{\sim}{k}} \Big\{ \Big[\frac{k_1 k_2}{k^2} u_{33} + \frac{k_3^2}{k^2} u_{12} - \frac{k_2 k_3}{k^2} u_{13} - \frac{k_1 k_3}{k^2} u_{23} \Big] \cos(\underset{\sim}{k}\cdot\underset{\sim}{r}) + \Big[\frac{k_3^2}{k^2} v_{21} + \frac{k_1 k_3}{k^2} v_{32} + \frac{k_2 k_3}{k^2} v_{13} \Big] \sin(\underset{\sim}{k}\cdot\underset{\sim}{r}) \Big\} d\underset{\sim}{k} \tag{30}$$

$$R_{13}(\underset{\sim}{r}) = R_{31}(-\underset{\sim}{r}) = -\int_{\underset{\sim}{k}} \Big\{ \Big[\frac{k_1 k_3}{k^2} u_{22} + \frac{k_2^2}{k^2} u_{13} - \frac{k_1 k_2}{k^2} u_{32} - \frac{k_2 k_3}{k^2} u_{12} \Big] \cos(\underset{\sim}{k}\cdot\underset{\sim}{r}) + \Big[\frac{k_2^2}{k^2} v_{31} + \frac{k_1 k_2}{k^2} v_{23} + \frac{k_2 k_3}{k^2} v_{12} \Big] \sin(\underset{\sim}{k}\cdot\underset{\sim}{r}) \Big\} d\underset{\sim}{k} \tag{31}$$

$$R_{22}(\underset{\sim}{r}) = \int_{\underset{\sim}{k}} \Big(\frac{k_3^2}{k^2} u_{33} + \frac{k_2^2}{k^2} u_{11} - 2 \frac{k_1 k_3}{k^2} u_{13} \Big) \cos(\underset{\sim}{k}\cdot\underset{\sim}{r})\, d\underset{\sim}{k} \tag{32}$$

$$R_{23}(\underset{\sim}{r}) = R_{32}(-\underset{\sim}{r}) = -\int_{\underset{\sim}{k}} \Big\{ \Big[\frac{k_1 k_3}{k^2} u_{11} + \frac{k_1^2}{k^2} u_{23} - \frac{k_1 k_3}{k^2} u_{12} - \frac{k_1 k_2}{k^2} u_{31} \Big] \cos(\underset{\sim}{k}\cdot\underset{\sim}{r}) + \Big[\frac{k_1^2}{k^2} v_{32} + \frac{k_1 k_2}{k^2} v_{13} + \frac{k_1 k_3}{k^2} v_{21} \Big] \sin(\underset{\sim}{k}\cdot\underset{\sim}{r}) \Big\} d\underset{\sim}{k} \tag{33}$$

$$R_{33}(\underset{\sim}{r}) = \int_{\underset{\sim}{k}} \Big(\frac{k_2^2}{k^2} u_{11} + \frac{k_1^2}{k^2} u_{22} - 2 \frac{k_1 k_2}{k^2} u_{12} \Big) \cos(\underset{\sim}{k}\cdot\underset{\sim}{r})\, d\underset{\sim}{k} \tag{34}$$

It can be shown from these expressions that to insure isotropy it is sufficient that

$$v_{21} = v_{31} = v_{23} = 0$$

$$u_{12} = u_{13} = u_{23} = 0$$

$$u_{11} = u_{22} = u_{33} = \frac{\Phi(k)}{4\pi}, \text{ say, or} \tag{35}$$

$$v_{ij} = 0$$

$$u_{ij} = \frac{\Phi(k)}{4\pi} \delta_{ij} \qquad i,j = 1,2,3 \tag{36}$$

Reproduced with permission of the copyright owner. Further reproduction prohibited without permission.

In this case, equation (20) reduces to the isotropic form,

$$\langle u_i(\underset{\sim}{x}) u_j(\underset{\sim}{x}+\underset{\sim}{r}) \rangle = \int_{\underset{\sim}{k}} \frac{\Phi(k)}{4\pi k^2} (k^2 \delta_{ij} - k_i k_j) \cos(\underset{\sim}{k}\cdot\underset{\sim}{r})\, d\underset{\sim}{k} . \tag{37}$$

Thus, in terms of the energy density $E(k)$ (Batchelor 1953) $\Phi(k)$ is

$$\Phi(k) = \frac{E(k)}{k^2} . \tag{38}$$

4. Some Identifications for the Model Field

Next consider velocity fields of the form to be used in the simulations, i.e.,

$$\underset{\sim}{u}'(\underset{\sim}{x},t) = \sum_{n=1}^{N} T(\underset{\sim}{k}_n, t_n) \frac{\underset{\sim}{k}_n}{k_n} \times \left\{ \underset{\sim}{\alpha}_n \cos(\underset{\sim}{k}_n\cdot\underset{\sim}{x}) + \underset{\sim}{\beta}_n \sin(\underset{\sim}{k}_n\cdot\underset{\sim}{x}) \right\} \tag{39}$$

Note again that $\underset{\sim}{k}_n$, $\underset{\sim}{\alpha}_n$, $\underset{\sim}{\beta}_n$, and $t_n = t - t_{0_n}$ $(n = 1, 2, \ldots, N)$ are all random quantities, whose statistical properties determine the statistical properties of $\underset{\sim}{u}'$. Also note that the amplitudes $g_n(\underset{\sim}{k}_n, t)$ and $f_n(\underset{\sim}{k}_n, t)$ in equation (1) have been assumed to be of the form $T(\underset{\sim}{k}_n, t_n)\underset{\sim}{\alpha}_n$ and $T(\underset{\sim}{k}_n, t_n)\underset{\sim}{\beta}_n$. To avoid unnecessary complications in the model, we define each quantity to be identically distributed for each n (e.g., $p_{\underset{\sim}{k}_n}(\underset{\sim}{\lambda}; n)$, the probability density of $\underset{\sim}{k}_n$, is defined to be independent of n).

Taking note of the restrictions imposed on $d\underset{\sim}{A}$ and $d\underset{\sim}{B}$ by equations (15) and (16), we require that $\underset{\sim}{\alpha}_n$ and $\underset{\sim}{\beta}_n$ satisfy:

$$\langle \alpha_{n_m} \alpha_{n_q} \rangle = \langle \beta_{n_m} \beta_{n_q} \rangle \equiv \hat{a}_{mq} \tag{40}$$

Reproduced with permission of the copyright owner. Further reproduction prohibited without permission.

$$\langle \alpha_{n_m} \beta_{n_q} \rangle = - \langle \beta_{n_m} \alpha_{n_q} \rangle = \hat{\sigma}_{mq} . \tag{41}$$

No summation is implied on n . Note that

$$\hat{u}_{mq} = \hat{u}_{qm} \tag{42}$$

$$\hat{\sigma}_{mq} = - \hat{\sigma}_{qm} \tag{43}$$

Also to insure homogeneity, the statistical orthogonality of $\underset{\sim}{\alpha}_n$ and $\underset{\sim}{\beta}_n$ for different n (and so $\underset{\sim}{\kappa}_n$) is required, i.e.,

$$\langle \alpha_{n_r} \alpha_{m_s} \rangle = \langle \alpha_{n_r} \beta_{m_s} \rangle = \langle \beta_{n_r} \beta_{m_s} \rangle = 0 \quad \text{for } n \neq m. \tag{44}$$

For any given n , the $(\underset{\sim}{\alpha}_n , \underset{\sim}{\beta}_n)$, the t_{0_n} , and the $\underset{\sim}{\kappa}_n$ will all be defined independently. (Thus, for example, t_{0_n} and $\underset{\sim}{\kappa}_n$ will be statistically independent.) So any one of the quantities can be "averaged out" independently of the others. For example, averaging the $\underset{\sim}{\alpha}_n$ and $\underset{\sim}{\beta}_n$ in the expression for $u_i'(\underset{\sim}{x},t)\, u_j'(\underset{\sim}{x}+\underset{\sim}{r},t)$ gives

$$\sum_{n=1}^{N} T^2(\underset{\sim}{\kappa}_n, t_n)\, \varepsilon_{ipm}\, \varepsilon_{jqg}\, \frac{\kappa_{n_p} \kappa_{n_p}}{\kappa_n^2} \Big\{ \langle \alpha_{n_m} \alpha_{n_g} \rangle \cos(\underset{\sim}{\kappa}_n \cdot \underset{\sim}{x}) \cos[\underset{\sim}{\kappa}_n \cdot (\underset{\sim}{x}+\underset{\sim}{r})]$$
$$+ \langle \alpha_{n_m} \beta_{n_g} \rangle \cos(\underset{\sim}{\kappa}_n \cdot \underset{\sim}{x}) \sin[\underset{\sim}{\kappa}_n \cdot (\underset{\sim}{x}+\underset{\sim}{r})] + \langle \beta_{n_m} \alpha_{n_g} \rangle \sin(\underset{\sim}{\kappa}_n \cdot \underset{\sim}{x}) \cos[\underset{\sim}{\kappa}_n \cdot (\underset{\sim}{x}+\underset{\sim}{r})]$$
$$+ \langle \beta_{n_m} \beta_{n_g} \rangle \cos(\underset{\sim}{\kappa}_n \cdot \underset{\sim}{x}) \cos[\underset{\sim}{\kappa}_n \cdot (\underset{\sim}{x}+\underset{\sim}{r})] \Big\} \tag{45}$$

Reproduced with permission of the copyright owner. Further reproduction prohibited without permission.

Noting that $(\underset{\sim}{\alpha}_n, \underset{\sim}{\beta}_n)$ is identically distributed for each n, such an average will be denoted by $\overline{(\,)}^{\alpha}$. Similarly, averaging the t_{0_n} alone will be denoted by $\overline{(\,)}^{t_0}$ and the $\underset{\sim}{K}_n$ alone by $\overline{(\,)}^{K}$. Note that averaging out the $(\underset{\sim}{\alpha}_n, \underset{\sim}{\beta}_n)$, the t_{0_n}, and the $\underset{\sim}{K}_n$ in succession gives the ensemble average, i.e.,

$$\overline{\overline{\overline{(\,)}^{\alpha}}^{t_0}}^{K} = \langle (\,) \rangle \tag{46}$$

Using equations (40) to (44) in expression (45) then gives

$$\overline{v_i'(\underset{\sim}{x},t)v_j'(\underset{\sim}{x}+\underset{\sim}{r},t)}^{\alpha} = \sum_{n=1}^{N} T^2(\underset{\sim}{K}_n, t_n) E_{i0m} E_{j\rho\beta} \frac{K_p K_{n\rho}}{K_n^2} \left\{ \hat{u}_{mq} \cos(\underset{\sim}{K}_n \cdot \underset{\sim}{r}) + \hat{w}_{mq} \sin(\underset{\sim}{K}_n \cdot \underset{\sim}{r}) \right\} \tag{47}$$

N is the number of modes on the field at any time, and so is a random function of time. Its statistics depends on those of the injection process, and hence t_{0_n}. Thus when averaging the t_{0_n}, one must take N into account.

t_n also depends statistically on t_{0_n}. To make computations appreciably easier, it will be assumed that t_n and N are statistically independent, an assumption which will be discussed more later. Also let

$$F(\underset{\sim}{K}_n) \equiv \overline{T^2(\underset{\sim}{K}_n, t_n)}^{t_0}. \tag{48}$$

(Note that $T(\underset{\sim}{K}_n, t_n)$ is a deterministic function of the random variables $\underset{\sim}{K}_n$ and t_n).

Reproduced with permission of the copyright owner. Further reproduction prohibited without permission.

This average will be computed later (see equation (87)) and will be shown to be a function of $K_n = |\underset{\sim}{K}_n|$ alone for the particular choice of $T(\underset{\sim}{k}_n, t_n)$ to be used. Defining $\overline{N} \equiv \langle N \rangle$, and with the independence assumption mentioned above, averaging the t_{0_n} in (47) gives

$$\overline{\overline{u_i'(\underset{\sim}{x},t)u_j'(\underset{\sim}{x}+\underset{\sim}{r},t)}^{\alpha}}^{t_0} = \overline{N}\, F(K_n)\,\varepsilon_{ilm}\varepsilon_{jpq}\frac{k_{nl}k_{np}}{K_n^2}\left\{\hat{u}_{mq}\cos(\underset{\sim}{k}_n\cdot\underset{\sim}{r}) + \hat{v}_{mq}\sin(\underset{\sim}{k}_n\cdot\underset{\sim}{r})\right\} \tag{49}$$

Writing $p_{\underset{\sim}{k}_n}(\underset{\sim}{\lambda})$ as the probability density of $\underset{\sim}{k}_n$, then, with (46), the ensemble is:

$$\langle u_i'(\underset{\sim}{x},t)u_j'(\underset{\sim}{x}+\underset{\sim}{r},t)\rangle = \overline{N}\int_{\underset{\sim}{\lambda}} \varepsilon_{ilm}\varepsilon_{jpq}\frac{\lambda_l\lambda_p}{\lambda^2}\left\{\hat{u}_{mq}\cos(\underset{\sim}{\lambda}\cdot\underset{\sim}{r}) + \hat{v}_{mq}\sin(\underset{\sim}{\lambda}\cdot\underset{\sim}{r})\right\} p_{\underset{\sim}{k}_n}(\underset{\sim}{\lambda})F(\lambda)\,d\underset{\sim}{\lambda} \tag{50}$$

Comparing (50) with (19), we make the identifications

$$u_{ij}(\underset{\sim}{k}) \Longleftrightarrow \hat{u}_{ij}\,\overline{N}\,p_{\underset{\sim}{k}_n}(\underset{\sim}{k})\,F(k) \tag{51}$$

$$v_{ij}(\underset{\sim}{k}) \Longleftrightarrow \hat{v}_{ij}\,\overline{N}\,p_{\underset{\sim}{k}_n}(\underset{\sim}{k})\,F(k) \tag{52}$$

Thus, in modelling an isotropic flow, for example, we have (see equations (35) and (36)):

$$\frac{\Phi(k)}{4\pi}\delta_{ij} = \overline{N}\,\hat{u}_{ij}\,p_{\underset{\sim}{k}_n}(\underset{\sim}{k})F(k)$$

$$0 = \overline{N}\,\hat{v}_{ij}\,p_{\underset{\sim}{k}_n}(\underset{\sim}{k})F(k) \qquad \text{, or}$$

$$\frac{\Phi(k)}{4\pi} = p_{\underset{\sim}{k}_n}(\underset{\sim}{k})\,F(k) \tag{53}$$

$$\hat{u}_{ij} = \delta_{ij}/\overline{N} \tag{54}$$

Reproduced with permission of the copyright owner. Further reproduction prohibited without permission.

$$\hat{\alpha}_{ij} = 0 . \tag{55}$$

The energy density $E(k)$ is thus given by

$$E(k) = k^2 \cdot 4\pi \oint_{\xi_k} (\xi) F(k) . \tag{56}$$

Similar identifications can be made for the case of the shear flow, but the expressions are much more complicated. They will be produced only when needed.

B. The Shear Flow Model

1. Conditions to be Satisfied by the Model

The shear flow chosen to be modelled was the nearly homogeneous, turbulent shear flow experimentally investigated by Rose (1966), by Champagne, Harris, and Corrsin (1970), and by Graham, Harris, and Corrsin (1970). This flow contains the complicated coupling of turbulent and mean velocity fields which is characteristic of most natural and technological turbulent flows, but it has the simplicity of statistical homogeneity. Furthermore, a considerable amount of data describing the field was available.

The model was required to satisfy in particular the following conditions:

I. Homogeneity of the spatial correlations (but not all possible space-time correlations).

II. With the mean flow $\underset{\sim}{U}(\underset{\sim}{x})$ given by $\underset{\sim}{U}(\underset{\sim}{x}) = \left(\frac{dU}{dx_2} x_2, 0, 0\right)$ (see figure 3),

Reproduced with permission of the copyright owner. Further reproduction prohibited without permission.

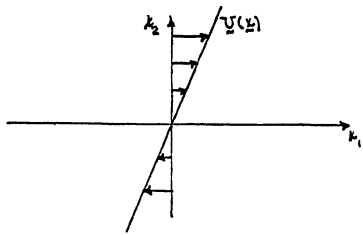

Figure 3

statistical invariance with respect to the following axes transformation $(y,t) \longleftrightarrow (x,t)$:

$$\left(x_1 + \frac{dU_1}{dx_2}t\,h,\, x_2 + h,\, x_3,\, t\right) = (y_1, y_2, y_3, t) \qquad (57)$$

where $\frac{dU_1}{dx_2}$ and h are constants.

III. Statistical stationarity.

IV. Statistical invariance of rotations of 180° about the x_3 - axis.

V. Statistical invariance for reflections in the x_1, x_2 plane.

VI. Tendency towards isotropy at high wave numbers.

Condition I is one that is approximately satisfied by the modeled flow, as are conditions IV, V, and VI. The transformation II results from: (i) a translation of distance h along the x_2 - axis, and (ii) a Galilean transformation such that the origin

Reproduced with permission of the copyright owner. Further reproduction prohibited without permission.

of the new coordinate system will coincide with the point of zero mean velocity (so that $y_1 = x_1 + \frac{dU_1}{dx_2} t + h$). (See figure 4.)

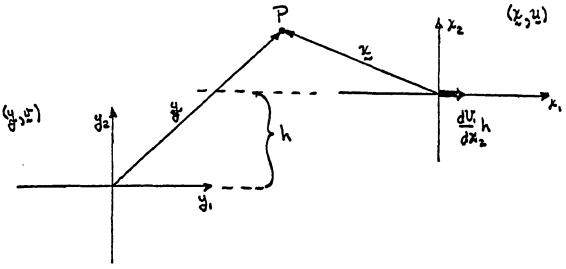

Figure 4

Thus this condition implies that the statistical properties of the flow should be identical in any two coordinate systems which are alined and whose origins are traveling with the local mean velocity.

That the condition imposes certain restrictions of the functional form of the space-time velocity correlation can be seen from the following argument: assume that the space-time correlation is of the form

$$\langle v_i(y,t) v_j(y+r, t+\tau) \rangle = Q_{ij}(r, \tau, y_2). \tag{58}$$

In the transformation defined in condition II, the turbulent velocities are related by

Reproduced with permission of the copyright owner. Further reproduction prohibited without permission.

$$\underset{\sim}{u}(x_1, x_2, x_3, t) = \underset{\sim}{u}\left(x_1 + \frac{du}{dx_2}\xi h, x_2 + h, x_3, t\right) \tag{59}$$

With condition II, R_{ij} can also be expressed as

$$R_{ij}(\xi, r, x_2) = \langle u_i(x, t)\, u_j(x + \xi, t + r)\rangle \tag{60}$$

Using (59) in (60) gives

$$R_{ij}(\xi, r, x_2) = \left\langle u_i\left(x_1 + \frac{du}{dx_2}\xi h, x_2 + h, x_3, t\right) u_j\left(x_1 + r_1 + \frac{du}{dx_2}(\xi + r)h, x_2 + \xi + h, x_3 + r_3, t + r\right)\right\rangle,$$

which is, with (58),

$$R_{ij}(r_1, r_2, r_3, r, x_2) = R_{ij}\left(r_1 + \frac{du}{dx_2}rh, r_2, r_3, r, x_2 + h\right) \tag{61}$$

This is a functional equation which has to be satisfied by R_{ij}.
Differentiating (61) with respect to h gives

$$\frac{\partial}{\partial\alpha} R_{ij}(\alpha, r_2, r_3, r, x_2 + h)\Big|_{\alpha = r_1 + \frac{du}{dx_2}rh} \cdot \frac{du_i}{dx_2} r + \frac{\partial}{\partial\beta} R_{ij}\left(r_1 + \frac{du}{dx_2}rh, r_2, r_3, r, \beta\right)\Big|_{\beta = x_2 + h} = 0 \tag{62}$$

This is an equation of the form

$$\frac{du_i}{dx_2} r \frac{\partial}{\partial\alpha} f(\alpha, \beta) + \frac{\partial}{\partial\beta} f(\alpha, \beta) = 0 \tag{63}$$

which has the general solution

$$f(\alpha, \beta) = g\left(\alpha - \frac{du_i}{dx_2} r\beta\right), \tag{64}$$

Reproduced with permission of the copyright owner. Further reproduction prohibited without permission.

where g is an arbitrary, differentiable function. Thus, the space-time correlation can be defined in the form

$$\langle u_i'(\underset{\sim}{x},t)\, u_j'(\underset{\sim}{x}+\underset{\sim}{r},t+\tau)\rangle = \mathcal{R}_{ij}\left(\underset{\sim}{r} - \frac{dU_1}{dx_2}\tau x_2 \underset{\sim}{i}_1, \tau\right). \tag{65}$$

This satisfies both condition II and condition I -- with $\tau = 0$.

The condition III of statistical stationary is desired for theoretical simplicity, although it is now generally held (Rose 1966, Corrsin 1962, Champagne et.al. 1970, Graham et.al. 1971, Lumley 1970) that homogeneous turbulent shear flows cannot be stationary.

Condition IV has several important ramifications. Consider the correlation

$$\mathcal{R}_{13}(0,0,r_3,0) = \langle u_1'(0,0,0,0)\, u_3'(0,0,r_3,0)\rangle$$

computed in the coordinate system A . (See figure 5.)

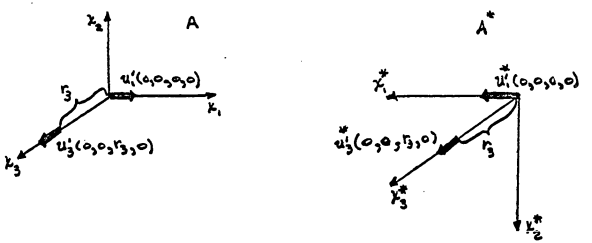

Figure 5.

Reproduced with permission of the copyright owner. Further reproduction prohibited without permission.

In the coordinate system A^* , obtained from A by a rotation of 180° about the x_3- axis, we have

$$\mathcal{R}^*_{13}(0,0,r_3,0) = \langle u_1'^*(0,0,0,0)\, u_3'^*(0,0,r_3,0)\rangle.$$

Now $u_3'^*(0,0,r_3,0) = u_3'(0,0,r_3,0)$ and $-u_1'^*(0,0,0,0) = u_1'(0,0,0,0)$.

So $$\mathcal{R}^*_{13}(0,0,r_3,0) = -\mathcal{R}_{13}(0,0,r_3,0).$$

However, condition IV requires that $\mathcal{R}^*_{13}(0,0,r_3,0) = \mathcal{R}_{13}(0,0,r_3,0)$.

So we conclude that condition IV implies:

$$\mathcal{R}_{13}(0,0,r_3,0) = 0. \tag{66}$$

A similar argument leads to

$$\mathcal{R}_{23}(0,0,r_3,0) = 0. \tag{67}$$

The implications of these conditions on the choice of $p_{\underset{\sim}{k}_n}(\underset{\sim}{\lambda})$ will be discussed later.

Condition V also implies that $\mathcal{R}_{ij}$ satisfy certain symmetry conditions. For example, it implies that

$$\langle u_1'(0,0,0,0)\, u_1'(r_1,r_2,r_3,0)\rangle = \langle u_1'(0,0,0,0)\, u_1'(r_1,r_2,-r_3,0)\rangle,$$

so that $$\mathcal{R}_{11}(r_1,r_2,r_3,0) = \mathcal{R}_{11}(r_1,r_2,-r_3,0), \tag{68}$$

using equation (65). Condition V also requires that

Reproduced with permission of the copyright owner. Further reproduction prohibited without permission.

$$\langle u_1'(o,o,o)\,u_3'(r_1,r_2,r_3,o)\rangle = -\langle u_1'(o,o,o)\,u_3'(r_1,r_2,-r_3,o)\rangle,$$

so that $$R_{13}(r_1,r_2,r_3,o) = -R_{13}(r_1,r_2,-r_3,o), \qquad (69)$$

again using (65). In a similar manner, the following results are obtained:

$$R_{12}(r_1,r_2,r_3,o) = R_{12}(r_1,r_2,-r_3,o) \qquad (70)$$

$$R_{22}(r_1,r_2,r_3,o) = R_{22}(r_1,r_2,-r_3,o) \qquad (71)$$

$$R_{23}(r_1,r_2,r_3,o) = -R_{23}(r_1,r_2,-r_3,o) \qquad (72)$$

$$R_{33}(r_1,r_2,r_3,o) = R_{33}(r_1,r_2,-r_3,o). \qquad (73)$$

Condition VI has been shown experimentally to be valid for extremely high Reynolds number flows (e.g., see Grant, Stewart, and Moilliet 1962), and there are indications that it is also valid (when applied to certain statistical quantities) in flows at moderate Reynolds numbers (e.g., see Champagne, et.al. 1970).

2. Selection of the statistical properties of the α_n and β_n

To meet condition I, the α_n and β_n were selected so as to satisfy the same statistical requirements as $dA(k)$ and $dB(k)$, namely (i) statistical orthogonality of α_n and β_n for different wave numbers; and (ii) conditions equivalent

Reproduced with permission of the copyright owner. Further reproduction prohibited without permission.

to equations (15) and (16). Also it will be shown later in this section that the requirements that $R_{13}(o,o,r_3,o) = R_{23}(o,o,r_3 o) = o$ imply that (see equation (94)

$$\hat{u}_{13} = \hat{u}_{23} = 0. \tag{74}$$

Furthermore, the tendency towards isotropy at the large wave numbers implies that (see equations (54) and (55):

$$\hat{u}_{22}, \hat{u}_{33} \to \hat{u}_{11} \quad \text{and} \quad \hat{u}_{12}, \hat{v}_{12}, \hat{v}_{13}, \hat{v}_{23} \to 0 \quad \text{as} \quad k_n \to \infty. \tag{75}$$

These conditions are all met by

(i) choosing all the quantities

$$\alpha_{n_1}, \alpha_{n_2}, \alpha_{n_3}, \beta_{n_1}, \beta_{n_2}, \beta_{n_3} \qquad (n = 1, 2, \ldots, N)$$

independently distributed for the different n (meeting the requirement of statistical orthogonality);

(ii) choosing $\underset{\sim}{\alpha}_n$ and $\underset{\sim}{\beta}_n$ to be independent and identically distributed [satisfying equations (15) and (16)], so that

$$\langle \alpha_{n_r} \alpha_{n_s} \rangle = \langle \beta_{n_r} \beta_{n_s} \rangle = \hat{u}_{rs}$$

$$\langle \alpha_{n_r} \beta_{n_s} \rangle = \hat{v}_{rs} = o \qquad \text{for all } r,s \tag{76}$$

(iii) requiring the third component to be independent of the first and second, so that

$$\hat{u}_{13} = \hat{u}_{23} = o$$

Reproduced with permission of the copyright owner. Further reproduction prohibited without permission.

(iv) selecting the quantities from Gaussian distributions with zero mean (so that $\langle \underset{\sim}{u}' \rangle = \underset{\sim}{0}$) such that

$$\langle \alpha_{n_1} \alpha_{n_1} \rangle = \langle \beta_{n_1} \beta_{n_1} \rangle = A_{11} \tag{77}$$

$$\langle \alpha_{n_2} \alpha_{n_2} \rangle = \langle \beta_{n_2} \beta_{n_2} \rangle = A_{11} \left(1 + \frac{a_{22}}{G(k_n)}\right) \tag{78}$$

$$\langle \alpha_{n_3} \alpha_{n_3} \rangle = \langle \beta_{n_3} \beta_{n_3} \rangle = A_{11} \left(1 + \frac{a_{33}}{G(k_n)}\right) \tag{79}$$

$$\langle \alpha_{n_1} \alpha_{n_2} \rangle = \langle \beta_{n_1} \beta_{n_2} \rangle = A_{11} \frac{a_{12}}{G(k_n)} \tag{80}$$

where A_{11}, a_{22}, a_{33}, and a_{12} were all constant parameters. The function $G(k_n)$ was defined so that it was equal to one for small values of k_n (non-isotropic range), and tended rapidly to infinity at large values of k_n (the isotropic range). It was chosen to be of the simple form:

$$G(k) = \begin{cases} 1 & k < k^* \\ 1 + [\gamma(k - k^*)]^2 & k \geq k^* \end{cases} \tag{81}$$

where k^* and γ are constant parameters.

3. Time Development of the Model Flow.

In order to satisfy condition II, the phases and wave numbers must be made functions of time, Instead of equation (39) we use the velocity fluctuation field in the generalized form,

Reproduced with permission of the copyright owner. Further reproduction prohibited without permission.

$$\underline{v}(\underline{x},t) = \sum_{n=1}^{N} T(\underline{k}_n, t_n) \frac{\underline{k}_n'}{k_n} \times \left\{ \alpha_n \cos(\underline{k}_n' \cdot \underline{x}) + \beta_n \sin(\underline{k}_n' \cdot \underline{x}) \right\} \qquad (82)$$

where $\underline{k}_n' = \underline{k}_n - \frac{dU}{dx_2} t_n k_{n_1} \underline{i}_2$ ($\underline{i}_m$ is a unit vector in the direction of k_{n_m}). Thus the fluctuation field is continually being strained by the mean velocity field. A physical space example of the straining of two modes in this manner is shown in figure 6.

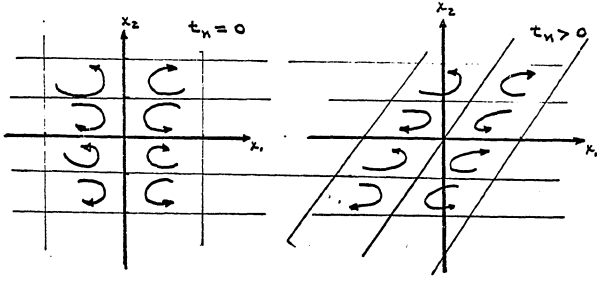

Figure 6.

Reproduced with permission of the copyright owner. Further reproduction prohibited without permission.

To see that condition II is satisfied, let $\overline{(\ )}^{\alpha}$ again represent an average over $\underset{\sim}{\alpha}_n$, $\underset{\sim}{\beta}_n$. Then (using the conditions already mentioned for $\underset{\sim}{\alpha}_n$ and $\underset{\sim}{\beta}_n$),

$$\overline{u_i'(\underset{\sim}{x},t)\,u_j'(\underset{\sim}{x}+\underset{\sim}{r},t+\tau)}^{\alpha} =$$

$$\sum_{n=1}^{N} T^2(\underset{\sim}{k}_n,t_n)\,\epsilon_{ilm}\epsilon_{jpq}\,\frac{k_{nq}'k_{np}'}{k_n^2}\langle\alpha_{n_m}\alpha_{n_q}\rangle\cos\left[k_1\left(r_1-\frac{dU_1}{dx_2}\tau x_2\right)+k_2r_2+k_3r_3+k_1\frac{dU_1}{dx_2}r_2(t_n+\tau)\right]. \quad (83)$$

Note that r_1 and x_2 appear only in the term $\left(r_1-\frac{dU_1}{dx_2}\tau x_2\right)$. Thus, averaging the t_{0_n} (which eliminates the t_n dependence) and then the $\underset{\sim}{k}_n$ will produce a function of the form $\mathcal{F}\left(r_1-\frac{dU_1}{dx_2}x_2\tau, r_2, r_3, \tau\right)$, as desired.

Because of the continual straining of the fluctuation field by the mean field, energy is transferred from lower to higher wave numbers, and so a source of energy is needed to keep the process stationary.

To provide a source of energy, new modes were continually fed onto the field in a stationary, random, Poisson manner. Thus, for example, at time t_{0_n}, the nth mode would be "injected" onto the field, i.e., it would be turned on. It would then increase in amplitude from zero, and finally decrease and decay to zero (governed by the function $T(\underset{\sim}{k}_n,t_n)$), all the while being strained by the mean field. By use of an exponentially distributed time between "injections", $t_{0_{n+1}}-t_{0_n}$, with probability density $\Gamma\exp(-\Gamma t)$, Γ^{-1} being the constant average time between injections, the stationary Poisson process was achieved. In any one realization, modes were injected into the field until a stationary

Reproduced with permission of the copyright owner. Further reproduction prohibited without permission.

process was established, and then dispersion was allowed to begin.

The modal time development function $T(\cdot,\cdot)$ was arbitrarily chosen to be of the form

$$T(\underline{k}_n, t_n) \equiv \begin{cases} 0, & t < t_{0_n} \\ \left[t_n / \tau(\underline{k}_n)\right]^2 \exp\left[-t_n / 2\tau(\underline{k}_n)\right], & t_{0_n} \le t \le t_{0_n} + \sigma_{T_M} \\ 0, & t > t_{0_n} + \sigma_{T_M} \end{cases} \tag{84}$$

σ_{T_M} is the maximum time interval that any mode is retained on the field. After σ_{T_M}, it is discarded; its magnitude has dropped below a predetermined minimum cutoff value. The "eddy circulation time", $\tau(\underline{k}_n)$, is defined by

$$\tau(\underline{k}_n)^{-1} \equiv \omega\left(1 + \sigma k_n\right), \tag{85}$$

ω and σ being constant, positive parameters. $\tau(\underline{k}_n)$ corresponds very roughly to the spectral time characteristic of inertial mechanisms in real turbulence.

This functional form was chosen for $T(\cdot,\cdot)$ because (i) it has the required qualitative properties of initiation at a predetermined instant (t_{0_n}), growth, and decay; (ii) it is of analytical form simple enough to permit some analysis to be done without a machine; (iii) it is of class C^1 at t_{0_n} (so that the velocity and acceleration fields are continuous functions of time). The "eddy circulation time" was chosen as such because it is a simple form, is bounded as $k_n \to 0$, and has the property that the time scale decreases with increasing wave number (a well

Reproduced with permission of the copyright owner. Further reproduction prohibited without permission.

known property of turbulent flows (for example, see Batchelor 1953).

This general manner of modeling the time development of the flow is a main difference between this model and Kraichnan's (see section II.C). It holds the flow stationary while at the same time continually straining it. It also includes crude modeling of turbulent energy "production" from the mean flow (the mode injection), redistribution among the different wave numbers due to mean flow inertial effects, and viscous dissipation.

To compute averages with respect to t_{o_n}, it will be assumed that the modes are not ordered monotonically with time (i.e., if $n > m$ then $t_{o_n} > t_{o_m}$ does not necessarily follow), but are ordered randomly in time. This assumption implies a knowledge of less information than is actually known. Thus, the calculations will not contain quite as much information as possible. From the assumption, it also follows that t_n is uniformly distributed, i.e.,

$$p_{t_n}(\mu) = \frac{1}{\sigma_M} \quad , \quad 0 < \mu < \sigma_M \, , \tag{86}$$

and also that N and t_n are statistically independent. Thus

$$F(k_n) \equiv \overline{T^2(\underline{k}_n, t_n)}^{t_o} \doteq \frac{1}{\sigma_M} \int_0^{\sigma_M} T^2(\underline{k}_n, t_n)\, d\mu$$

$$\doteq \int_0^{\infty} \frac{\left[\mu/\tau(k_n)\right]^4 \exp\left[-\mu/\tau(k_n)\right]}{\sigma_M} = \frac{4!\,\tau(k_n)}{\sigma_M} \, .$$

Reproduced with permission of the copyright owner. Further reproduction prohibited without permission.

So $$F(K_n) \doteq \frac{4!}{\omega \tau_M (1+\sigma K_n)^4} \,. \tag{87}$$

Similarly,

$$F_m(K_n) \equiv \overline{t_n^m T^2(\underline{K}_n, t_n)}^{t_o} \doteq \frac{(m+2)!}{\omega \tau_m (1+\sigma K_n)} \frac{1}{\omega^m (1+\sigma K_n)^m} \tag{88}$$

4. Choice of the Statistical Properties of the $\underline{K}_n$

The choice of the probability density of the $\underline{K}_n$ is influenced by the third of the six conditions mentioned at the beginning of this section. This condition implies that $Q_{13}(o, o, r_3, o) = Q_{23}(o, o, r_3, o) = o$. Now

$$\overline{u_i'(\underline{x}, t) u_j'(\underline{x}+\underline{r}, \underline{i}_3, t)}^{\alpha} = \sum_{n=1}^{N} T^2(\underline{K}_n, t_n) \hat{\epsilon}_{ilm} \hat{\epsilon}_{jpq} \frac{K_n' K_n'}{K_n^2} \hat{u}_{lnq} \cos(K_n r_3), \tag{89}$$

so $$\overline{u_1'(\underline{x}, t) u_3'(\underline{x}+\underline{r}, \underline{i}_3, t)}^{\alpha} = \sum_{n=1}^{N} T^2(\underline{K}_n, t_n) \left\{ \frac{K_{n_1}' K_{n_3}'}{K_n^2} \hat{u}_{22} + \frac{K_{n_2}'^2}{K_n^2} \hat{u}_{13} \right.$$

$$\left. - \frac{K_{n_1}' K_{n_2}'}{K_n^2} \hat{u}_{23} - \frac{K_{n_2}' K_{n_3}'}{K_n^2} \hat{u}_{12} \right\} \cos(K_{n_3} r_3) = \sum_{n=1}^{N} T^2(\underline{K}_n, t_n) \left\{ K_{n_1} K_{n_3} \hat{u}_{22} + \left[K_{n_2}^2 \right.\right.$$

$$-2 \frac{dU}{dk_2} t_n K_{n_1} K_{n_2} + \left(\frac{dU}{dk_2}\right)^2 t_n^2 K_{n_1}^2 \Big] \frac{\hat{u}_{13}}{K_n^2} - \left[K_{n_1} k_{n_2} - \frac{dU}{dk_2} t_n K_{n_1}^2 \right] \frac{\hat{u}_{23}}{K_n^2}$$

$$\left. - \left[K_{n_2} K_{n_3} - \frac{dU}{dk_2} t_n K_{n_1} K_{n_3} \right] \frac{\hat{u}_{12}}{K_n^2} \right\} \cos(k_{n_3} r_3), \tag{90}$$

using $\underline{K}_n' = \underline{K}_n - \frac{dU}{dx_2} t_n K_{n_1} \underline{i}_2$. Averaging with respect to t_{o_A} gives [with $c_i = K_{n_i} / K_n$, and equation (88)],

$$\overline{u_1'(\underline{x}_3, t) u_3'(\underline{x}+\underline{r}_3 \underline{i}_3, t)}^{t_o} \overset{\alpha}{=} \frac{4! \bar{N}}{\omega \tau_M (1+\sigma K_n)} \left\{ c_1 c_3 \hat{u}_{22} - \left[c_2^2 - 10 \left(\frac{1}{\omega} \frac{dU}{dx_2}\right) \frac{c_1 c_2}{(1+\sigma K_n)} \right.\right. \tag{91}$$

$$\left. + 30 \frac{\left(\frac{1}{\omega} \frac{dU}{dx_2}\right)^2 c_2^2}{(1+\sigma K_n)^2} \right] \hat{u}_{13} - \left[c_2 c_3 - 5 \frac{\left(\frac{1}{\omega} \frac{dU}{dx_2}\right) c_1^2}{(1+\sigma K_n)} \right] \hat{u}_{32} - \left[c_2 c_3 - 5 \frac{\left(\frac{1}{\omega} \frac{dU}{dx_2}\right) c_1 c_3}{(1+\sigma K_n)} \right] \hat{u}_{12} \Big\} \cos(K_{n_3} r_3).$$

Reproduced with permission of the copyright owner. Further reproduction prohibited without permission.

Finally, with $\Lambda = \frac{1}{\omega}\frac{dU_1}{dx_2}$, averaging with respect to $\underline{K}_n$ gives

$$\langle u_1'(\underline{x},t)u_3'(\underline{x}+\underline{r}\underline{i}_3,t)\rangle = \frac{4!\,\bar{N}}{\omega\tau_m}\int_{\underline{K}}\Big\{c_1c_3\hat{u}_{22}+\Big[c_2^2-10\frac{\Lambda c_1c_2}{(1+\sigma K)}+30\frac{\Lambda^2c_2^2}{(1+\sigma K)^2}\Big]\hat{u}_{13}$$
$$-\Big[c_1c_2-5\frac{\Lambda c_1^2}{(1+\sigma K)}\Big]\hat{u}_{32}-\Big[c_2c_3-5\frac{\Lambda c_1c_3}{(1+\sigma K)}\Big]\hat{u}_{12}\Big\}\frac{p_{\underline{K}_n}(\underline{K})\cos(k_3r_3)}{(1+\sigma K)}\,d\underline{K}. \tag{92}$$

Similarly,

$$\langle u_2'(\underline{x},t)u_3'(\underline{x}+\underline{r}\underline{i}_3,t)\rangle = \frac{4!\,\bar{N}}{\omega\tau_m}\int_{\underline{K}}\Big\{\Big[c_2c_3-5\frac{\Lambda c_1c_3}{(1+\sigma K)}\Big]\hat{u}_{11}+c_1^2\hat{u}_{23}$$
$$-c_1c_2\hat{u}_{12}-\Big[c_1c_2-5\frac{\Lambda c_1^2}{(1+\sigma K)}\Big]\hat{u}_{31}\Big\}\frac{p_{\underline{K}_n}(\underline{K})\cos(k_3r_3)}{(1+\sigma K)}\,d\underline{K}. \tag{93}$$

As a sufficient condition for these two integrals to be zero, we require that each term in the coefficients be zero. Thus

$$\hat{u}_{13} = \hat{u}_{23} = 0 \tag{94}$$

(since they both multiply positive definite quantities), and

$$\int_{\underline{K}}\frac{k_1k_3}{k^2}H_1(k)\,p_{\underline{K}_n}(\underline{K})\cos(k_3r_3)\,d\underline{K} = 0 \tag{95}$$

$$\int_{\underline{K}}\frac{k_2k_3}{k^2}H_2(k)\,p_{\underline{K}_n}(\underline{K})\cos(k_3r_3)\,d\underline{K} = 0 \tag{96}$$

Here $H_1(K)$ and $H_2(K)$ represent several different functions, all of which depend on K alone.

The conditions given by equations (94) have already been taken into account in the model (see equation (74)). Conditions given by (92) and (93) will be satisfied if $p_{\underline{K}_n}(\underline{K})$ is such that

Reproduced with permission of the copyright owner. Further reproduction prohibited without permission.

$$\underset{\underline{K}_n}{\beta}(K_1, K_2, K_3) = \underset{\underline{K}_n}{\beta}(K_1, K_2, -K_3). \tag{97}$$

To see this, consider

$$\int_{-\infty}^{\infty}\int_{-\infty}^{\infty}\int_{-\infty}^{\infty} \frac{K_1 K_3}{k^2} H_1(k) \underset{\underline{K}_n}{\beta}(K_1, K_2, K_3) \cos(k_3 r_3)\, dK_1\, dK_2\, dK_3$$

$$= \underset{K_3 \to -K_3}{\int_{-\infty}^{\infty}\int_{-\infty}^{\infty}\int_{-\infty}^{\infty}} \frac{K_1(-K_3)}{k^2} H_1(k) \underset{\underline{K}_n}{\beta}(K_1, K_2, -K_3) \cos(-k_3 r_3)\, dK_1\, dK_2\, d(-K_3)$$

$$= -\int_{-\infty}^{\infty}\int_{-\infty}^{\infty}\int_{-\infty}^{\infty} \frac{K_1 K_3}{k^2} H_1(k) \underset{\underline{K}_n}{\beta}(K_1, K_2, K_3) \cos(k_3 r_3)\, dK_1\, dK_2\, dK_3 .$$

So $$\int_{-\infty}^{\infty}\int_{-\infty}^{\infty}\int_{-\infty}^{\infty} \frac{K_1 K_3}{k^2} H_1(k) \underset{\underline{K}_n}{\beta}(K_1, K_2, K_3) \cos(k_3 r_3)\, dK_1\, dK_2\, dK_3 = 0.$$

Similarly, $$\int_{-\infty}^{\infty}\int_{-\infty}^{\infty}\int_{-\infty}^{\infty} \frac{K_2 K_3}{k^2} H_2(k) \underset{\underline{K}_n}{\beta}(K_1, K_2, K_3) \cos(k_3 r_3)\, dK_1\, dK_2\, dK_3 = 0.$$

In order to determine the implications of condition V, consider the following expressions, which are obtained in the same manner as equations (92) and (93). [For example, using the Fourier series expression for $u_1'(\underline{x},t)\, u_1'(\underline{x}+\underline{r},t)$, average the $(\underline{x}_n, \beta_n)$ then the t_{0_n} , and finally the $\underline{K}_n$.]

$$R_{11}(\underline{r},0) = \frac{4!\,\bar{N}}{\omega^2 \tau_M} \int_{\underline{K}} \left\{ c_3^2 \hat{u}_{22} + \left[c_2^2 - 10\, \frac{\Lambda c_1 c_2}{(1+\sigma K)} + 30\, \frac{\Lambda^2 c_1^2}{(1+\sigma K)^2} \right] \hat{u}_{33} \right\} \frac{\underset{\underline{K}_n}{\beta}(\underline{K}) \cos(\underline{K}\cdot\underline{r})}{(1+\sigma K)}\, d\underline{K} \tag{98}$$

$$R_{12}(\underline{r},0) = \frac{4!\,\bar{N}}{\omega^2 \tau_M} \int_{\underline{K}} \left\{ \left[c_1 c_2 - 5\, \frac{\Lambda c_1^2}{(1+\sigma K)} \right] \hat{u}_{33} + c_3^2 \hat{u}_{12} \right\} \frac{\underset{\underline{K}_n}{\beta}(\underline{K}) \cos(\underline{K}\cdot\underline{r})}{(1+\sigma K)}\, d\underline{K} \tag{99}$$

Reproduced with permission of the copyright owner. Further reproduction prohibited without permission.

$$\mathcal{R}_{13}(r,0) = \frac{4!\,\bar{N}}{\omega\tau_M}\int_{\underline{K}}\left\{c_1c_3\hat{u}_{22} - \left[c_2c_3 - 5\frac{\Lambda c_1c_3}{(1+\sigma K)}\right]\hat{u}_{12}\right\}\frac{\hat{p}_{\underline{K}_n}(\underline{K})\cos(\underline{K}\cdot\underline{r})}{(1+\sigma K)}\,d\underline{K} \tag{100}$$

$$\mathcal{R}_{22}(r,0) = \frac{4!\,\bar{N}}{\omega\tau_M}\int_{\underline{K}}\left[c_1^2\hat{u}_{33} + c_3^2\hat{u}_{11}\right]\frac{\hat{p}_{\underline{K}_n}(\underline{K})\cos(\underline{K}\cdot\underline{r})}{(1+\sigma K)}\,d\underline{K} \tag{101}$$

$$\mathcal{R}_{23}(r,0) = \frac{4!\,\bar{N}}{\omega\tau_M}\int_{\underline{K}}\left\{\left[c_2c_3 - 5\frac{\Lambda c_1c_3}{(1+\sigma K)}\right]\hat{u}_{11} - c_1c_3\hat{u}_{12}\right\}\frac{\hat{p}_{\underline{K}_n}(\underline{K})\cos(\underline{K}\cdot\underline{r})}{(1+\sigma K)}\,d\underline{K} \tag{102}$$

$$\mathcal{R}_{33}(r,0) = \frac{4!\,\bar{N}}{\omega\tau_M}\int_{\underline{K}}\left\{\left[c_2^2 - 10\frac{\Lambda c_1c_2}{(1+\sigma K)} + 30\frac{\Lambda^2c_1^2}{(1+\sigma K)^2}\right]\hat{u}_{11} + c_1^2\hat{u}_{22} - 2\left[c_1c_2 - 5\frac{\Lambda c_1^2}{(1+\sigma K)}\right]\hat{u}_{12}\right\}\frac{\hat{p}_{\underline{K}_n}(\underline{K})\cos(\underline{K}\cdot\underline{r})}{(1+\sigma K)}\,d\underline{K} \tag{103}$$

(Again $c_i = \frac{K_i}{K}$, $\Lambda = \frac{1}{\omega}\frac{dU}{dx_2}$.)

It can be seen from these expressions that the results of condition V -- equations (68) to (73) -- are satisfied if $\hat{p}_{\underline{K}_n}(\underline{K})$ is selected so that equation (97) holds. For example, assuming that $\hat{p}_{\underline{K}_n}(\underline{K})$ satisfies (97), then

$$\mathcal{R}_{22}(r_1,r_2,r_3,0) = \frac{4!\,\bar{N}}{\omega\tau_M}\int_{\underline{K}}\left[\frac{K_1^2}{K^2}\hat{u}_{33} + \frac{K_3^2}{K^2}\hat{u}_{11}\right]\frac{\hat{p}_{\underline{K}_n}(K_1,K_2,K_3)\cos(K_1r_1+K_2r_2+K_3r_3)}{(1+\sigma K)}\,d\underline{K}$$

$$= \frac{4!\,\bar{N}}{\omega\tau_M}\int_{-\infty}^{\infty}\int_{-\infty}^{\infty}\int_{-\infty}^{\infty}\left[\frac{\lambda_1^2}{\lambda^2}\hat{u}_{33} + \frac{(\lambda_3)_2^2}{\lambda^2}\hat{u}_{11}\right]\frac{\hat{p}_{\underline{K}_n}(\lambda_1,\lambda_2,\lambda_3)\cos(\lambda_1r_1+\lambda_2r_2-\lambda_3r_3)}{(1+\sigma\lambda)}\,d\lambda_1\,d\lambda_2(-d\lambda_3)$$

$$(K_1,K_2,K_3)\to(\lambda_1,\lambda_2,-\lambda_3)$$

$$= \frac{4!\,\bar{N}}{\omega\tau_M}\int_{-\infty}^{\infty}\int_{-\infty}^{\infty}\int_{-\infty}^{\infty}\left[\frac{\lambda_1^2}{\lambda^2}\hat{u}_{33} + \frac{\lambda_3^2}{\lambda^2}\hat{u}_{11}\right]\frac{\hat{p}_{\underline{K}_n}(\lambda_1,\lambda_2,\lambda_3)\cos[\lambda_1r_1+\lambda_2r_2+\lambda_3(-r_3)]}{(1+\sigma\lambda)}\,d\lambda_1\,d\lambda_2\,d\lambda_3$$

$$= \mathcal{R}_{22}(r_1,r_2,-r_3,0).$$

Reproduced with permission of the copyright owner. Further reproduction prohibited without permission.

In a similar manner, it can be shown that (69) to (73) hold if (97) is satisfied. So both condition IV and condition V lead to equation (97).

In order to simplify the modelling of anisotropy at small wave numbers, the density of $\underset{\sim}{K}_h$ in polar form is used. With the transformation $(k_1,k_2,k_3) \longleftrightarrow (k,\theta,\phi)$ given by

$$k_1 = k\cos\phi \qquad k = (k_1^2 + k_2^2 + k_3^2)^{1/2}$$

$$k_2 = k\sin\phi\sin\theta \qquad \phi = \tan^{-1}\left\{\frac{(k_3^2+k_2^2)^{1/2}}{k_1}\right\}$$

$$k_3 = k\sin\phi\cos\theta \qquad \theta = \tan^{-1}\left(\frac{k_2}{k_3}\right)$$

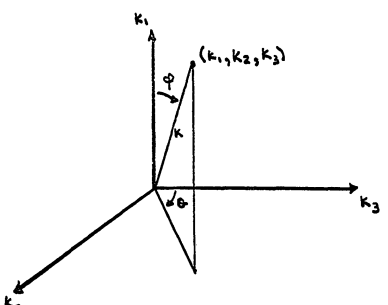

Figure 7.

elementary probability theory tells us that the densities of

(k_1,k_2,k_3) $\left[\underset{k_1k_2k_3}{\rho}(\lambda_1,\lambda_2,\lambda_3)\right]$ and (k,θ,ϕ) $\left[\underset{k\theta\phi}{\rho}(\lambda,\chi,\psi)\right]$

Reproduced with permission of the copyright owner. Further reproduction prohibited without permission.

are related by

$$p_{K_1K_2K_3}(\lambda_1,\lambda_2,\lambda_3) =$$

$$p_{K\Theta\phi}\left[(\lambda_1^2+\lambda_2^2+\lambda_3^2)^{1/2}, \tan^{-1}\left(\frac{K_2}{K_3}\right), \tan^{-1}\left\{\frac{(K_2^2+K_3^2)^{1/2}}{K_1}\right\}\right] \frac{1}{(K_1^2+K_2^2+K_3^2)^{1/2}(K_2^2+K_3^2)^{1/2}} \qquad (104)$$

Now $p_{K\Theta\phi}(\lambda,\chi,\psi) = p_{\Theta\phi}(\chi,\psi/K=\lambda)\, p_K(\lambda)$, where $p_{\Theta\phi}(\chi,\psi/K=\lambda)$ is the probability density of (Θ,ϕ) conditional upon $K=\lambda$.

With local isotropy, the probability density of $\underset{\sim}{K}_n'$ (say $p_{K_{n_1}K_{n_2}K_{n_3}}$) at any point in time must tend towards an isotropic limit as $K_n' \longrightarrow \infty$. However, because the "eddy circulation time" decreases as $K_n' \longrightarrow \infty$, the effect of the shear also decreases, since the mean velocity has less time to strain the "eddy". So

$$p_{K_{n_1}'K_{n_2}'K_{n_3}'} \longrightarrow p_{K_{n_1}K_{n_2}K_{n_3}}$$

for large K_n' (or K_n). Thus local isotropy will be produced by requiring that

$$p_{\Theta_n\phi_n}(\chi,\psi/k_n=\lambda) \longrightarrow \text{(isotropic form) as } \lambda\to\infty. \qquad (105)$$

The isotropic form of $p_{\Theta_n\phi_n}(\chi,\psi/k_n=\lambda)$ is

$$p_{\Theta_n\phi_n}(\chi,\psi/K_n=\lambda)\Big|_{\text{ISOTROPIC}} = \frac{\sin\psi}{4\pi} \qquad (106)$$

Reproduced with permission of the copyright owner. Further reproduction prohibited without permission.

With conditions given by (97) and (105) in mind, $\rho_{\theta_n \varphi_n}(\chi, \psi / k_n = \lambda)$ is chosen to be of the form:

$$\rho_{\theta_n \varphi_n}(\chi, \psi / k_n = \lambda) = C \frac{\sin \psi}{(1 + A \cos 2\psi)} \cdot \frac{\rho^*}{\pi} \frac{1}{[(1+\beta^2) + (1-\beta^2)\cos 2\chi]} \tag{107}$$

where, in order to normalize $\rho_{\theta_n \varphi_n}$,

$$C = \frac{\frac{1}{2}\sqrt{2A(1-A)}}{\tan^{-1}\left\{\frac{\sqrt{2A(1-A)}}{1-A}\right\}} \tag{108}$$

Also $A = \frac{B}{G(\lambda)}$ and $\rho^* = 1 + \frac{R}{G(\lambda)}$, (109)

where $G(k)$ has been previously defined, and B and R are constant parameters. Note that $\rho_{k_1 k_2 k_3}(\lambda_1, \lambda_2, \lambda_3)$

$$= C \frac{\sin\left\{\tan^{-1}\left[\frac{(\lambda_2^2+\lambda_3^2)^{1/2}}{\lambda_1}\right]\right\}}{1 + A\cos\left\{2\tan^{-1}\left[\frac{(\lambda_2^2+\lambda_3^2)^{1/2}}{\lambda_1}\right]\right\}} \cdot \frac{\rho^*}{\pi} \frac{\rho_{k_n}(\lambda) \frac{1}{\lambda} \frac{1}{(\lambda_2^2+\lambda_3^2)^{1/2}}}{[(1+\beta^2)+(1-\beta^2)\cos\{2\tan^{-1}(\frac{\lambda_2}{\lambda_3})\}}$$

$$= C \frac{\sin\left\{\tan^{-1}\left[\frac{(\lambda_2^2+(-\lambda_3)^2)^{1/2}}{\lambda_1}\right]\right\}}{1 + A\cos\left\{2\tan^{-1}\left[\frac{(\lambda_2^2+(-\lambda_3)^2)^{1/2}}{\lambda_1}\right]\right\}} \cdot \frac{\rho^*}{\pi} \frac{\rho_{k_n}(\lambda) \frac{1}{\lambda} \frac{1}{(\lambda_2^2+(-\lambda_3)^2)^{1/2}}}{[(1+\beta^2)+(1-\beta^2)\cos\{2\tan^{-1}[\frac{\lambda_2}{(-\lambda_3)}]\}}$$

$$= \rho_{k_n, k_{n2}, k_{n3}}(\lambda_1, \lambda_2, -\lambda_3) ,$$

so that the condition given by (97) is satisfied. Also, since $G(\lambda) \to \infty$ as $K \to \infty$, $\rho_{\theta_n \varphi_n}(\chi, \psi / k_n = \lambda)$ tends to its isotropic form as $\lambda \to \infty$.

For simplicity in understanding the density of (θ_n, φ_n), it might have been better to choose (θ_n, φ_n) with constant

Reproduced with permission of the copyright owner. Further reproduction prohibited without permission.

probability surfaces of elliptical form, i.e.,

$$P_{\theta_n \phi_n}(\chi, \psi / K_n = \lambda) = \frac{a}{\frac{\cos^2\psi}{a_1^2} + \sin^2\psi\left[\frac{\sin^2\chi}{a_2^2} + \frac{\cos^2\chi}{a_3^2}\right]} .$$

However, the expression chosen above (equation (107)), which is of a similar form, simplified the non-machine analysis.

The constant probability contours for K_n look qualitatively like those in figure 8.

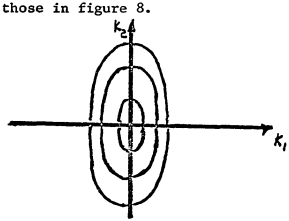

Figure 8.

The effect of the shear qualitatively is to tilt the ovals (figure 9):

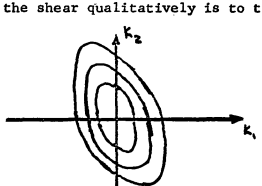

Figure 9.

Reproduced with permission of the copyright owner. Further reproduction prohibited without permission.

Thus the velocity isocorrelation curves should be of the proper qualitative form.

The density $p_{k_n}(\lambda)$ was chosen as

$$p_{k_n}(\lambda) = \begin{cases} K \dfrac{(\xi\lambda)^2}{(1+\xi\lambda)^3} & \lambda \le K_M \\ 0 & \lambda > K_M \end{cases} \qquad K = \frac{\xi}{\ln(1+\xi K_M) - \dfrac{\xi K_M (1+\frac{3}{2}\xi K_M)}{(1+\xi K_M)^2}} \tag{110}$$

where K_M and ξ are fixed parameters.

ξ^{-1} is a characteristic (large) scale of the field. The function $p_{k_n}(\lambda) F(\lambda)$ peaks at $\lambda = \xi^{-1}$. K_M, the high wave number cutoff, is selected with the following restrictions in mind. In the numerical integration scheme the time step size must be much less than the inverse of the highest frequencies in the flow. But increasing K_M increases the highest frequencies in the flow [through $\tau(k_n)^{-1} = \omega(1+\sigma k_n)$], forcing a decrease in the integration step size, thus increasing the required computer time. However, larger K_M corresponds to a better modelling of the flow; higher Reynolds numbers can be modelled through greater separations between small and large scales.

Because computer time (cost) was a limiting factor, and because a simple form for p_{k_n} was necessary for computational purposes, it was decided to model the spectrum only out to the beginning of the dissipation range, and cut the spectrum off there. Also K_M was chosen to be 10, so that the model flow was necessarily of low turbulent Reynolds number. In the shear case also (see equa-

Reproduced with permission of the copyright owner. Further reproduction prohibited without permission.

tion (53) for the isotropic expression), the energy density is proportional to $\phi_{K_n}(\lambda)F(\lambda)$, or $\frac{(\xi\lambda)^2}{(1+\xi\lambda)^3(1+\sigma\lambda)}$, which varies as λ^{-2} for large λ.

C. The Isotropic Turbulence Model

This started as an investigation of dispersion in shear flow, but it was soon realized that simulations in isotropic turbulence were needed. One reason was that it provided a basis for comparison, to obtain the effects of the shear alone. Also any spurious effects due to model defects should hopefully appear in both models, and so be recognized for what they were. With these reasons in mind, and to eliminate any further effects that might arise because of differences in the models, an isotropic model was developed as nearly as possible like the shear flow model. The main differences were (i) energy was fed into the isotropic model isotropically at all scales [i.e., $\phi_{\theta_n}\phi_{\gamma_n}(\chi,\psi/K_n=\lambda)$ was of isotropic form for all λ] whereas, as mentioned, energy was fed into the shear flow anisotropically at larger scales; (ii) the mean strain rate was omitted in the isotropic case.

For the isotropic field the time development function T and the injection process (t_{o_n}) were chosen to be exactly the same as in the shear flow case.

The $\underset{\sim}{\alpha}_n$'s and β_n's were also chosen in a similar manner, but now they were of isotropic form (see equations (54) and (55)) for all λ, i.e.,

$$\hat{a}_{ij} = \delta_{ij}/\sqrt{N} \tag{111}$$

Reproduced with permission of the copyright owner. Further reproduction prohibited without permission.

$$\dot{v}_{ij} = 0. \tag{112}$$

$p_{\kappa_n}(\lambda)$ was chosen <u>exactly</u> the same as in the shear flow case, while $p_{\theta_n \phi_n}(\chi, \psi / \kappa_n = \lambda)$ was of the isotropic form

$$p_{\theta_n \phi_n}(\chi, \psi / \kappa_n = \lambda) = \frac{\sin \psi}{4\pi} . \tag{113}$$

Reproduced with permission of the copyright owner. Further reproduction prohibited without permission.

IV. A DISCUSSION OF THE EQUATIONS OF MOTION FOR "SMALL" SPHERICAL PARTICLES

A. Introduction

A rather detailed form of the equations of translational motion for "small" spherical particles moving at vanishingly small Reynolds-number in a general fluid motion has been given by Corrsin and Lumley (1956). The application to turbulent fluid, along with various conditions under which the equations in their various forms may be applied, were presented at some length by Lumley (1957, chapter 2). The following analysis is to fill in several gaps in Lumley's analysis. Thus the procedure is similar to his. The technique for deriving the equations was first used by Tchen (1947).

B. Development of a Force Balance

Assume that $\underset{\sim}{u}(\underset{\sim}{x},t)$ is a turbulent velocity field satisfying the constant density Navier-Stokes and continuity equations,

$$\frac{\partial}{\partial t}\underset{\sim}{u} + (\underset{\sim}{u}\cdot\nabla)\underset{\sim}{u} = -\frac{1}{\rho}\nabla p + \nu\nabla^2\underset{\sim}{u} \tag{1}$$

$$\nabla\cdot\underset{\sim}{u} = 0 \tag{2}$$

and initial and boundary conditions appropriate to the problem under discussion. If a "small" spherical particle of radius r is placed on this

Reproduced with permission of the copyright owner. Further reproduction prohibited without permission.

field, the resulting velocity field $\bar{\underset{\sim}{u}}(\underset{\sim}{x},t)$ will then differ from $\underset{\sim}{u}(\underset{\sim}{x},t)$ by an amount $\underset{\sim}{u}^*(\underset{\sim}{x},t)$, say:

$$\bar{\underset{\sim}{u}}(\underset{\sim}{x},t) \equiv \underset{\sim}{u}(\underset{\sim}{x},t) + \underset{\sim}{u}^*(\underset{\sim}{x},t) \tag{3}$$

where $\bar{\underset{\sim}{u}}(\underset{\sim}{x},t)$ also satisfies the Navier-Stokes equations

$$\frac{\partial}{\partial t}\bar{\underset{\sim}{u}} + (\bar{\underset{\sim}{u}}\cdot\nabla)\bar{\underset{\sim}{u}} = -\frac{1}{\rho}\nabla\bar{p} + \nu\nabla^2\bar{\underset{\sim}{u}} \tag{4}$$

$$\nabla\cdot\bar{\underset{\sim}{u}} = 0 \tag{5}$$

In addition to possible initial and boundary conditions satisfied by $\underset{\sim}{u}$, $\bar{\underset{\sim}{u}}$ also satisfies the boundary condition (where $\underset{\sim}{x}_s$ is any point on the surface of the sphere)

$$\bar{\underset{\sim}{u}}(\underset{\sim}{x}_s,t) = \underset{\sim}{V}(t) + \underset{\sim}{\Omega}(t)\times\left\{\underset{\sim}{x}_s - \underset{\sim}{Y}(t)\right\}, \tag{6}$$

where $\underset{\sim}{V}(t)$ is the velocity of the sphere, $\underset{\sim}{\Omega}(t)$ its angular velocity, and $\underset{\sim}{Y}(t)$ the position of its center. Note that, if $\underset{\sim}{b}$ is the initial position of the center of the sphere, i.e., $\underset{\sim}{b} = \underset{\sim}{Y}(t_0)$ then $\underset{\sim}{Y}(t)$ satisfies

$$\underset{\sim}{Y}(t) = \underset{\sim}{b} + \int_{t_0}^{t} \underset{\sim}{V}(t')\,dt'. \tag{7}$$

Reproduced with permission of the copyright owner. Further reproduction prohibited without permission.

Since the particle is assumed to be "small", its disturbance $\underset{\sim}{u}^*$ will (hopefully) also be small in some sense, to be clarified in the following analysis.

To obtain the equations for $\underset{\sim}{u}^*$, substitute equations (3) into (4) and (5), and subtract equations (1) and (2) from the result of (4) and (5) respectively. This gives:

$$\frac{\partial}{\partial t}\underset{\sim}{u}^* + (\underset{\sim}{u}\cdot\nabla)\underset{\sim}{u}^* + (\underset{\sim}{u}^*\cdot\nabla)\underset{\sim}{u} + (\underset{\sim}{u}^*\cdot\nabla)\underset{\sim}{u}^* = -\frac{1}{\rho}\nabla p^* + \nu\nabla^2\underset{\sim}{u}^* \qquad (8)$$

$$\nabla\cdot\underset{\sim}{u}^* = 0 \qquad (9)$$

where p^* is defined by

$$\bar{p}(\underset{\sim}{x},t) = p(\underset{\sim}{x},t) + p^*(\underset{\sim}{x},t) . \qquad (10)$$

We assume that "far" from the particle (i.e., a distance large compared to the sphere's radius r), $\bar{\underset{\sim}{u}} \to \underset{\sim}{u}$ and $\bar{p} \to p$, so that, using (3) and (10), $\underset{\sim}{u}^*$ and p^* must satisfy the boundary conditions

$$\underset{\sim}{u}^* \longrightarrow \underset{\sim}{0} \qquad (11)$$

"far"from the particle

$$p^* \longrightarrow 0 \qquad (12)$$

Also, combining (3) and (6) gives

Reproduced with permission of the copyright owner. Further reproduction prohibited without permission.

$$\underset{\sim}{u}^{*}(\underset{\sim}{\chi}_s,t) = \underset{\sim}{V}(t) + \underset{\sim}{\Omega}(t) \times \left\{ \underset{\sim}{\chi}_s - \underset{\sim}{Y}(t) \right\} - \underset{\sim}{u}(\underset{\sim}{\chi}_s,t) \qquad (13)$$

Next the equations are transformed to a coordinate system in which the undisturbed fluid $\underset{\sim}{u}$ is at rest in the vicinity of the particle. (The problem is then set up in the same manner as the Basset-Boussinesq-Oseen problem (Oseen 1927), and a force balance on the sphere can be more easily computed.) The transformation $(\underset{\sim}{\chi},t) \longrightarrow (\underset{\sim}{\xi},t)$ which accomplishes this is:

$$\underset{\sim}{\chi} = \underset{\sim}{\xi} + \int_{t_0}^{t} \underset{\sim}{u}\left[\underset{\sim}{Y}(t'),t' \right] dt' \qquad (14)$$
$$t = t$$

where $\underset{\sim}{Y}(t)$ again is the position (of the center) of the particle [in the coordinate system $(\underset{\sim}{\chi},t)$] at time t , and t_0 is some past time at which the two coordinate systems are coincident. (See figure 10.)

Writing any quantity in the new coordinate system, corresponding to the quantity $f(\underset{\sim}{\chi},t)$ in the original system, as $\hat{f}(\underset{\sim}{\xi},t)$, the following relationships exist:

$$\underset{\sim}{u}(\underset{\sim}{\chi},t) = \hat{\underset{\sim}{u}}\left\{ \underset{\sim}{\chi} - \int_{t_0}^{t} \underset{\sim}{u}\left[\underset{\sim}{Y}(t'),t' \right] dt', t \right\} + \underset{\sim}{u}\left[\underset{\sim}{Y}(t),t \right] \qquad (15)$$

$$\underset{\sim}{u}^{*}(\underset{\sim}{\chi},t) = \hat{\underset{\sim}{u}}^{*}\left\{ \underset{\sim}{\chi} - \int_{t_0}^{t} \underset{\sim}{u}\left[\underset{\sim}{Y}(t'),t' \right] dt', t \right\} \qquad (16)$$

$$p^{*}(\underset{\sim}{\chi},t) = \hat{p}^{*}\left\{ \underset{\sim}{\chi} - \int_{t_0}^{t} \underset{\sim}{u}\left[\underset{\sim}{Y}(t'),t' \right] dt', t \right\} \qquad (17)$$

Reproduced with permission of the copyright owner. Further reproduction prohibited without permission.

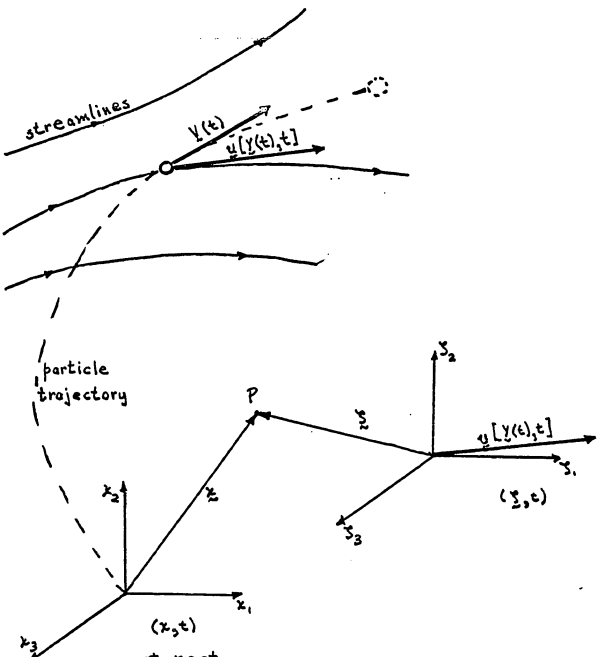

Figure 10.

Reproduced with permission of the copyright owner. Further reproduction prohibited without permission.

Thus

$$\frac{\partial}{\partial t} \underset{\sim}{u}^*(\underset{\sim}{\xi},t) = \frac{\partial}{\partial t} \hat{\underset{\sim}{u}}^*(\underset{\sim}{\xi},t) - \left\{ \underset{\sim}{u}\left[\underset{\sim}{Y}(t),t\right] \cdot \nabla \right\} \hat{\underset{\sim}{u}}^*(\underset{\sim}{\xi},t) \tag{18}$$

$$\nabla \underset{\sim}{u}^*(\underset{\sim}{\xi},t) = \nabla \hat{\underset{\sim}{u}}^*(\underset{\sim}{\xi},t) \tag{19}$$

$$\nabla \underset{\sim}{u}(\underset{\sim}{x},t) = \nabla \hat{\underset{\sim}{u}}(\underset{\sim}{\xi},t) \tag{20}$$

$$\nabla p^*(\underset{\sim}{x},t) = \nabla \hat{p}^*(\underset{\sim}{\xi},t) \tag{21}$$

So, substituting (15) to (21) into (8) and (9), then transforming to the new $(\underset{\sim}{\xi},t)$ coordinate system gives:

$$\frac{\partial}{\partial t} \hat{\underset{\sim}{u}}^* + (\hat{\underset{\sim}{u}}^* \cdot \nabla)\hat{\underset{\sim}{u}}^* + (\hat{\underset{\sim}{u}}^* \cdot \nabla)\hat{\underset{\sim}{u}} + (\hat{\underset{\sim}{u}}^* \cdot \nabla)\hat{\underset{\sim}{u}}^* = -\frac{1}{\rho}\nabla \hat{p}^* + \nu \nabla^2 \hat{\underset{\sim}{u}}^* \tag{22}$$

$$\nabla \cdot \hat{\underset{\sim}{u}}^* = 0 \tag{23}$$

Note that although $(\underset{\sim}{\xi},t)$ is a non-inertial frame, its acceleration $\frac{d}{dt}\underset{\sim}{u}\left[\underset{\sim}{Y}(t),t\right]$ does not appear in the equation for $\hat{\underset{\sim}{u}}^*$ (although it would appear in the equation for $\hat{\underset{\sim}{u}}$) .

Using (16) and (17), boundary conditions (11), (12), and (13) transform to:

$$\hat{\underset{\sim}{u}}^* \longrightarrow \underset{\sim}{0} \qquad \text{"far" from the particle} \tag{24}$$

$$\hat{p}^* \longrightarrow 0 \tag{25}$$

Reproduced with permission of the copyright owner. Further reproduction prohibited without permission.

and

$$\hat{\underset{\sim}{u}}^{**}(\underset{\sim}{\xi}_p,t) = \underset{\sim}{V}(t) - \underset{\sim}{u}\left[\underset{\sim}{y}(t),t\right] + \underset{\sim}{\Omega}(t)\times\left\{\underset{\sim}{\xi}_p - \hat{\underset{\sim}{y}}(t)\right\} - \hat{\underset{\sim}{u}}(\underset{\sim}{\xi}_p,t) \qquad (26)$$

where $\underset{\sim}{\xi}_p$ is any point on the surface of the sphere, and $\hat{\underset{\sim}{y}}(t)$ is the position of the center of the sphere in the coordinate system $(\underset{\sim}{\xi},t)$. Note that from (14)

$$\underset{\sim}{y}(t) = \hat{\underset{\sim}{y}}(t) + \int_{t_o}^{t} \underset{\sim}{u}\left[\underset{\sim}{y}(t'),t'\right]dt' . \qquad (27)$$

Our immediate objective is to obtain a force balance for the sphere in the $(\underset{\sim}{\xi},t)$ frame. It will be assumed that the sphere is small enough compared to the smallest scales in the turbulent velocity field so that the following two conditions are approximately satisfied: a) the flow in the neighborhood of the sphere is an unsteady, linear shear flow; and b) a volume enclosing the sphere can be defined, which is large with respect to the volume of the sphere, but small enough with respect to the turbulence scales that the velocity field is approximately uniform in it. These conditions will be approximately satisfied provided that

(i) $r/\eta \ll 1$,

where η is the Kolmogorov length scale of the turbulence. Using this requirement and others to be determined below, the second, third, and fourth terms on the left sides of equations (22), and the third and

Reproduced with permission of the copyright owner. Further reproduction prohibited without permission.

fourth terms on the right sides of (26) can be neglected. Thus equations (22) and (23), along with boundary conditions (24), (25), and (26) reduce to the Basset-Bousinesq-Oseen problem. And so a force balance on the sphere can easily be computed.

Since $\hat{\underset{\sim}{u}}(\underset{\sim}{x}, t)$ is $\underset{\sim}{0}$ at the center of the sphere (by the definition of the coordinate system $(\underset{\sim}{y}, t)$), then at the surface of the sphere $\hat{\underset{\sim}{u}}$ is at most of order r/η. So with condition (i), boundary condition (26) becomes

$$\hat{\underset{\sim}{u}}^{*}(\underset{\sim}{x}_{\beta}, t) = \underset{\sim}{V}(t) - \underset{\sim}{y}\left[\underset{\sim}{y}(t), t\right] + \underset{\sim}{\Omega}(t) \times \left\{\underset{\sim}{x}_{\beta} - \hat{\underset{\sim}{y}}(t)\right\}. \tag{28}$$

Furthermore, it has been shown by several authors (see, for example, Faxen 1927, Rubinow and Keller 1961, Saffman 1965, and Harper and Chang 1968) that, for steady flows, the effect of the rotation of the sphere upon the force balance of the sphere is to add a term of order $R_{\Omega} = \frac{|\underset{\sim}{\Omega}| r^2}{\nu}$. (Note that for a freely rotating sphere, $|\underset{\sim}{\Omega}| = \frac{1}{2} K$, where K is the local velocity gradient.)

Thus, assuming that this result also applies in the unsteady case, and that

(ii) $\frac{|\underset{\sim}{\Omega}| r^2}{\nu} \ll 1$,

then the boundary condition (28) reduces to

Reproduced with permission of the copyright owner. Further reproduction prohibited without permission.

$$\hat{\underset{\sim}{u}}^{*}(\underset{\sim}{\xi},t) = \underset{\sim}{V}(t) - \underset{\sim}{u}[\underset{\sim}{y}(t),t] \,. \tag{29}$$

Harper and Chang (1968) have shown, using a generalization of the method of Saffman (1965), that, for steady, linear shear flows, the effect of the shear on the force balance for a sphere is to add a force term of order $R_k^{1/2} = \left\{ \frac{\kappa r^2}{\nu} \right\}^{1/2}$, where κ is the velocity gradient. In a turbulent velocity field, an upper bound for κ would be $\kappa = u'/\eta$ (see, for example, Batchelor 1953), where u' is the rms turbulent velocity. Thus, assuming that this result applies in the unsteady case, and that

(iii) $\left\{ \frac{u'}{\eta} \frac{r^2}{\nu} \right\}^{1/2} = \left\{ \frac{u'\eta}{\nu} \right\}^{1/2} r/\eta \ll 1$,

then the $(\hat{\underset{\sim}{u}} \cdot \nabla)\hat{\underset{\sim}{u}}$ and $(\hat{\underset{\sim}{u}} \cdot \nabla)\hat{\underset{\sim}{u}}^{*}$ terms (representing the effect on $\hat{\underset{\sim}{u}}^{*}$ of the spatial non-uniformities in $\hat{\underset{\sim}{u}}$) can be neglected in equation (22).

For isotropic flows, with v the Kolmogorov velocity scale, $\frac{u'}{v} = 15^{-1/4} R_{\lambda g}^{1/2}$, where $R_{\lambda g} = \frac{u'\lambda_g}{\nu}$, a turbulence Reynolds number (e.g., Hinze, 1959, p. 185). So

$$\frac{u'\eta}{\nu} = \frac{v\eta}{\nu}\left(\frac{u'}{v}\right) = 15^{-1/4} R_{\lambda g}^{1/2} \,,$$

Reproduced with permission of the copyright owner. Further reproduction prohibited without permission.

since the Kolmogorov scale Reynolds number $\frac{v\eta}{\nu}$ equals one by definition. So in this case, condition (iii) reduces to

(iii') $R_{Ig}^{1/4} \frac{r}{\eta} \ll 1$.

Several authors (for example Oseen, 1927, Kaplun and Lagerstrom, 1957, Proudman and Pearson, 1957, Rubinow and Keller, 1961, and Harper and Chang, 1968) have shown that the effect of the non-linear term in (22) on the sphere force balance is to add a term of order $R_U = \frac{Ur}{\nu}$, U being a measure of the relative velocity of the sphere and the fluid (i.e., a measure of $\underset{\sim}{V}(t) - \underset{\sim}{u}[\underset{\sim}{Y}(t), t]$). So, assuming that

(iv) $\frac{Ur}{\nu} \ll 1$,

the term $(\hat{\underset{\sim}{u}}^* \cdot \nabla)\hat{\underset{\sim}{u}}^*$ can be neglected in (22).

So if conditions (iii) and (iv) are satisfied, then equation (22) reduces to

$$\frac{\partial}{\partial t}\hat{\underset{\sim}{u}}^* = -\frac{1}{\rho}\nabla\hat{p}^* + \nu\nabla^2\hat{\underset{\sim}{u}}^*. \tag{30}$$

And if conditions (i) to (iv) are satisfied, $\hat{\underset{\sim}{u}}^*$ and $\hat{p}^*$ are solutions to the differential equations (30), and boundary conditions (24), (25), and (29).

Reproduced with permission of the copyright owner. Further reproduction prohibited without permission.

To this order of approximation then, $\hat{\underset{\sim}{u}}^{*}$ and $\hat{p}^{*}$ are equal to the B-B-O solutions, say $\hat{\underset{\sim}{u}}_{BBO}$ and $\hat{p}_{BBO}$, and so the solution to the problem in the $(\underset{\sim}{\xi}, t)$ coordinate system is

$$\hat{\overline{\underset{\sim}{u}}}(\underset{\sim}{\xi}, t) = \hat{\underset{\sim}{u}}(\underset{\sim}{\xi}, t) + \hat{\underset{\sim}{u}}_{BBO}(\underset{\sim}{\xi}, t) \tag{31}$$

$$\hat{\overline{p}}(\underset{\sim}{\xi}, t) = \hat{p}(\underset{\sim}{\xi}, t) + \hat{p}_{BBO}(\underset{\sim}{\xi}, t) \tag{32}$$

When transformed back to the original coordinate system, this is

$$\overline{\underset{\sim}{u}}(\underset{\sim}{x}, t) = \underset{\sim}{u}(\underset{\sim}{x}, t) + \underset{\sim}{u}_{BBO}(\underset{\sim}{x}, t) \tag{33}$$

$$\overline{p}(\underset{\sim}{x}, t) = p(\underset{\sim}{x}, t) + p_{BBO}(\underset{\sim}{x}, t) \tag{34}$$

where

$$\underset{\sim}{u}_{BBO}(\underset{\sim}{x}, t) = \hat{\underset{\sim}{u}}_{BBO}\left\{\underset{\sim}{x} - \int_{t_0}^{t} \underset{\sim}{u}\left[\underset{\sim}{\chi}(t'), t'\right] dt', t\right\} \tag{35}$$

$$p_{BBO}(\underset{\sim}{x}, t) = \hat{p}_{BBO}\left\{\underset{\sim}{x} - \int_{t_0}^{t} \underset{\sim}{u}\left[\underset{\sim}{\chi}(t'), t'\right] dt', t\right\} \tag{36}$$

The force on the particle is obtained by integrating the total stress $\overline{\sigma}_{ij}$ over the surface of the particle. The stress is given by

$$\begin{aligned} \overline{\sigma}_{ij} &= -\bar{p}\delta_{ij} + \mu\left(\frac{\partial}{\partial x_j}\overline{u}_i + \frac{\partial}{\partial x_i}\overline{u}_j\right) \\ &= -(p + p_{BBO})\delta_{ij} + \mu\left[\frac{\partial}{\partial x_j}(u_i + u_{BBO_i}) + \frac{\partial}{\partial x_i}(u_j + u_{BBO_j})\right] \end{aligned} \tag{37}$$

Reproduced with permission of the copyright owner. Further reproduction prohibited without permission.

where μ is the fluid viscosity.

The B-B-O terms integrate to give the B-B-O force (F_{BBO}), i.e.,

$$F_{BBO_i} = \int_{\substack{\text{sphere}\\\text{surface}}} \sigma_{BBO_{ij}} n_j \, dA = \int_{\substack{\text{sphere}\\\text{surface}}} \left\{ -p_{BBO_i} \delta_{ij} + \mu \left(\frac{\partial}{\partial x_j} u_{BBO_i} + \frac{\partial}{\partial x_i} u_{BBO_j} \right) \right\} n_j \, dA$$

$$= -\frac{2\pi r^3}{3} \rho (\dot{V}_i - \dot{u}_i) - 6\pi\mu r \left\{ (V_i - u_i) + \frac{r}{\sqrt{\pi\nu}} \int_{-\infty}^{t} d\tau \, \frac{[\dot{V}_i(\tau) - \dot{u}_i(\tau)]}{\sqrt{t-\tau}} \right\} \qquad (38)$$

where again r is the radius of the particle, ρ the density of the fluid, and ν the kinematic viscosity. Also

$$u_i \equiv u_i \left[\underset{\sim}{Y}(t), t \right] \qquad (39)$$

$$\dot{u}_i \equiv \left\{ \frac{\partial u_i}{\partial t} + V_j \frac{\partial}{\partial x_j} u_i \right\}_{\underset{\sim}{x} = \underset{\sim}{Y}(t)} \equiv \dot{u}_i(t) \, . \qquad (40)$$

Other force terms are due to the acceleration of the (turbulent) fluid, and are computed as follows (where σ_{ij} is the stress tensor of the turbulent velocity field $\underset{\sim}{u}$):

$$F_i = \int_{\substack{\text{sphere}\\\text{surface}}} \sigma_{ij} n_j \, dA = \int_{\substack{\text{sphere}\\\text{volume}}} \frac{\partial}{\partial x_j} \sigma_{ij} \, dV \qquad (41)$$

by the divergence theorem. So

$$F_i = \int_{\substack{\text{sphere}\\\text{volume}}} \left(-\frac{\partial p}{\partial x_i} + \mu \nabla^2 u_i \right) dV \qquad (42)$$

Reproduced with permission of the copyright owner. Further reproduction prohibited without permission.

Since (r/η) has been assumed to be small, the integrand is approximately constant over the volume, and so

$$F_i = \left\{ -\frac{\partial p}{\partial x_i} + \mu \nabla^2 u_i \right\}_{\substack{x = x(t) \\ y = y(t)}} \cdot \frac{4}{3}\pi r^3 \left[1 + O(r/\eta) \right]. \tag{43}$$

So the total force on the sphere (F_T), assuming that (r/η) is sufficiently small, and assuming the presence of a gravitational field g, is

$$F_{T_i} = \frac{4}{3}\pi r^3 \left\{ -\frac{\partial p}{\partial x_i} + \mu \nabla^2 u_i \right\} - \frac{2\pi r^3}{3}\rho(\dot{V}_i - \dot{u}_i) - 6\pi\mu r \Big\{ (V_i - u_i) + \frac{r}{\sqrt{\pi\nu}} \int_{-\infty}^{t} d\tau \frac{[\dot{V}_i(\tau) - \dot{u}_i(\tau)]}{\sqrt{t-\tau}} \Big\} - \frac{4\pi r^3}{3}(\rho' - \rho) g_i \tag{44}$$

where, as in equation (38), everything is evaluated at the center of the sphere and where ρ' is the density of the sphere.

Using equation (1), the first two terms on the right hand side of equation (44) can be expressed as

$$\begin{aligned} \frac{4}{3}\pi r^3 \left\{ -\frac{\partial p}{\partial x_i} + \mu \nabla^2 u_i \right\} &= \frac{4}{3}\pi r^3 \rho \left\{ \frac{\partial u_i}{\partial t} + v_j \frac{\partial}{\partial x_j} u_i \right\} \\ &= \frac{4}{3}\pi r^3 \rho \left\{ \frac{\partial u_i}{\partial t} + V_j \frac{\partial}{\partial x_j} u_i + (v_j - V_j)\frac{\partial}{\partial x_j} u_i \right\} \\ &= \frac{4}{3}\pi r^3 \rho \left\{ \dot{v}_i + (v_j - V_j)\frac{\partial}{\partial x_j} u_i \right\}. \end{aligned} \tag{45}$$

Reproduced with permission of the copyright owner. Further reproduction prohibited without permission.

Using (45) in (44), the equations of motion for the "small" spherical particles are:

$$\frac{4}{3}\pi r^3\rho' \dot{V}_i = \frac{4}{3}\pi\rho r^3 \left\{ \dot{u}_i + (u_j - V_j)\frac{\partial}{\partial y_j} u_i \right\} - \frac{3\pi r^3}{3}\rho(\dot{V}_i - \dot{u}_i)$$
$$-6\mu\pi r\left\{ (V_i - u_i) + \frac{r}{\sqrt{\pi\nu}} \int_{-\infty}^{t} d\tau \frac{(\dot{V}_i - \dot{u}_i)}{\sqrt{t-\tau}} \right\} - \frac{4\pi r^3}{3}(\rho' - \rho) g_i \,. \qquad (46)$$

So finally,

$$\dot{V}_i = -\alpha(V_i - u_i) + \kappa \dot{u}_i + \frac{2}{3}\kappa(u_j - V_j)\frac{\partial}{\partial y_j} u_i - \frac{\kappa}{r\sqrt{\pi\nu}} \int_{-\infty}^{t} d\tau \frac{(\dot{V}_i - \dot{u}_i)}{\sqrt{t-\tau}} + g_i \qquad (47)$$

where $\alpha = \dfrac{9\nu}{r^2\left(2\frac{\rho'}{\rho} + 1\right)}$, $\kappa = \dfrac{3}{\left(2\frac{\rho'}{\rho} + 1\right)}$, $g_i = -g_i \dfrac{\left(\frac{\rho'}{\rho} - 1\right)}{\left(\frac{\rho'}{\rho} + \frac{1}{2}\right)}$.

C. Some Special Cases

Note that, when $\rho' = \rho$, then $\kappa = 1$ and $g_i = 0$. The equation can then be factored in terms of ($\dot{V}_i - \dot{u}_i$) and ($V_i - u_i$), so that the sphere moves with the fluid. That is,

$$V_i(t) = u_i[\underset{\sim}{y}(t), t] \qquad (48)$$

is a solution to the equation. With $\frac{d}{dt}\underset{\sim}{y}(t) = \underset{\sim}{V}(t)$, this equation is

$$\frac{d}{dt}\underset{\sim}{y}(t) = \underset{\sim}{u}[\underset{\sim}{y}(t), t] \,, \qquad (49)$$

Reproduced with permission of the copyright owner. Further reproduction prohibited without permission.

or the equation for a fluid particle trajectory.

Lumley (1957, chapter 2, section 4) has shown that the integral term in (47) can be neglected provided that

(v) $\left(\frac{r^2}{\nu}\omega\right)^{1/2} \ll 1$,

where ω is a characteristic high frequency of the Eulerian turbulent field.

Furthermore, Lumley (1957, chapter 2, section 5) established that a mean measure of $\frac{\kappa}{\alpha}\frac{\partial u_i}{\partial x_j}$ was small compared to one when

(vi) $R_{\lambda_g}\left(\frac{r}{\lambda_g}\right)^2 \ll 1$.

When these conditions are satisfied, equation (47) reduces to [1]

$$\dot{V}_i = -\alpha(V_i - u_i) + \kappa\dot{u}_i + g_i \qquad (50)$$

---

1. Lumley's (1957) final reduced form of the equations of translational motion (his equation 2.9.1) does not contain the term $\kappa\dot{u}_i$. In neglecting various terms to obtain the reduced form he compared terms such as $\kappa\frac{\partial u_i}{\partial t}$ and $\kappa V_j\frac{\partial}{\partial x_j}u_i$ with αV_i and αu_i. However, for "large" α (i.e., large $\alpha\tau_F$, where τ_F is a particle velocity microscale),

$$\alpha V_i, \alpha u_i = \alpha\tau_F \cdot O[\alpha(V_i - u_i)]$$

(see, for example, Lumley's equation 6.5.8). Thus, although a term may be small compared to αV_i or αu_i, it may not be small compared to $\alpha(V_i - u_i)$. In that case, such terms as $\kappa\frac{\partial u_i}{\partial t}$ and $\kappa V_j\frac{\partial}{\partial x_j}u_i$ can only be neglected for κ "very small".

Reproduced with permission of the copyright owner. Further reproduction prohibited without permission.

This is the most general form of the equations of motion that is used in the present simulations.

Note that in the case where $\frac{\rho'}{\rho} \to \infty$, so that $\psi \to 0$, but α remains finite (for finite $r^2 \frac{\rho'}{\rho}$), then equation (50) reduces to

$$V_i = -\alpha(V_i - u_i) + g_i \tag{51}$$

D. Summary

Summing up the conditions to be satisfied for equation (50) to hold,

(i) $r/\eta \ll 1$,

(ii) $\frac{|\underline{\Omega}| r^2}{\nu} \ll 1$,

(iii) $\left\{\frac{u'\eta}{\nu}\right\}^{1/2} r/\eta \ll 1$,

(iv) $\frac{Ur}{\nu} \ll 1$,

(v) $\left\{\frac{r^2\omega}{\nu}\right\}^{1/2} \ll 1$,

(vi) $R_{\lambda g}\left(\frac{r}{\lambda g}\right)^2 \ll 1$.

Reproduced with permission of the copyright owner. Further reproduction prohibited without permission.

V. EULERIAN FIELD SIMULATION RESULTS

A. Determination of the Parameters

1. Homogeneous, Stationary Shear Flow

To summarize some of the discussion in the third chapter, the mathematical form of the model random shear flow field $\underline{u}(\underline{x},t)$ is

$$\underline{u}(\underline{x},t) = \left(\frac{dU_1}{dx_2}\right) x_2 \underline{i}_1 + \sum_{n=1}^{N} T(\underline{k}_n, t_n) \frac{\underline{k}'_n}{k_n} \times \left\{ \underline{\alpha}_n \cos(\underline{k}'_n \cdot \underline{x}) + \underline{\beta}_n \sin(\underline{k}'_n \cdot \underline{x}) \right\} \tag{1}$$

where $\underline{k}'_n = \underline{k}_n - \frac{dU_1}{dx_2} k_{n_1} t_n \underline{i}_2$, and $t_n = t - t_{o_n}$. (2)

$(t_{o_{n+1}} - t_{o_n})$ has probability density $\Gamma \exp(-\Gamma t)$, where Γ^{-1} is the average time between Fourier mode injections. Also

$$T(\underline{k}_n, t_n) = \begin{cases} 0 & t_n = t - t_{o_n} < 0 \\ \left[t_n / \tau(\underline{k}_n)\right]^2 \exp\left[-t_n / 2\tau(\underline{k}_n)\right] & 0 \le t_n \le \sigma_M \\ 0 & \sigma_M < t_n \end{cases} \tag{3}$$

where $\tau(\underline{k}_n)^{-1} = \omega(1 + \sigma k_n)$. (4)

The probability density of injected wave numbers, in spherical polar variables, is

$$p_{k_n \beta_n \phi_n}(\lambda, \chi, \psi) = C \frac{\sin\psi}{1 + A\cos 2\psi} \cdot \frac{\rho^*}{\pi} \cdot \frac{p_{k_n}(\lambda)}{\left[(1+\rho^{*2}) + (1-\rho^{*2})\cos 2\chi\right]} \tag{5}$$

with $C = \frac{\frac{1}{2}\sqrt{2A(1-A)}}{\tan^{-1}\left\{\frac{\sqrt{2A(1-A)}}{1-A}\right\}}$, $A = \frac{B}{G(\lambda)}$, $\rho^* = 1 + \frac{R}{G(\lambda)}$ (6)

and

Reproduced with permission of the copyright owner. Further reproduction prohibited without permission.

$$G(\lambda) = \begin{cases} 1 & \lambda < K^* \\ 1 + [\gamma(\lambda - K^*)]^2 & \lambda \geq K^* \end{cases} \tag{7}$$

$$\frac{p}{K_n}(\lambda) = \begin{cases} \mathcal{K} \dfrac{(\xi\lambda)^2}{(1+\xi\lambda)^3} & \lambda < K_M \\ 0 & \lambda \geq K_M \end{cases} \quad \text{, where} \tag{8}$$

$$\mathcal{K} = \frac{\xi}{\ln(1+\xi K_M) - \dfrac{\xi K_M (1 + 3/2\, \xi K_M)}{(1+\xi K_M)^2}} \tag{9}$$

$\underset{\sim}{\alpha}_n$ and $\underset{\sim}{\beta}_n$ are independent, identically distributed Gaussian vectors, with

$$\left.\begin{aligned} \langle \underset{\sim}{\alpha}_n \rangle &= \langle \underset{\sim}{\beta}_n \rangle = \underset{\sim}{0} \\ \langle \alpha_{n_1} \alpha_{n_1} \rangle &= \langle \beta_{n_1} \beta_{n_1} \rangle = A_{11} \\ \langle \alpha_{n_2} \alpha_{n_2} \rangle &= \langle \beta_{n_2} \beta_{n_2} \rangle = A_{11}\left(1 + \frac{a_{22}}{G(\lambda)}\right) \\ \langle \alpha_{n_3} \alpha_{n_3} \rangle &= \langle \beta_{n_3} \beta_{n_3} \rangle = A_{11}\left(1 + \frac{a_{33}}{G(\lambda)}\right) \\ \langle \alpha_{n_1} \alpha_{n_2} \rangle &= \langle \beta_{n_1} \beta_{n_2} \rangle = A_{11} \frac{a_{12}}{G(\lambda)} \end{aligned}\right\} \tag{10}$$

for n = 1, 2, . . , N. (Note again that $\langle ( ) \rangle$ denotes the ensemble average of ( ) .) All other combinations (e.g. $\langle \alpha_{n_1} \alpha_{n_3} \rangle$, $\langle \alpha_{n_1} \beta_{n_1} \rangle$, etc.) are zero.

Reproduced with permission of the copyright owner. Further reproduction prohibited without permission.

In this choice of velocity field, values of the following parameters need to be specified:

$$\tau_M, \Gamma, K_M, \frac{dU}{dx_2}, \xi, \sigma, K^*, \gamma, \omega, \beta, R, A_{11}, a_{22}, a_{33}, a_{12}$$

The following paragraphs explain how the values were selected.

τ_M. τ_M is the maximum time interval that a mode remains on the field. (That is, for $t_n = t - t_{0_n} > \tau_M$, the amplitude of the nth mode is defined to be identically zero.) It is selected using the following criteria. Let $\mu = t_n / \tau(\xi_n)$. Then

$$T(\xi_n, t_n) = f(\mu) = \mu^2 \exp(-\mu/2).$$

So $\frac{\partial}{\partial \mu} f(\mu) = 2\mu\left(1 - \frac{\mu}{4}\right)\exp(-\mu/2) = 0$ for $\mu = 0, 4$.

Thus $f(\mu)$ has its maximum at $\mu = 4$:

$$f_{MAX} \equiv f(4) = 4^2 \exp(-2).$$

So $f(\mu)/f_{MAX} = \left(\frac{\mu}{4}\right)^2 \exp\left(-\frac{\mu}{2} + 2\right)$.

$\mu_M \equiv \tau_M / \tau(\xi_n)$ is chosen so that $f(\mu)/f_{MAX}$ has fallen below a predetermined "small" value, i.e. $f(\mu_M)/f_{MAX} < 2*10^{-3}$. This is satisfied for $\mu_M = 24$, so we set $\tau_M = 24\,\tau(\xi_n)$.

Γ. Since the cutoff time τ_M is the total time interval that a mode is on the field, then the average time interval, say ATI, is given by

Reproduced with permission of the copyright owner. Further reproduction prohibited without permission.

$$ATI = \langle \tau_M \rangle = \langle 24\, r(k_n) \rangle = \frac{24}{\omega} \left\langle \frac{1}{(1+\sigma k_n)} \right\rangle .$$

If it is desired that on the average $\bar{N}$ modes be on the field at any instant, then on the average $\bar{N}$ modes must be injected during a time interval ATI. So the average time between injections Γ^{-1} should be

$$\Gamma^{-1} = \frac{ATI}{\bar{N}} = \frac{24}{\omega \bar{N}} \left\langle \frac{1}{(1+\sigma k_n)} \right\rangle . \qquad (11)$$

The computation time for any one realization is roughly proportional to $\bar{N}$, so $\bar{N}$ was bounded from above by the amount of computer time (or money) available. $\bar{N}$ was chosen to be 25.

Using this $\bar{N}$ along with values of ω, σ, ξ, and K_M explained below, and using $p_{k_n}(\lambda)$ as given by equation (8) to compute the average $\left\langle \frac{1}{(1+\sigma k_n)} \right\rangle$, then $\Gamma^{-1} = 0.1$.

K_M. Taking into consideration the reasons stated in Chapter III, section B.4, K_M was chosen to be 10. Thus one decade of the wave number is modeled, restricting the modeling to very low Reynolds number turbulent flows.

$\frac{dU_1}{dx_2}$. Choosing the time $\left(\frac{dU_1}{dx_2}\right)^{-1} = 1$ scales all the other times by $\left(\frac{dU_1}{dx_2}\right)^{-1}$. That is, any other time T in the simulations can be considered to be $T \frac{dU_1}{dx_2}$, and thus be non-dimensionalized by $\left(\frac{dU_1}{dx_2}\right)^{-1}$.

ξ. In the same manner, ξ^{-1} (a characteristic (large) length scale of the field) is chosen as the basic length scale, so $\xi^{-1} = 1$.

Reproduced with permission of the copyright owner. Further reproduction prohibited without permission.

σ. For all the simulations computed, σ (an inverse length scale) was chosen to be equal to ξ, or $\sigma = 1$. This was done because there was no serious reason to bring in another length scale.

K^*, γ. K^* and γ are an inverse length scale and a length scale used in the definition of the function $G(\lambda)$ (see equation (7)). Together they help to determine how the wave number spectrum tends to its isotropic form as λ becomes large. (That is, they determine how fast $G(\lambda)$ increases with λ. Note that, in the definition of $\beta_{\underline{\kappa}_n}(\lambda)$, $\langle \alpha_{n_i} \alpha_{n_j} \rangle$, and $\langle \beta_{n_i} \beta_{n_j} \rangle$, $G(\lambda) = \infty$ corresponds to their isotropic forms.) The criteria used for $G(\lambda)$ was that as $\lambda \to K_M$, $G(\lambda) \to 10$. Thus, for example, $\rho^*(K_M) = 1 + \frac{R}{G(K_M)} = 1 + \frac{R}{10} = 1.08$ (using the value of R determined below), which is close to the isotropic value of $\rho^* = 1$. Furthermore, it was found that if the spectrum tended to its isotropic from too rapidly, then the desired values of the ratios $\frac{\langle u_1'^2 \rangle}{\langle u_2'^2 \rangle}$, $\frac{\langle u_1'^2 \rangle}{\langle u_3'^2 \rangle}$, and $\frac{\langle u_1' u_2' \rangle}{\langle u_1'^2 \rangle^{1/2} \langle u_2'^2 \rangle^{1/2}}$ could not be attained. With these two things in mind, K^* was chosen to be 5.0, and γ to be 2/3.

ω. Since $\tau(\underline{\kappa}_n)^{-1} = \omega(1 + \sigma K_n)$, then $\tau(\underline{0})^{-1} = \omega$. So ω^{-1} is the characteristic time of the large scale structure. Because of this, ω is the main parameter which determines the integral time scales of the flow. Thus by adjusting the value of ω, the non-dimensional parameter $T_{11}\left(\frac{dU_1}{dx_2}\right)$ (where

$$T_{11} = \int_0^\infty \frac{\langle u_1'(\underline{0},t) u_1'(\underline{0},t+\tau) \rangle}{\langle u_1'^2(\underline{0},t) \rangle} \, d\tau \quad)$$

Reproduced with permission of the copyright owner. Further reproduction prohibited without permission.

was set approximately equal to 0.8[1], the value which was estimated for the real shear flow being roughly modeled (Champagne, Harris, and Corrsin 1970, pp. 125 and 126). This led to $\omega = 2.0$.

R. The shape of isoprobability contours of $p_{k_n}(\lambda)$ in the $\lambda_2\lambda_3$ plane is determined mainly by the factor $\frac{1}{[(1+\rho^{*2})+(1-\rho^{*2})\cos 2\chi]}$ in the definition of $p_{\theta_n\phi_n}(\chi,\psi/k_n=\lambda)$. This term can be rearranged as

$$\frac{1}{[(1+\rho^{*2})+(1-\rho^{*2})\cos 2\chi]} = \frac{1}{[(1+\rho^{*2})+(1-\rho^{*2})(\cos^2\chi-\sin^2\chi)]} = \frac{1/2}{\cos^2\chi+\rho^{*2}\sin^2\chi} .$$

Since $\lambda_2 = \lambda \sin\psi\sin\chi$, $\lambda_3 = \lambda\sin\psi\cos\chi$, this term is proportional to

$$g(\lambda_2,\lambda_3) = \frac{1}{\lambda_3^2+\rho^{*2}\lambda_2^2} .$$

g has constant contours qualitatively like those shown in figure 11.

It can be seen from the expression for g that if σ_2 is a characteristic scale of λ_2, and σ_3 the corresponding characteristic scale for λ_3, then $\rho^* = \frac{\sigma_3}{\sigma_2}$ so that g can be written as

---

1. In fixing the relative values of the mean flow time scale $\left(\frac{dU_1}{dx_2}\right)^{-1}$ and turbulence time scales (e.g., T_{11} , $L_{11}/\langle u_1^2\rangle^{1/2}$, etc.), the choice of matching $T_{11}\left(\frac{dU_1}{dx_2}\right)$ instead of some other non-dimensional parameter was arbitrary.

Reproduced with permission of the copyright owner. Further reproduction prohibited without permission.

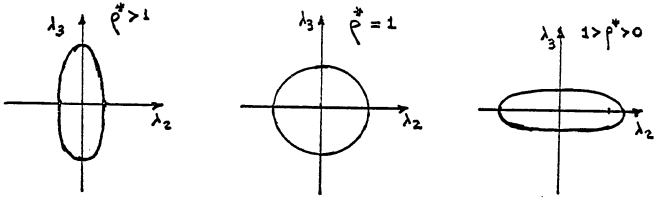

Figure 11.

$$g(\lambda_2, \lambda_3) = \frac{1}{\left(\frac{\lambda_3^2}{\sigma_3^2} + \frac{\lambda_2^2}{\sigma_2^2}\right)\sigma_3^2} .$$

Noting that (i) $p_{\underset{\sim}{k}_n}(\underset{\sim}{\lambda})$ is proportional to the energy density (see equation (III.56) for the isotropic expression), and that (ii) $\rho^*(0) = 1 + \frac{R}{G(0)} = 1 + R$ is the ratio of the characteristic scales of λ_2 and λ_3 for small wave numbers (large scales), say $\frac{\sigma_3^0}{\sigma_2^0}$, the following assumptions are made to determine R:

a) assume that the characteristic scales of λ_2 and λ_3 for g are also the characteristic scales of λ_2 and λ_3 for $p_{\underset{\sim}{k}_n}$;

b) assume that the ratio $\frac{\sigma_3^0}{\sigma_2^0}$ determines the ratio L_2/L_3 of integral scales of $\mathcal{R}_{11}(r_1, r_2, r_3, 0)$ along the r_2 and r_3 axes respectively, and that in fact

Reproduced with permission of the copyright owner. Further reproduction prohibited without permission.

$$\frac{\sigma_3^2}{\sigma_2^2} = \frac{L_2}{L_3} .$$

These assumptions were made because no inexpensive method was available to compute the ratio L_2/L_3 for the simulation fields.

Using the "pseudo-integral scales" L_2 and L_3, defined by Champagne, Harris, and Corrsin to be the integral of R_{11} out to the first zero of R_{11}, then the ratio of L_2/L_3 determined from their results is $L_2/L_3 \doteq 1.8$. Thus, from assumption (b), $\frac{\sigma_3^2}{\sigma_2^2} = 1 + \frac{R}{q(0)}$ $= 1 + R = 1.8$, or, $R = 0.8$.

B. The direction of the velocity vector $\underset{\sim}{u}'$ is determined by $\underset{\sim}{k}_n$, $\underset{\sim}{\alpha}_n$, and β_n through the vector cross-products $\underset{\sim}{k}_n \times \underset{\sim}{\alpha}_n$ and $\underset{\sim}{k}_n \times \underset{\sim}{\beta}_n$. [See equation (1).] One way to insure that

$$\langle u_1'^2 \rangle > \langle u_2'^2 \rangle, \langle u_3'^2 \rangle$$

(as is observed in most turbulent shear flows with nearly rectilinear mean velocity in the x_1 direction) is to have $\underset{\sim}{k}_n \times \underset{\sim}{\alpha}_n$ and $\underset{\sim}{k}_n \times \underset{\sim}{\beta}_n$ with a larger component along x_1 than along x_2 and x_3 on the average. This can be accomplished to a certain extent by choosing $\underset{\sim}{\alpha}_n$ and $\underset{\sim}{\beta}_n$ to be on the average near the x_2x_3 plane (see the discussion below on the choice of q_{22} and q_{33}).

But also if the $\underset{\sim}{k}_n$ are selected so that it is more probable that a $\underset{\sim}{k}_n$ is perpendicular to x_1 (i.e., lying in the vicinity of the x_2x_3 plane), then it is also more probable that $\underset{\sim}{u}'$ has a larger component along x_1 than perpendicular to x_1.

This fact is used in the selection of $\mathcal{B}$. For $\mathcal{B}$ determines the

Reproduced with permission of the copyright owner. Further reproduction prohibited without permission.

shape of the isoprobability contours of $p_{K_n}(\lambda)$ in the $\lambda_1 \cdot (\lambda_2^2+\lambda_3^2)^{1/2}$ plane through the factor [see equations (5) and (6-ii)]

$$\frac{1}{1+A\cos 2\psi} \quad ; \quad A = \frac{\beta}{G(\lambda)} \; .$$

This can be rearranged as

$$\frac{1}{1+A\cos 2\psi} = \frac{1}{(1+A)\cos^2\psi + (1-A)\sin^2\psi}$$

and has constant contours as shown in figure 12. The third example in the figure, for $0<A<1$, corresponds to selecting K_n so that it is more probable that K_n is perpendicular to x_1.

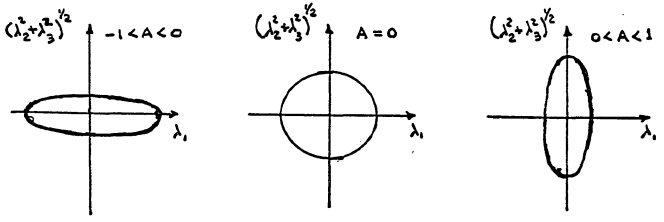

Figure 12.

Reproduced with permission of the copyright owner. Further reproduction prohibited without permission.

Thus β was selected (in conjunction with the selection of a_{22} and a_{33} discussed below) to match the ratio $\frac{\langle u_1'^2\rangle}{\langle u_2'^2\rangle}$ and $\frac{\langle u_1'^2\rangle}{\langle u_3'^2\rangle}$ in the model and the real flows. It was also attempted to take into account the ratios L_1/L_2 and L_1/L_3 in the choice of β.

The value determined for β was 0.888.

a_{22}, a_{33}, a_{12}. Values for these parameters were obtained by matching the ratios $\frac{\langle u_1'^2\rangle}{\langle u_2'^2\rangle}$, $\frac{\langle u_1'^2\rangle}{\langle u_3'^2\rangle}$, $\frac{-\langle u_1'u_2'\rangle}{\langle u_1'^2\rangle^{1/2}\langle u_2'^2\rangle^{1/2}}$ with those in the real flow. The first and third ratios taken together determine the orientation of the Reynolds stress tensor $\langle u_i'u_j'\rangle$ in the $u_1'u_2'$ plane. It has principal axes tilted by the amount

$$\alpha_{RS} = \frac{1}{2}\tan^{-1}\left\{\frac{2\langle u_1'u_2'\rangle}{\langle u_1'^2\rangle - \langle u_2'^2\rangle}\right\}. \qquad (12)$$

By choosing $a_{22} = a_{33} = 0.75$, and $a_{12} = 0.052$, the model had approximately

$$\frac{\langle u_1'^2\rangle}{\langle u_2'^2\rangle} = 2.1\,, \quad \frac{\langle u_1'^2\rangle}{\langle u_3'^2\rangle} = 1.7\,, \quad \frac{-\langle u_1'u_2'\rangle}{[\langle u_1'^2\rangle\langle u_2'^2\rangle]^{1/2}} = 0.5\,,$$

which are close to the values measured in the real flow.

A_{11}. Finally, the parameter A_{11} was determined by matching the ratio of the turbulent strain rate to the mean strain rate $\frac{\langle s^2\rangle^{1/2}}{\frac{dU_1}{dx_2}}$ with that of the real flow. It was found that with $A_{11} = 0.04$, $\langle s^2\rangle^{1/2}/\frac{dU_1}{dx_2}$ was approximately 8.0, a value comparable with those of the homogeneous shear and some traditional shear flows (Champagne, Harris, and Corrsin).

Reproduced with permission of the copyright owner. Further reproduction prohibited without permission.

2. Stationary, Isotropic Flow

The stationary, isotropic field $\underline{u}(\underline{x},t)$ was defined to be of the form (see Chapter III, section C):

$$\underline{u}(\underline{x},t) = \sum_{n=1}^{N} T(\underline{\kappa}_n, t_n) \frac{\underline{\kappa}_n}{\kappa_n} \times \left\{ \underline{\alpha}_n \cos(\underline{\kappa}_n \cdot \underline{x}) + \underline{\beta}_n \sin(\underline{\kappa}_n \cdot \underline{x}) \right\}. \quad (13)$$

Again $t_n = t - t_{0_n}$, where $t_{0_{n+1}} - t_{0_n}$ is exponentially distributed with density $\Gamma \exp(-\Gamma t)$. Also again

$$T(\underline{\kappa}_n, t_n) = \begin{cases} 0 & t_n = t - t_{0_n} < 0 \\ [t_n/\tau(\underline{\kappa}_n)]^2 \exp[-t_n/2\tau(\underline{\kappa}_n)] & 0 \le t_n \le \sigma_M \\ 0 & \sigma_M < t_n \end{cases} \quad (14)$$

where $\tau(\underline{\kappa}_n)^{-1} = \omega(1 + \sigma\kappa_n)$. To insure isotropy at all wave numbers,

$$f_{\kappa_n} Q_n P_m(\lambda, \chi, \psi) = \frac{\sin\psi}{4\pi} f_{\kappa_n}(\lambda), \quad (15)$$

where again

$$f_{\kappa_n}(\lambda) = \begin{cases} K \dfrac{(\xi\lambda)^2}{(1+\xi\lambda)^3} & \lambda \le \kappa_M \\ 0 & \lambda > \kappa_M \end{cases} \quad (16)$$

and

$$K = \frac{\xi}{\ln(1+\xi\kappa_M) - \dfrac{\xi\kappa_M(1+3/2\,\xi\kappa_M)}{(1+\xi\kappa_M)^2}} \quad (17)$$

$\underline{\alpha}_n$ and $\underline{\beta}_n$ are chosen to be independent, identically distributed

Reproduced with permission of the copyright owner. Further reproduction prohibited without permission.

Gaussian vectors such that

$$\langle \alpha_n \rangle = \langle \beta_n \rangle = 0$$

$$\langle \alpha_{n_r} \alpha_{n_s} \rangle = \langle \beta_{n_r} \beta_{n_s} \rangle = A_{11} \delta_{rs} \tag{18}$$

for n = 1, 2, . . , N. All other combinations are zero.

Thus the following parameters need to be determined.

$$\tau_M , \Gamma , K_M , \xi , \sigma , \omega , A_{11}$$

As has been mentioned, it was decided to keep the isotropic field and the shear field as similar as possible. Thus the parameters τ_M, Γ, K_M, ξ, σ, and ω were all chosen to be of the same values as used in the shear flow model.

The value of A_{11} was obtained by matching the non-dimensional parameter $\frac{u_1' T_{11}}{L_f}$ in the simulation flow field with that measured in an isotropic wind tunnel turbulence (Comte-Bellot and Corrsin 1971). Here u_1' is the rms velocity fluctuation, T_{11} the integral time scale of R_{11} (rescaled in a "stationary" frame), and L_f the integral scale of the Karman-Howarth "f-function". Behind a biplane, square rod, 5.08 cm. mesh grid with mean speed of 10 m/sec. (mesh Reynolds number of 34,000), u_1' = 22.3 cm./sec., T_{11} = 84 msec., and L_f = 2.54 cm. With these values, A_{11} is 0.2.

B. Simulation Results

1. Homogeneous, Stationary Shear Flow

Reproduced with permission of the copyright owner. Further reproduction prohibited without permission.

Table 1 contains information about both the Reynolds stress tensor computed for the shear flow model field and that measured by Champagne, Harris, and Corrsin. Results are listed for three different, independent ensembles of the model field, to give a rough idea of the scatter in the computer "measurements". Appendix B gives an error analysis for random sampling, the technique used to obtain the results. The simulation values of $\langle u_1' u_3' \rangle$ and $\langle u_2' u_3' \rangle$ were zero to within the accuracy of the measurements (never exceeding 2% of the value of $\langle u_1'^2 \rangle$), and so are not listed.

α_{RS} is the angle of the principal axes of the Reynolds stress tensor [equation (12)].

	C.H.& C.	Run I	Run II	Run III
$\langle u_1'^2 \rangle$	–	1.874	1.789	1.895
$\langle u_2'^2 \rangle$	–	0.927	0.868	0.857
$\langle u_3'^2 \rangle$	–	1.070	1.044	1.026
$-\langle u_1' u_2' \rangle$	–	0.518	0.491	0.561
$\langle u_1'^2 \rangle / \langle u_2'^2 \rangle$	1.96	2.021	2.060	2.210
$\langle u_1'^2 \rangle / \langle u_3'^2 \rangle$	1.70	1.751	1.714	1.845
$-\langle u_1' u_2' \rangle / \langle u_1'^2 \rangle^{1/2} \langle u_2'^2 \rangle^{1/2}$	0.50	0.394	0.394	0.440
α_{RS}	-28°, 62°	-24°, 66°	-21°, 69°	-24°, 66°

Table 1.

Reproduced with permission of the copyright owner. Further reproduction prohibited without permission.

Figure 13 is a plot of the Eulerian time autocorrelation coefficients

$$\frac{\langle u_1'(\varrho_3,t)u_1'(\varrho_3,t+\tau)\rangle}{\langle u_1'^2(\varrho_3,t)\rangle}\ ,\quad \frac{\langle u_2'(\varrho_3,t)u_2'(\varrho_3,t+\tau)\rangle}{\langle u_2'^2(\varrho_3,t)\rangle}\ ,\quad \frac{\langle u_3'(\varrho_3,t)u_3'(\varrho_3,t+\tau)\rangle}{\langle u_3'^2(\varrho_3,t)\rangle}\ .$$

Note that these are time autocorrelations evaluated at the origin of the coordinate system, at which point the mean velocity is zero. At any other x_2 value we would get the same function by moving with the mean velocity.

We know of no reason why the three autocorrelation coefficient functions should or should not be identical. However, in these simulations, they appear to be almost identical. Their differences may be partially due to errors resulting from the finite sampling size. The error bound in figure 13 is approximately 0.07 (see Appendix B). In all the results reported in this project the sample size -- i.e., the number of realizations in an ensemble -- was 2000.

The integral time scales, defined by

$$\mathcal{T}_{ij} \equiv \frac{1}{\langle u_i'(\varrho_3,t)u_j'(\varrho_3,t)\rangle}\int_0^\infty \langle u_i'(\varrho_3,t)u_j'(\varrho_3,t+\tau)\rangle\, d\tau \quad \text{(no sum)} \qquad (19)$$

were found to be $\mathcal{T}_{11} = 0.991$, $\mathcal{T}_{22} = 0.868$, and $\mathcal{T}_{33} = 1.031$. Again, the deviations may result from the finite sample size. With these values, then $\mathcal{T}_{11}\left(\frac{dU_1}{dx_2}\right) \doteq 0.991$, compared to the value of about 0.80 estimated by Champagne, Harris, and Corrsin from their wind tunnel measurements. The corresponding microscales (defined for the correlation coefficient $\mathcal{R}_{ij}(\tau)$ to be $\mathcal{T}_{\varepsilon_{ij}} = \sqrt{\frac{2}{-\mathcal{R}_{ij}''(0)}}$)

Reproduced with permission of the copyright owner. Further reproduction prohibited without permission.

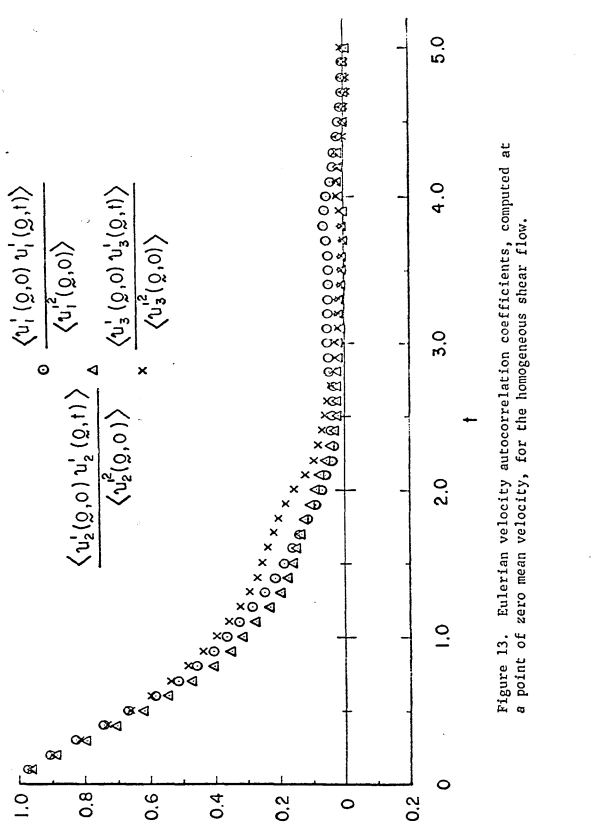

Figure 13. Eulerian velocity autocorrelation coefficients, computed at a point of zero mean velocity, for the homogeneous shear flow.

Reproduced with permission of the copyright owner. Further reproduction prohibited without permission.

are $\gamma_{\xi_{11}} = 0.612$, $\gamma_{\xi_{22}} = 0.525$, and $\gamma_{\xi_{33}} = 0.548$. Note that the relatively large γ_{ξ}/T shows that this model corresponds to low Reynolds number turbulence.

Figure 14 is a plot of the cross-correlation coefficient

$$\frac{\langle u_i'(\varrho,t)\, u_2'(\varrho,t+\tau)\rangle}{\langle u_i'(\varrho,t)\, u_2'(\varrho,t)\rangle}$$

for both positive and negative values of τ. Note that since the process is stationary, $\langle u_i'(\varrho,t)\, u_2'(\varrho,t+\tau)\rangle = \langle u_2'(\varrho,t)\, u_i'(\varrho,t-\tau)\rangle$. The function appears to be quite unsymmetric about the origin. The integral time scales were found to be $T_{12} = 1.010$ (for $\tau > 0$) and $T_{21} = 0.660$ (for $\tau < 0$). It should be noted that in all the calculations completed, the cross-correlation coefficient consistently had a high degree of scatter, much more that the other correlations measured.

Figures 15, 16, and 17 display Eulerian velocity spatial autocorrelations along the x_1, x_2, and x_3 axes. The results for $\langle u_i'(\underline{x},t)\, u_i'(\underline{x}+\underline{r},t)\rangle$ are in qualitative agreement with those of Champagne, Harris, and Corrsin, i.e., the correlation drops off faster along the x_2 and x_3 axes than along the x_1 axis (in a fashion similar to that of the f and g functions for isotropic fields). However, it was not determined if the correlation along the x_3 axis will go negative as is usual in shear flows, and in fact it appears that the correlation along the x_2 axis may be going negative instead.

Figures 18, 19, and 20 display the cross-correlations

$$\langle v_i'(\underline{x},t)\, u_2'(\underline{x}+\underline{r},t)\rangle$$

Reproduced with permission of the copyright owner. Further reproduction prohibited without permission.

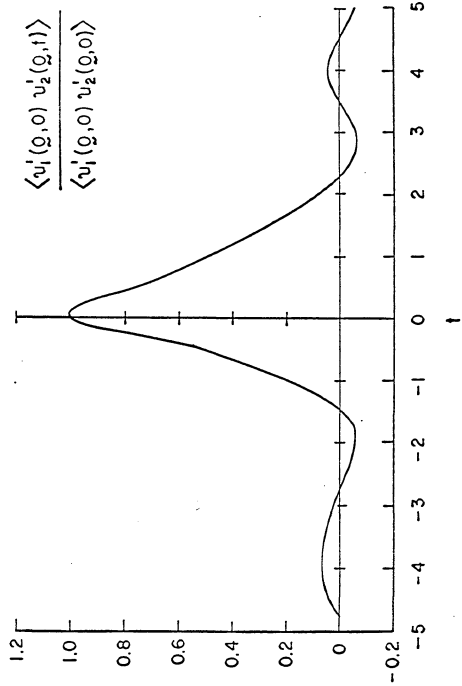

Figure 14. The Eulerian velocity time cross-correlation coefficient, computed at a point of zero mean velocity, for the homogeneous shear flow.

Reproduced with permission of the copyright owner. Further reproduction prohibited without permission.

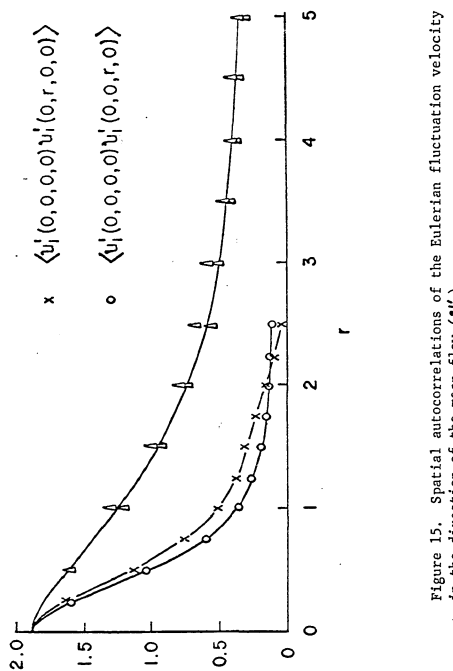

Figure 15. Spatial autocorrelations of the Eulerian fluctuation velocity in the direction of the mean flow (u_i').

Reproduced with permission of the copyright owner. Further reproduction prohibited without permission.

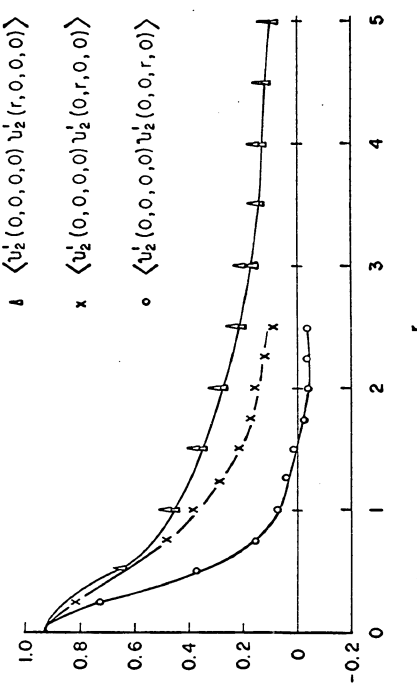

Figure 16. Spatial autocorrelations of the Eulerian fluctuation velocity in the direction of the mean velocity gradient (u_2').

Reproduced with permission of the copyright owner. Further reproduction prohibited without permission.

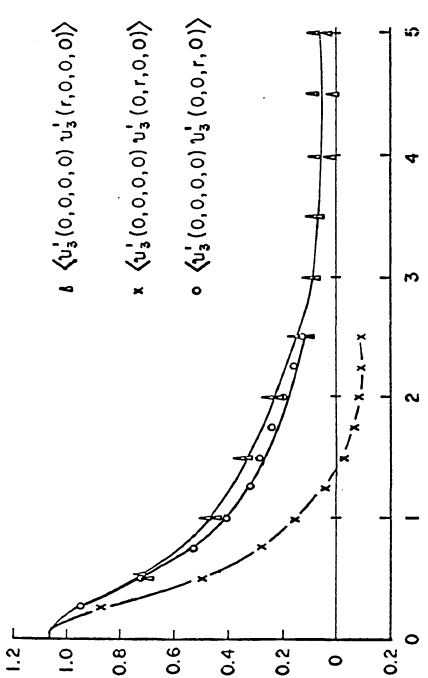

Figure 17. Spatial autocorrelations of the Eulerian fluctuation velocity in the direction normal to both the mean velocity and mean velocity gradient (u'_3).

Reproduced with permission of the copyright owner. Further reproduction prohibited without permission.

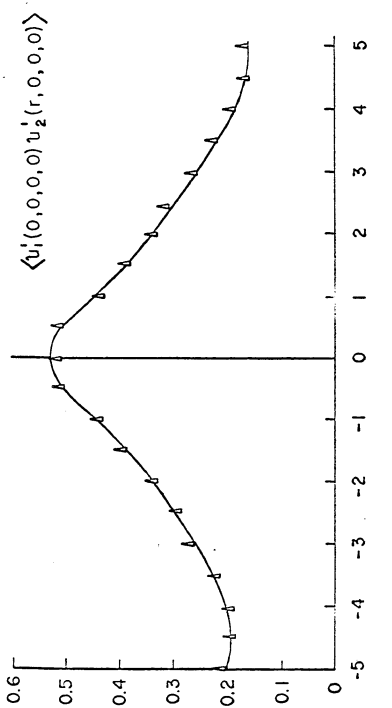

Figure 18. Eulerian velocity spatial cross-correlation $\langle u_i'(\vec{x},t)\, u_j'(\vec{x}+\vec{r},t)\rangle$ along the direction of the mean velocity (r_1).

Reproduced with permission of the copyright owner. Further reproduction prohibited without permission.

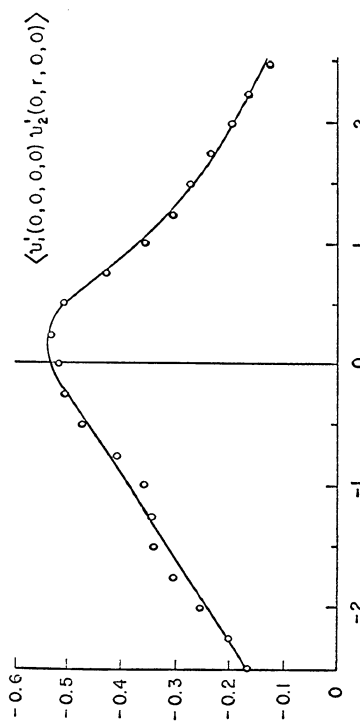

Figure 19. Eulerian velocity spatial cross-correlation $\langle u_i'(x_1,x_2,x_3,t)u_j'(x_1+r_1,x_2+r_2,x_3+r_3,t)\rangle$ along the direction of the mean velocity gradient (r_2).

Reproduced with permission of the copyright owner. Further reproduction prohibited without permission.

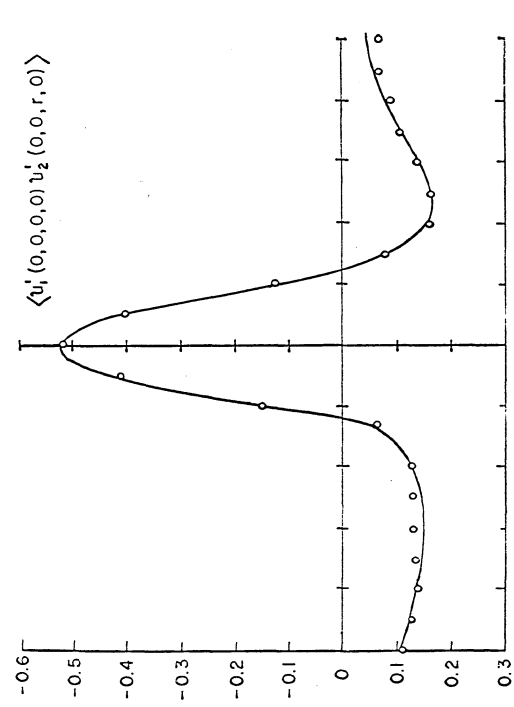

Figure 20. Eulerian velocity spatial cross-correlation $\langle u_1'(x_2,t)u_2'(x+r,t)\rangle$ along the direction normal to both the mean velocity and mean velocity gradient (r_3).

Reproduced with permission of the copyright owner. Further reproduction prohibited without permission.

along the three cartesian axes. The integral length scale along x_1 appears to be much greater than those along x_2 and x_3. We also note the large negative regions of the cross-correlation along the x_3 axis. This is apparently a result of the fact that the motion is isochoric. For in isochoric motions, $\nabla \cdot \underline{u}' = 0$, which results in the constraint

$$\frac{\partial}{\partial r_i} R_{ij}(\underline{r},0) = \frac{\partial}{\partial r_j} R_{ij}(\underline{r},0) = 0 \tag{20}$$

for statistically homogeneous flows. (See Batchelor 1953, page 27.) It can be shown that this implies

$$\int_{-\infty}^{\infty}\int_{-\infty}^{\infty} R_{12}(r_1,r_2,r_3,0)\, dr_1\, dr_3 = 0$$
$$\int_{-\infty}^{\infty}\int_{-\infty}^{\infty} R_{12}(r_1,r_2,r_3,0)\, dr_2\, dr_3 = 0 \tag{21}$$

so that somewhere in the r_1r_3 and r_2r_3 planes there are regions of negative R_{12}.

Figure 21 is a plot of the spatial correlation $\langle u_1'(\underline{x},t)u_1'(\underline{x}+\underline{r},t)\rangle$ along the streamwise (r_1) direction for a series of values of r_2. The plot is in qualitative agreement with results obtained by Champagne, Harris, and Corrsin. The figure gives a rough indication of $\langle u_1'(\underline{x},t)\, u_1'(\underline{x}+\underline{r},t)\rangle$ in the r_1r_2 plane.

A better indication of the spatial correlations $\langle u_i'(\underline{x},t)u_j'(\underline{x}+\underline{r},t)\rangle$ in the r_1r_2 plane is given by isocorrelation contours plotted in this plane. Curves of this type are displayed in figure 22

Reproduced with permission of the copyright owner. Further reproduction prohibited without permission.

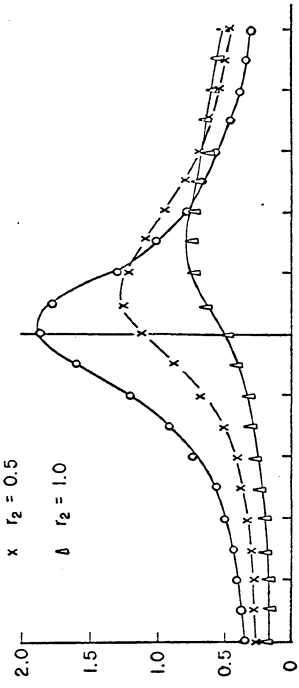

Figure 21. Spatial autocorrelation functions along the streamwise direction (r_1) for a series of values of r_2.

Reproduced with permission of the copyright owner. Further reproduction prohibited without permission.

($\frac{\langle u_1'(\underline{x},t)\,u_1'(\underline{x}+\underline{r},t)\rangle}{\langle u_1'^2(\underline{x},t)\rangle}$), figure 23 ($\frac{\langle u_2'(\underline{x},t)\,u_2'(\underline{x}+\underline{r},t)\rangle}{\langle u_2'^2(\underline{x},t)\rangle}$), figure 24 ($\frac{\langle u_3'(\underline{x},t)\,u_3'(\underline{x}+\underline{r},t)\rangle}{\langle u_3'^2(\underline{x},t)\rangle}$), figure 25 ($\frac{\langle u_1'(\underline{x},t)\,u_2'(\underline{x}+\underline{r},t)\rangle}{\langle u_1'(\underline{x},t)\,u_2'(\underline{x},t)\rangle}$), and figure 26 ($\frac{\langle u_2'(\underline{x},t)\,u_1'(\underline{x}+\underline{r},t)\rangle}{\langle u_2'(\underline{x},t)\,u_1'(\underline{x},t)\rangle}$).

These plots were obtained by computing values for the correlation coefficients from the simulations on a 20x10 point grid in the r_1r_2 plane (from -5 to 5 in r_1 and from 0 to 2.5 in r_2), and using the NCAR library subroutine CALCNT to interpolate values throughout the plane and to determine the constant contours. Because of the comparatively small number of points used, and because of the error inherent in the computed values, the curves are far from exact. However they do give a good indication of the spatial structure of the field.

The isocorrelation contours for $u_1'u_1'$ are in qualitative agreement with those measured in nearly homogeneous shear flow (Champagne, Harris, and Corrsin 1970; Graham, Harris, and Corrsin 1971). However, the results for $u_1'u_2'$ are qualitatively different from those of Graham, Harris, and Corrsin.

2. Stationary, Isotropic Flow

Figure 27 is a plot of the Eulerian velocity autocorrelation coefficients in time,

$$\frac{\langle u_1(\underline{x},t)\,u_1(\underline{x},t+\tau)\rangle}{\langle u_1^2(\underline{x},t)\rangle}\ ,\quad \frac{\langle u_2(\underline{x},t)\,u_2(\underline{x},t+\tau)\rangle}{\langle u_2^2(\underline{x},t)\rangle}\ ,\quad \frac{\langle u_3(\underline{x},t)\,u_3(\underline{x},t+\tau)\rangle}{\langle u_3^2(\underline{x},t)\rangle}$$

for the isotropic model flow. Since the field was generated in a

Reproduced with permission of the copyright owner. Further reproduction prohibited without permission.

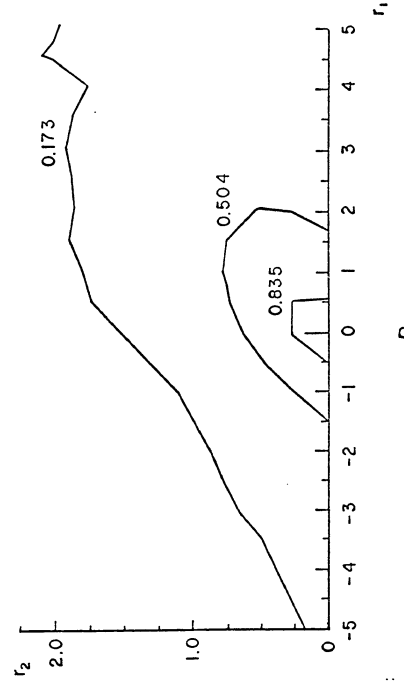

Figure 22. Spatial isocorrelation contours in the plane of the mean velocity (r_1) and mean velocity gradient (r_2).

Reproduced with permission of the copyright owner. Further reproduction prohibited without permission.

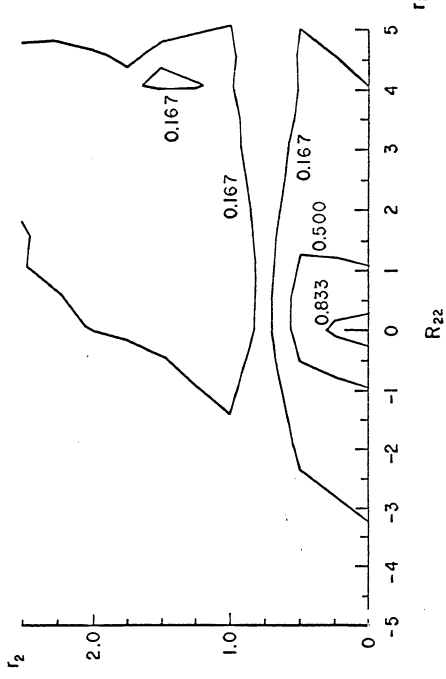

Figure 23. Spatial isocorrelation contours in the plane of the mean velocity (r_1) and mean velocity gradient (r_2).

Reproduced with permission of the copyright owner. Further reproduction prohibited without permission.

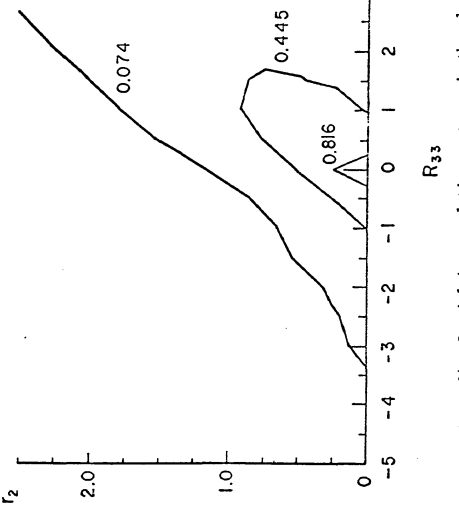

Figure 24. Spatial isocorrelation contours in the plane of the mean velocity (r_1) and mean velocity gradient (r_2).

Reproduced with permission of the copyright owner. Further reproduction prohibited without permission.

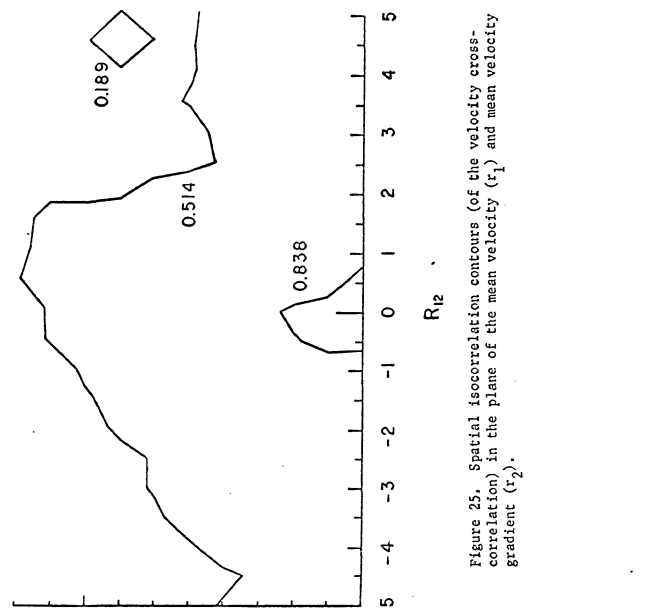

Figure 25. Spatial isocorrelation contours (of the velocity cross-correlation) in the plane of the mean velocity (r_1) and mean velocity gradient (r_2).

Reproduced with permission of the copyright owner. Further reproduction prohibited without permission.

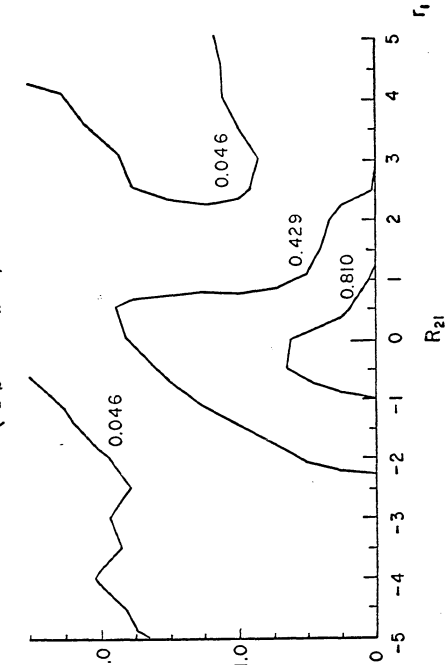

Figure 26. Spatial isocorrelation contours (of the velocity cross-correlation) in the plane of the mean velocity (r_1) and mean velocity gradient (r_2).

Reproduced with permission of the copyright owner. Further reproduction prohibited without permission.

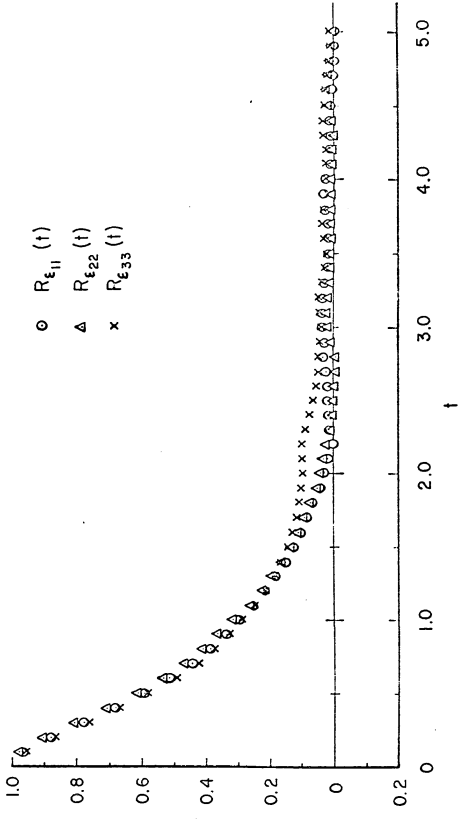

Figure 27. Eulerian velocity time autocorrelation coefficients for the isotropic model flow.

Reproduced with permission of the copyright owner. Further reproduction prohibited without permission.

statistically isotropic manner [$f_{\xi_n}(\lambda)$ being a function of $|\lambda|$ alone], the correlations should be identical. The differences thus give an indication of the errors resulting from the finite sample size.

The integral time scales were computed to be approximately 0.812, 0.824, and 0.891, while the microscales (defined by $\sqrt{\frac{2}{-R''(0)}}$) were found to be 0.516, 0.695, and 0.4775.

Figure 28 is a plot of the Kármán-Howarth f and g functions computed in the simulations. Two separate computations were made for the g function, corresponding to two perpendicular directions. The f function integral length L_f was approximately 1.50, while the g function integral lengths L_g were 0.808 and 0.858. Also the f function Taylor microscale ($\lambda_f \equiv [-f''(0)]^{-1/2}$) and the g function microscales ($\lambda_g \equiv [-g''(0)]^{-1/2}$) were computed to be 0.900, 0.443, and 0.386 respectively. The results for the integral lengths are in approximate agreement with the isotropic relationship (Batchelor 1953, page 47)

$$L_f = 2 L_g$$

However, the microscale results[1] do not agree well with the isotropic

---

1. In practice, the microscales are computed from the formula

$$\lambda = \frac{r}{\sqrt{2[1 - R(r)]}} \qquad \text{(for "small" r).}$$

Very small errors in $R(r)$ result in relatively large errors in $1-R(r)$. Thus the microscales are subject to a high degree of statistical scatter.

Reproduced with permission of the copyright owner. Further reproduction prohibited without permission.

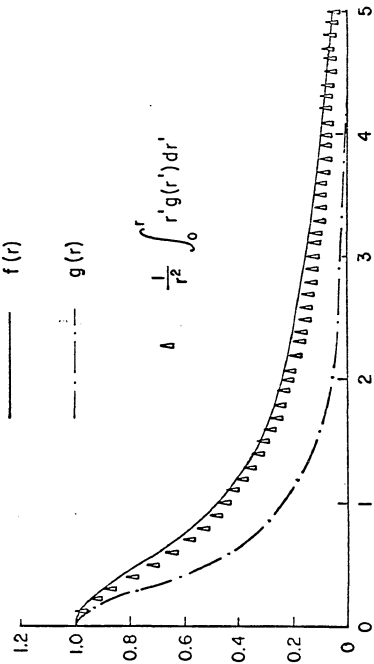

Figure 28. The Kármán-Howarth f and g functions for the isotropic model flow. Also included are values of $\frac{1}{r^2}\int_0^r r'^2 g(r')dr'$, which should equal $f(r)$ in a truly isotropic flow.

Reproduced with permission of the copyright owner. Further reproduction prohibited without permission.

relationship

$$\lambda_f = \sqrt{2}\,\lambda_g \ .$$

Figure 28 also includes values of $\frac{1}{r^2}\int_0^r r' g(r')\,dr'$ computed using the simulation values of g. In a truly isotropic flow,

$$f(r) = \frac{1}{r^2}\int_0^r r' g(r')\,dr' \ ,$$

a result which is valid in the simulations within their computed accuracy (which is about ± 0.07 in this case).

Note that for large separations, the values for f have still not quite reached zero, while those for g have not yet gone negative. This may indicate that there is some large scale coherence in the field, perhaps due to the choices for $f_{\xi_n}(\xi)$ and $T(\xi_n, t_n)$.

Reproduced with permission of the copyright owner. Further reproduction prohibited without permission.

VI. FLUID PARTICLE AND "ALIEN" PARTICLE DISPERSION

A. Simulation Results of Fluid Particle Diffusion on the Homogeneous, Stationary Shear Flow

1. Introduction

2000 realizations were completed of fluid particle diffusion on the homogeneous, stationary shear flow. In each realization, the fluid particle which was initially (t = 0) at the origin of the coordinate system was tracked, and its position and velocity as functions of (necessarily discrete) time were recorded. At the origin of the coordinate system (in fact in the plane $x_2 = 0$), the Eulerian mean velocity was identically zero. (See figure 29.)

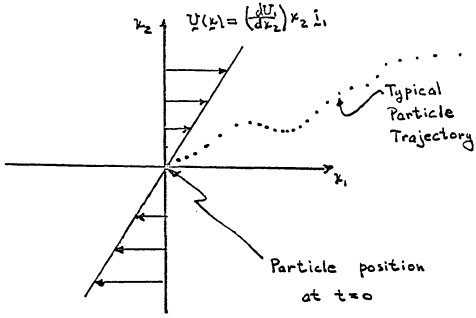

Figure 29.

Reproduced with permission of the copyright owner. Further reproduction prohibited without permission.

This particular initial position was chosen to simplify mathematical analysis, as well as conceptual vizualization of the problem. It permits easy comparison of simulation results with the theoretical predictions of Corrsin (1953). Furthermore, because of the way in which the field was defined (Chapter III), the statistical results for particles tracked starting from any other point in the fluid can be obtained by applying a Galilean transformation to these results.

The position and velocity of a fluid particle at time t, which started at a at time t_0, will be denoted in the Lagrangian (or "material") frame by $\underline{X}(a,t)$ and $\underline{U}(a,t)$ respectively. The Eulerian velocity field is always denoted by $\underline{u}(\underline{x},t)$.

The fluid particle velocity decomposition introduced by Corrsin (1953, 1959a) will be used: since the Eulerian field can be expressed as

$$\underline{u}(\underline{x},t) = \left(\frac{dU_1}{dx_2}\right) x_2 \underline{i}_1 + \underline{u}'(\underline{x},t) \qquad (1)$$

where $\langle \underline{u}'(\underline{x},t) \rangle = \underline{0}$, the fluid particle velocity $\underline{U}(a,t)$ can be decomposed as

$$\underline{U}(a,t) = \underline{u}\left[\underline{X}(a,t),t\right] = \left(\frac{dU_1}{dx_2}\right) X_2(a,t)\,\underline{i}_1 + \underline{u}'\left[\underline{X}(a,t),t\right]$$

$$= \left(\frac{dU_1}{dx_2}\right) X_2(a,t)\,\underline{i}_1 + \underline{U}'(a,t) \qquad (2)$$

where $\underline{U}'(a,t) = \underline{u}'\left[\underline{X}(a,t),t\right]$. Also, a fluid particle velocity

Reproduced with permission of the copyright owner. Further reproduction prohibited without permission.

autocorrelation coefficient $\mathcal{R}_{f_{ij}}(r)$ will be defined by

$$\mathcal{R}_{f_{ij}}(r) \equiv \frac{\langle U_i'(a,t)U_j'(a,t+r)\rangle}{\langle U_i'(a,t)U_j'(a,t)\rangle} \quad . \tag{3}$$

Since the velocity $\underset{\sim}{U}'(a,t)$ defined above is not the traditional Lagrangian fluctuation velocity [which is defined by the decomposition $\underset{\sim}{U}(a,t) = \langle \underset{\sim}{U}(a,t)\rangle + \underset{\sim}{U}^*(a,t)$], the autocorrelation introduced by equation (3) is not the "genuine" Lagrangian velocity autocorrelation. However, $\underset{\sim}{U}'(a,t)$ does have the following desirable characteristics:

(i) Since it is the Lagrangian quantity corresponding to $\underset{\sim}{u}'(\underset{\sim}{x},t)$ [i.e., it is defined by $\underset{\sim}{U}'(a,t) = \underset{\sim}{u}'[\underset{\sim}{X}(a,t),t]$], theoretical analyses are sometimes simplified. Examples of this are Corrsin's (1953, 1959a) kinematic predictions (see Chapter I, section C), and also possible extensions (e.g., to a homogeneous, shear flow) of Lumley's (1961) results (see Chapter I, section C).

(ii) There is reason to believe that $\underset{\sim}{U}'(a,t)$ is a stationary random function, and that $\underset{\sim}{U}^*(a,t)$ is not. In fact, this was observed in the simulations.

It was also observed in the simulation results (and was expected as a result of the choice of the initial position of the fluid particles) that $\langle \underset{\sim}{X}(a,t)\rangle = \langle \underset{\sim}{U}'(a,t)\rangle = \underset{\sim}{0}$ to within the accuracy of the measurements (so that also $\langle \underset{\sim}{U}(a,t)\rangle = \underset{\sim}{0}$). Thus all of the discussion below implies

$$\langle \underset{\sim}{X}(a,t)\rangle = \langle \underset{\sim}{U}'(a,t)\rangle = \underset{\sim}{0} \quad . \tag{4}$$

Reproduced with permission of the copyright owner. Further reproduction prohibited without permission.

2. Statistical Properties of the Displacement Covariance Tensor $\langle X_i(\underline{\varrho},t)X_j(\underline{\varrho},t)\rangle$.

Figure 30 is a plot of the mean square displacements $\langle X_2^2(\underline{\varrho},t)\rangle$ and $\langle X_3^2(\underline{\varrho},t)\rangle$. From equation (I.23), and from a similar equation for $\langle X_3^2(\underline{\varrho},t)\rangle$, it is seen that these quantities behave in a manner similar to their equivalents in an isotropic field. For "short" times (small compared to fluid particle velocity microscales), they should vary as

$$\langle X_2^2(\underline{\varrho},t)\rangle = \langle U_2'^2(\underline{\varrho},t)\rangle t^2 + O(t^3), \text{ and} \tag{5}$$

$$\langle X_3^2(\underline{\varrho},t)\rangle = \langle U_3'^2(\underline{\varrho},t)\rangle t^2 + O(t^3), \tag{6}$$

while for "large" times (compared with a fluid particle integral time scale),

$$\langle X_2^2(\underline{\varrho},t)\rangle \longrightarrow 2\langle U_2'^2(\underline{\varrho},t)\rangle T_{F_{22}} t \text{ , and} \tag{7}$$

$$\langle X_3^2(\underline{\varrho},t)\rangle \longrightarrow 2\langle U_3'^2(\underline{\varrho},t)\rangle T_{F_{33}} t, \tag{8}$$

where the fluid particle integral time scales, $T_{F_{ij}}$, are defined by

$$T_{F_{ij}} \equiv \int_0^\infty R_{F_{ij}}(\tau)\, d\tau . \tag{9}$$

It was found in all the measurements completed that, within the

Reproduced with permission of the copyright owner. Further reproduction prohibited without permission.

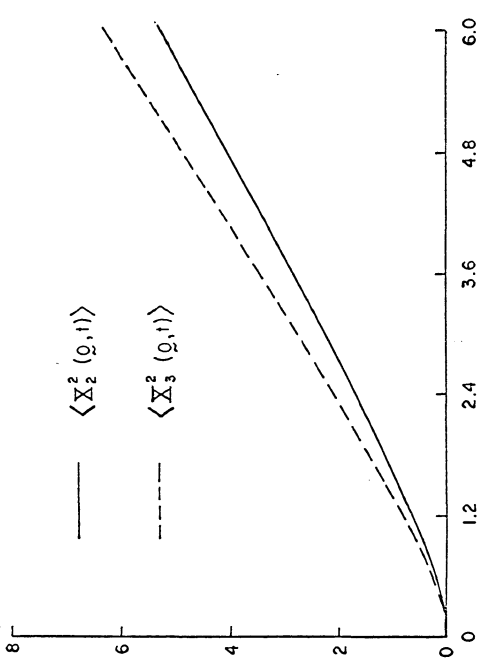

Figure 30. Dispersion in the direction of the mean velocity gradient, $\langle X_1^2(\xi,t)\rangle$, and normal to both the mean velocity and the mean velocity gradient, $\langle X_3^2(\xi,t)\rangle$.

Reproduced with permission of the copyright owner. Further reproduction prohibited without permission.

accuracy of the experiments, the one point moments of $\underset{\sim}{U}'$ (e.g., $\langle U_i' U_j' \rangle$) equaled the one point moments of $\underset{\sim}{v}'$ [1]. Computed results for $\langle U_i' U_j' \rangle$ are

$$\langle U_1'^2(\underset{\sim}{\xi},t) \rangle = 1.855 \pm 0.178 \tag{10}$$

$$\langle U_2'^2(\underset{\sim}{\xi},t) \rangle = 0.891 \pm 0.077 \tag{11}$$

$$\langle U_3'^2(\underset{\sim}{\xi},t) \rangle = 1.060 \pm 0.056 \tag{12}$$

$$\langle U_1'(\underset{\sim}{\xi},t) U_2'(\underset{\sim}{\xi},t) \rangle = -0.522 \pm 0.080 \tag{13}$$

$$\langle U_1'(\underset{\sim}{\xi},t) U_3'(\underset{\sim}{\xi},t) \rangle = \langle U_2'(\underset{\sim}{\xi},t) U_3'(\underset{\sim}{\xi},t) \rangle = 0 \tag{14}$$

With the $T_{F_{ij}}$ values discussed below, it was found that the simulation results shown in figure 30 agreed with the asymptotic predictions of equations (5), (6), (7), and (8).

Figure 31 is a log-log plot of $\langle \Sigma_1^2(\underset{\sim}{\xi},t) \rangle$. From equation (I.21), we note that for "short" times,

---

1. Note that Lumley's (1961) theoretical result (see Chapter I, section C), equating the one point probability densities of $\underset{\sim}{U}'(\underset{\sim}{\xi},t)$ and $\underset{\sim}{v}'(\underset{\sim}{x},t)$ (and thus their various moments) does not apply in this case, since the complete Eulerian field -- $\left(\frac{dU_i}{dx_2}\right) x_2 \underset{\sim}{i}_1 + \underset{\sim}{v}'(\underset{\sim}{x},t)$ -- is not homogeneous. Thus there is still no theoretical basis for equating the moments of $\underset{\sim}{U}'(\underset{\sim}{\xi},t)$ with those of $\underset{\sim}{v}'(\underset{\sim}{x},t)$ in this case.

Reproduced with permission of the copyright owner. Further reproduction prohibited without permission.

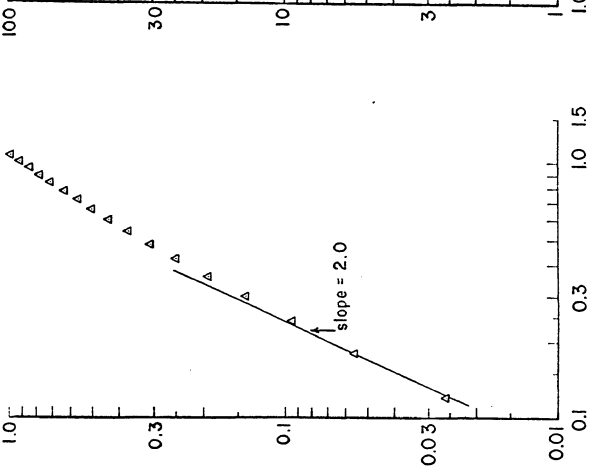

Figure 31. Lagrangian dispersion in the direction of the mean velocity, $\langle X_1^2(0,t)\rangle$.

Reproduced with permission of the copyright owner. Further reproduction prohibited without permission.

$$\langle X_1^2(\varrho,t)\rangle = \langle U_1'^2(\varrho,t)\rangle t^2 + O(t^3), \tag{15}$$

as for diffusion in an isotropic flow.

For "large" times (Corrsin 1953, 1959a),

$$\langle X_1^2(\varrho,t)\rangle \longrightarrow \frac{2}{3}\left(\frac{dU_1}{dx_2}\right)^2 \langle U_2'^2(\varrho,t)\rangle T_{F_{22}} t^3, \tag{16}$$

a result which is radically different from the isotropic case, where $\langle X_1^2(\varrho,t)\rangle \longrightarrow 2\langle U_1'^2(\varrho,t)\rangle T_{F_{11}} t$. Equation (16) reflects the effect of the mean velocity gradient on the dispersion process.

The simulation results agree well with both asymptotic expressions in equations (15) and (16). Furthermore, the results indicate that the "long" time regime has been established for non-dimensional times greater than about 3. [Note that $T_{F_{22}} = 0.545$ (see below), and $\left(\frac{dU_1}{dx_2}\right)^{-1} = 1.0$.]

Figures 32 and 33 are plots of the covariance function, $\langle X_1(\varrho,t) X_2(\varrho,t)\rangle$, and display other effects of the mean velocity gradient. From equation (I.22), for "short" times this function goes as

$$\langle X_1(\varrho,t) X_2(\varrho,t)\rangle = \langle U_1'(\varrho,t) U_2'(\varrho,t)\rangle t^2 + O(t^3), \tag{17}$$

which is also valid for homogeneous flows without shear. For "long" times (Corrsin 1953),

$$\langle X_1(\varrho,t) X_2(\varrho,t)\rangle \longrightarrow \left(\frac{dU_1}{dx_2}\right)\langle U_2'^2(\varrho,t)\rangle T_{F_{22}} t^2, \tag{18}$$

Reproduced with permission of the copyright owner. Further reproduction prohibited without permission.

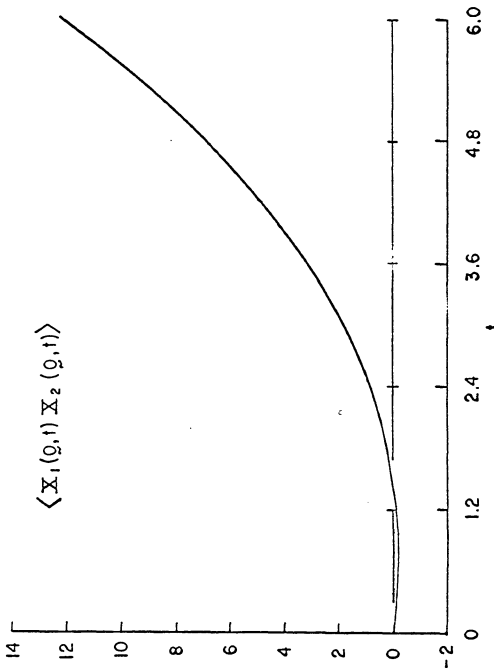

Figure 32. The fluid particle covariance function $\langle \Delta_1(\underline{\varrho},\underline{\xi},t)\Delta_2(\underline{\varrho},\underline{\xi},t)\rangle$ for the shear flow simulations.

Reproduced with permission of the copyright owner. Further reproduction prohibited without permission.

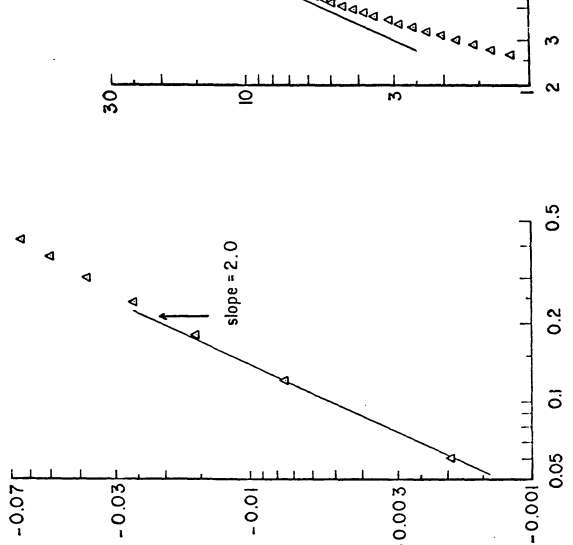

Figure 33. A log-log plot of the covariance function $\langle X_1(\underset{\sim}{\rho},t)X_2(\underset{\sim}{\rho},t)\rangle$.

Reproduced with permission of the copyright owner. Further reproduction prohibited without permission.

which is qualitatively different from the corresponding result for homogeneous flows without shear:

$$\langle X_1(\underline{\varrho},t)X_2(\underline{\varrho},t)\rangle \longrightarrow \langle U_1'(\underline{\varrho},t)U_2'(\underline{\varrho},t)\rangle\left(T_{F_{12}}+T_{F_{21}}\right)t\,.$$

Since $\langle U_1'(\underline{\varrho},t)U_2'(\underline{\varrho},t)\rangle$ is negative, equation (17) predicts that initially the covariance will go parabolicly negative. However, equation (18) shows that it will eventually become positive, with asymptote $\sim t^2$.

The simulation results are not in disagreement with these theoretical findings. For "short" times, the simulation follows (17), but for the largest times computed (up to a non-dimensional time of 6.0), a t^2 regime [equation (18)] had not quite been established.

Figure 34 is a plot of the cross-correlation coefficient

$$\frac{\langle X_1(\underline{\varrho},t)X_2(\underline{\varrho},t)\rangle}{\langle X_1^2(\underline{\varrho},t)\rangle^{1/2}\langle X_2^2(\underline{\varrho},t)\rangle^{1/2}}$$

which provides another view of the joint statistics of $X_1(\underline{\varrho},t)$ and $X_2(\underline{\varrho},t)$. Using the "short" time results for $\langle X_1^2(\underline{\varrho},t)\rangle$, $\langle X_2^2(\underline{\varrho},t)\rangle$, and $\langle X_1(\underline{\varrho},t)X_2(\underline{\varrho},t)\rangle$ [equations (15), (5), and (17)],

$$\frac{\langle X_1(\underline{\varrho},t)X_2(\underline{\varrho},t)\rangle}{\langle X_1^2(\underline{\varrho},t)\rangle^{1/2}\langle X_2^2(\underline{\varrho},t)\rangle^{1/2}} = \frac{\langle U_1'(\underline{\varrho},t)U_2'(\underline{\varrho},t)\rangle}{\langle U_1'^2(\underline{\varrho},t)\rangle^{1/2}\langle U_2'^2(\underline{\varrho},t)\rangle^{1/2}} + O(t)\,. \quad (19)$$

For "large" times [equations (16), (7), and (18), Corrsin (1953, 1959a)],

Reproduced with permission of the copyright owner. Further reproduction prohibited without permission.

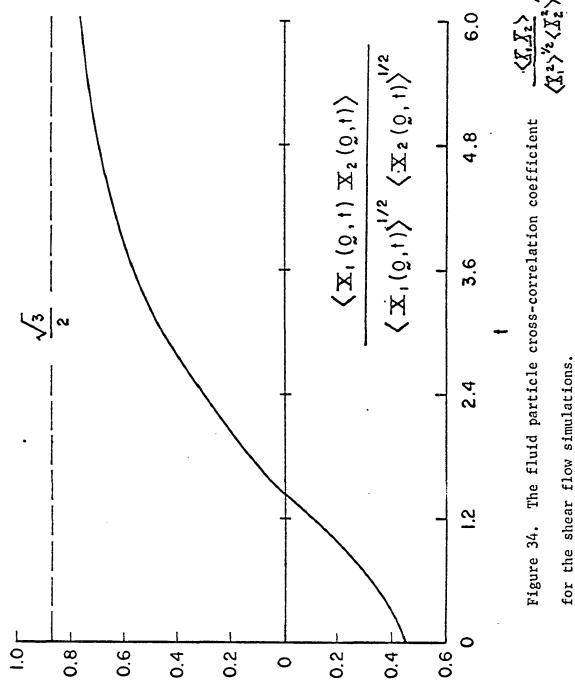

Figure 34. The fluid particle cross-correlation coefficient $\frac{\langle X_1 X_2\rangle}{\langle X_1^2\rangle^{1/2}\langle X_2^2\rangle^{1/2}}$ for the shear flow simulations.

Reproduced with permission of the copyright owner. Further reproduction prohibited without permission.

$$\frac{\langle X_1(\varrho,t)X_2(\varrho,t)\rangle}{\langle X_1^2(\varrho,t)\rangle^{1/2}\langle X_2^2(\varrho,t)\rangle^{1/2}} \longrightarrow \frac{\sqrt{3}}{2} \quad . \tag{20}$$

The "short" time simulation result agrees well with equation (19). However, the "long" time asymptotic result is not reached (since the asymptotic regime for $\langle X_1(\varrho,t)X_2(\varrho,t)\rangle$ had not been established) although the curve seems to head in the right direction. It appears that several more integral time scales will be needed before the asymptote is essentially attained.

Figure 35 is a plot of the angle of tilt α_{DT} of the major principal axis of the tensor $\langle X_i(\varrho,t)X_j(\varrho,t)\rangle$ in the x_1x_2 plane as a function of time. α_{DT} is

$$\alpha_{DT} = \frac{1}{2}\tan^{-1}\left\{\frac{2\langle X_1(\varrho,t)X_2(\varrho,t)\rangle}{\langle X_1^2(\varrho,t)\rangle - \langle X_2^2(\varrho,t)\rangle}\right\} . \tag{21}$$

The orientation of the principal axes of $\langle X_i(\varrho,t)X_j(\varrho,t)\rangle$ indicates in a sense the orientation of the joint probability density of $\{X_1(\varrho,t), X_2(\varrho,t)\}$, $f_{X_1X_2}(x_1,x_2;t)$. For "small" times, equations (15), (5), and (17) give

$$\alpha_{DT} \doteq \frac{1}{2}\tan^{-1}\left\{\frac{2\langle U_1'(\varrho,t)U_2'(\varrho,t)\rangle}{\langle U_1'^2(\varrho,t)\rangle - \langle U_2'^2(\varrho,t)\rangle}\right\} \tag{22}$$

which is equal to α_{RS} for the Reynolds stress tensor. For "large" times, (16), (7), and (18) give

$$\alpha_{DT} \longrightarrow \frac{1}{2}\tan^{-1}\left\{\frac{2\left(\frac{dU_1}{dx_2}\right)\langle U_2'^2(\varrho,t)\rangle T_{F_{22}}t^2}{2/3\left(\frac{dU_1}{dx_2}\right)^2\langle U_2'^2(\varrho,t)\rangle T_{F_{22}}t^3}\right\}$$

$$= \frac{1}{2}\tan^{-1}\left\{\frac{3}{\left(\frac{dU_1}{dx_2}\right)t}\right\} \doteq \frac{3}{2}\frac{1}{\left(\frac{dU_1}{dx_2}\right)t} \quad ,$$

Reproduced with permission of the copyright owner. Further reproduction prohibited without permission.

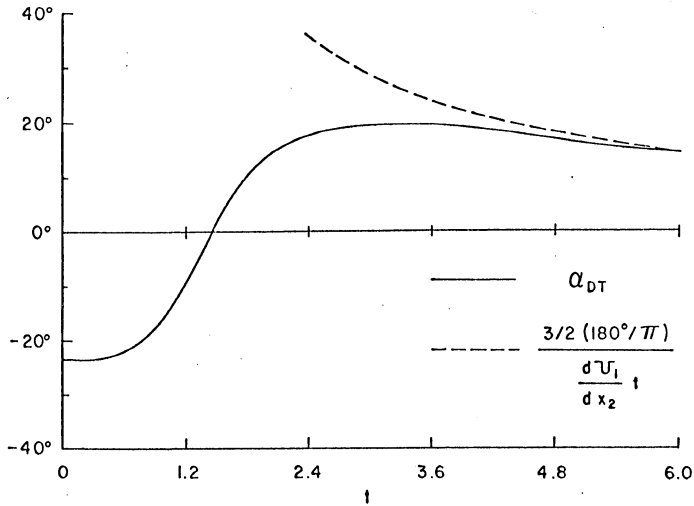

Figure 35. The angle of the major principal axis of the tensor $\langle \underline{X}_i(\underline{e},t)\underline{X}_j(\underline{e},t)\rangle$ in the x_1x_2 plane for the shear flow simulations (see equation (21)).

Reproduced with permission of the copyright owner. Further reproduction prohibited without permission.

that is, $$\alpha_{pT} \longrightarrow \frac{3}{2}\left(\frac{dU_1}{dx_2}t\right)^{-1}. \qquad (23)$$

The simulation values for $\langle U_i'(\underline{\xi},t)\,U_j'(\underline{\xi},t)\rangle$ [equations (10), (11), and (13)] give

$$\frac{1}{2}\tan^{-1}\left\{\frac{2\langle U_1'(\underline{\xi},t)U_2'(\underline{\xi},t)\rangle}{\langle U_1'^2(\underline{\xi},t)\rangle - \langle U_2'^2(\underline{\xi},t)\rangle}\right\} \doteq 23.5^\circ. \qquad (24)$$

Thus it is seen from figure 35 that the simulation results agree well with (22). Also, from figure 35, the asymptotic regime of equation (23) appears to be established for non-dimensional times greater than about 5.0.

3. Isoprobability Contours

It is desirable to compute contours of constant displacement probability in the x_1x_2 plane, i.e. contours of constant $p_{X_1X_2}(x_1,x_2;t)$, the joint probability density function of $X_1(\underline{\xi},t)$ and $X_2(\underline{\xi},t)$. Such plots give a clear conceptual picture of the shear effect, and offer easy comparisons with other related phenomena, such as fluid particle diffusion on isotropic turbulent fields, and molecular diffusion in the presence of shear. [Note that for the case of the convective dispersion from a point source of $\Theta(\underline{x},t)$ without molecular diffusion, i.e. satisfying

$$\frac{\partial}{\partial t}\Theta + (\underline{u}\cdot\nabla)\Theta = 0,$$

the normalized mean value of Θ, say $\langle\Theta(\underline{x},t)\rangle_N$, is equal to

Reproduced with permission of the copyright owner. Further reproduction prohibited without permission.

$p_{X_1 X_2 X_3}(x_1, x_2, x_3; t)$, the probability density of fluid point displacement. This was explicitly shown (for example) by Corrsin (1961), and clearly was understood by Taylor (1921, 1935).

However, it was estimated (see Appendix B) that to compute $p_{X_1 X_2}(x_1, x_2; t)$ directly from the simulations would require a minimum of about 125,000 realizations to give a reasonable (10% of peak value) accuracy. This would have required far more computer time than was available.

Fortunately, an indirect method was of use in determining $p_{X_1 X_2}(x_1, x_2, t)$ approximately. It is a well known fact (e.g. Batchelor 1949, page 446) that if the component of a vector $\{X_1(\underline{o}, t), X_2(\underline{o}, t)\}$ in any arbitrary direction is normally distributed, then $X_1(\underline{o}, t)$ and $X_2(\underline{o}, t)$ are joint normally distributed. Furthermore, since the vector $\{X_1(\underline{o}, t), X_2(\underline{o}, t)\}$ had been recorded for each realization, then any component, say $R_\beta(t)$, of this vector (say at an angle β with respect to the x_1-axis) can be computed using

$$R_\beta(t) = X_1(\underline{o}, t) \cos\beta + X_2(\underline{o}, t) \sin\beta \qquad (25)$$

One point probability densities [e.g., $p_{R_\beta}(r; t)$, the probability density of $R_\beta(t)$] were accurately attainable (to within 7% of peak value) with 2000 realizations, so that it was possible to compute $p_{R_\beta}(r; t)$ for any value of β.

The above observation cannot be used to prove that $X_1(\underline{o}, t)$

Reproduced with permission of the copyright owner. Further reproduction prohibited without permission.

and $X_2(\varrho,t)$ are joint normally distributed in the simulations (though it could be used to establish that they are not), since $p_{R_\beta}(r;t)$ can only be measured for a few values of β (because of limitations on computer time, etc.). However, if the densities for several arbitrary β's were found to be essentially normal, it can be inferred that the joint distribution of $X_1(\varrho,t)$ and $X_2(\varrho,t)$ is at least approximately normal, and the constant contours of $p_{X_1X_2}(x_1,x_2;t)$ can be approximated by ellipses, appropriate to a joint normal density.

Figures 36 and 37 show the probability distributions of $R_\beta(t)$ at angles β = 0°, 45°, 90°, and 135°, for two different values of time. A straight line on the plots corresponds to a "normal" distribution. It is seen that, over the range from about 2% to 98%, the distributions of $R_\beta(t)$ for each β are nearly normal. The scatter in the "tails" is due to the large errors involved in computing the relative magnitudes of these relatively rare "events".

These plots are characteristic of the same type of plots for other points in time. Thus it was concluded that the distribution of $X_1(\varrho,t)$ and $X_2(\varrho,t)$ was approximately joint normal for all times covered in the simulations. Since $\langle X_i(\varrho,t)X_j(\varrho,t)\rangle$ is available, the approximate form of $p_{X_1X_2}(x_1,x_2;t)$ is known as a function of time. Figures 38 and 39 are plots of the corresponding isoprobability contours for a sequence of times. For each t, the curve

$$\frac{p_{X_1X_2}(x_1,x_2;t)}{p_{X_1X_2}(0,0;t)} = e^{-1/2} \tag{26}$$

Reproduced with permission of the copyright owner. Further reproduction prohibited without permission.

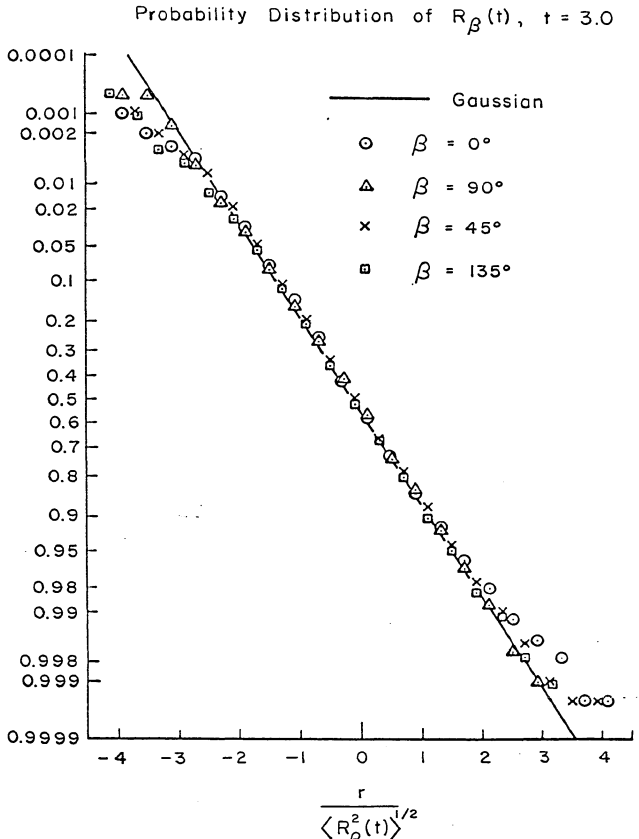

Figure 36.

Reproduced with permission of the copyright owner. Further reproduction prohibited without permission.

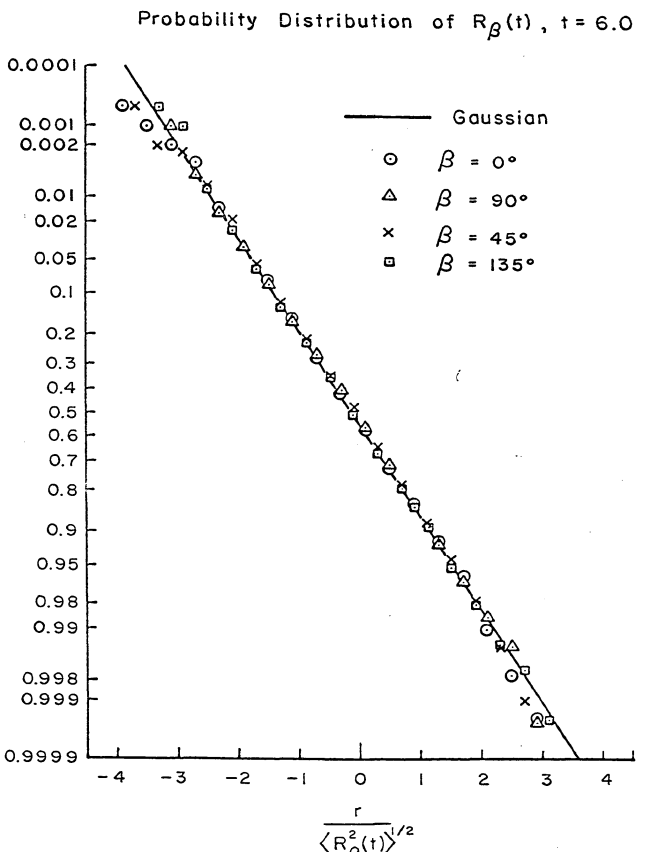

Figure 37.

Reproduced with permission of the copyright owner. Further reproduction prohibited without permission.

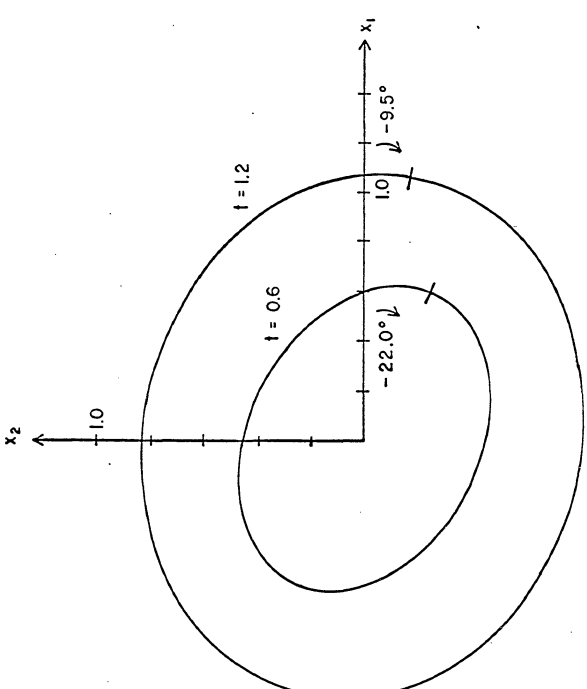

Figure 38. Contours of constant displacement probability in the x_1x_2 plane, for "short" and "moderate" times (see equation (28)).

Reproduced with permission of the copyright owner. Further reproduction prohibited without permission.

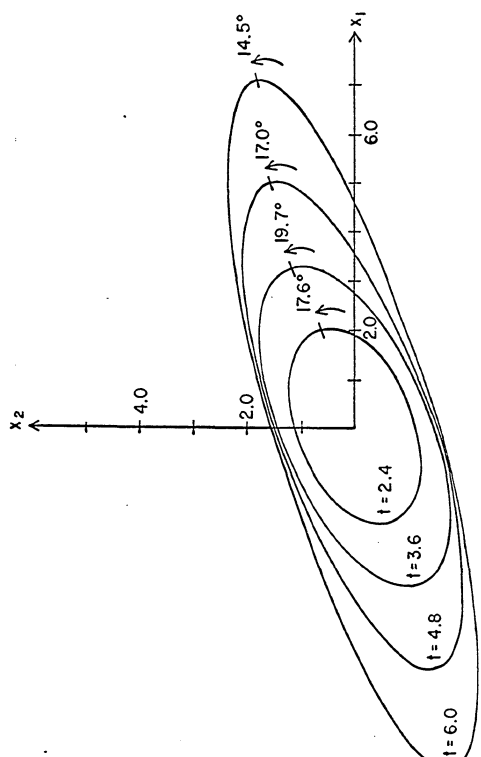

Figure 39. Contours of constant displacement probability in the x_1x_2 plane, for "moderate" to "long" times (see equation (28)).

Reproduced with permission of the copyright owner. Further reproduction prohibited without permission.

is plotted.

Since the densities are assumed joint normal,

$$\underset{X_1 X_2}{p}(x_1, x_2; t) = \frac{1}{2\pi\sigma_1\sigma_2\sqrt{1-\rho^2}} \exp\left\{\frac{-1}{2(1-\rho^2)}\left[\frac{x_1^2}{\sigma_1^2} - \frac{2\rho x_1 x_2}{\sigma_1\sigma_2} + \frac{x_2^2}{\sigma_2^2}\right]\right\} \qquad (27)$$

where $\sigma_1^2 \equiv \langle X_1^2(\underline{o},t)\rangle$, $\sigma_2^2 \equiv \langle X_2^2(\underline{o},t)\rangle$, and $\rho \equiv \dfrac{\langle X_1(\underline{o},t) X_2(\underline{o},t)\rangle}{\sigma_1\sigma_2}$.

Thus (26) is

$$\exp\left\{\frac{-1}{2(1-\rho^2)}\left[\frac{x_1^2}{\sigma_1^2} - \frac{2\rho x_1 x_2}{\sigma_1\sigma_2} + \frac{x_2^2}{\sigma_2^2}\right]\right\} = \exp(-1/2),$$

or,

$$\frac{x_1^2}{\sigma_1^2} - \frac{2\rho x_1 x_2}{\sigma_1\sigma_2} + \frac{x_2^2}{\sigma_2^2} = \sqrt{1-\rho^2}\,. \qquad (28)$$

This is the equation for an ellipse, with principal axis angles

$$\alpha = \frac{1}{2}\tan^{-1}\left\{\frac{2\rho\sigma_1\sigma_2}{\sigma_1^2 - \sigma_2^2}\right\}, \qquad (29)$$

which also defines the principal axes of $\langle X_i(\underline{o},t) X_j(\underline{o},t)\rangle$ [equation (21)]. The major and minor axes of the ellipse are the principal values of the tensor $\langle X_i(\underline{o},t) X_j(\underline{o},t)\rangle$.

The principal axes of these ellipses are initially (t = 0) oriented with the principal axes of the Reynolds stress tensor [equation (22)]. As time goes on, the tilt of the major axis tends to zero as the effect of the mean velocity begins to predominate.

In contrast, for simple Brownian motion or molecular diffusion, the major axis is always located in the first quadrant.

Reproduced with permission of the copyright owner. Further reproduction prohibited without permission.

This emphasizes the well-known fact that molecular type analyses must be used with caution (in fact, are wrong in principle) when applied to turbulent diffusion for short and moderate times. There is further discussion of this point in the later section on turbulent diffusivities.

For longer times, the tilt of the major axis goes positive, reaches a maximum, and asymptotically goes to zero as the isoprobability contours are being simultaneously elongated by the mean velocity gradient. The long time asymptotic behavior is qualitatively like that of molecular diffusion (e.g., see Elrick 1962).

4. Statistical Properties of the Lagrangian Velocity Autocorrelation Coefficients

Figure 40 shows fluid particle velocity autocorrelation coefficients $\mathcal{R}_{F_{11}}(\tau)$, $\mathcal{R}_{F_{22}}(\tau)$, and $\mathcal{R}_{F_{33}}(\tau)$ [see equation (3) for the definition of $\mathcal{R}_{F_{ij}}(\tau)$]. As in the case of the Eulerian field (figure 13), the correlations are approximately equal, differences being less than the maximum error or 0.07. The integral scales were found to be $\mathcal{T}_{F_{11}} = 0.614$, $\mathcal{T}_{F_{22}} = 0.545$, and $\mathcal{T}_{F_{33}} = 0.543$. The Taylor-type microscales, defined by

$$\gamma_{F_{ij}} = \sqrt{\frac{-2}{\mathcal{R}''_{F_{ij}}(0)}}, \tag{30}$$

were found to be $\gamma_{F_{11}} = 0.347$, $\gamma_{F_{22}} = 0.254$, and $\gamma_{F_{33}} = 0.310$.

Figure 41 is a comparison of the fluid particle velocity autocorrelation, $\mathcal{R}_{F_{22}}(\tau)$, and the Eulerian velocity autocorrelation coefficient, $\frac{\langle v'_2(\xi,t)\, v'_2(\xi,t+\tau)\rangle}{\langle v'^2_2(\xi,t)\rangle}$. The result is that the Eulerian

Reproduced with permission of the copyright owner. Further reproduction prohibited without permission.

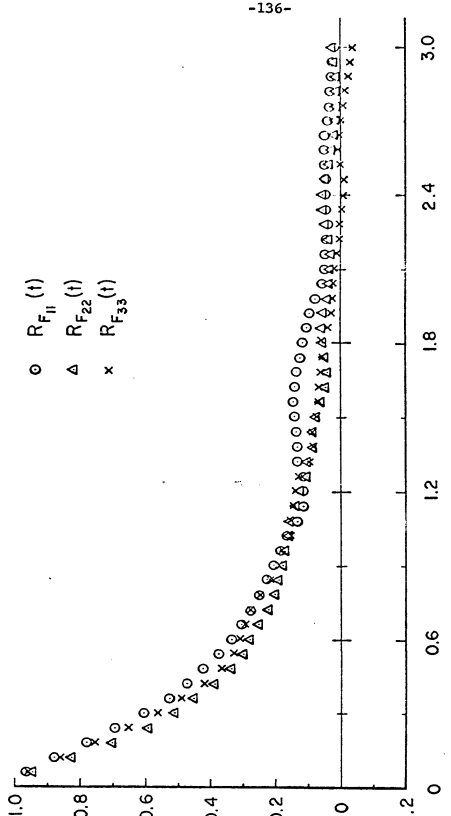

Figure 40. Fluid particle velocity autocorrelation coefficients for the shear flow simulations.

Reproduced with permission of the copyright owner. Further reproduction prohibited without permission.

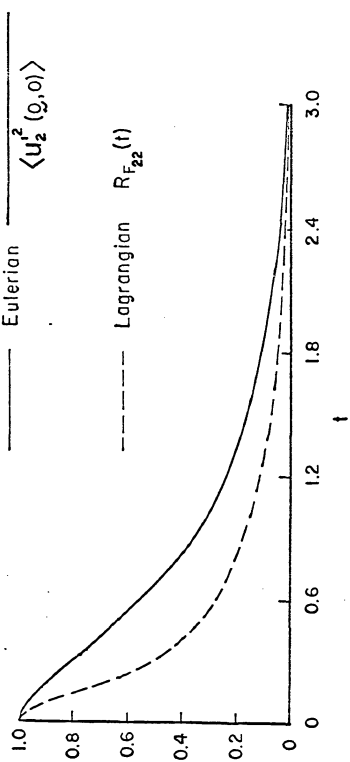

Figure 41. A comparison of a one-point Eulerian time autocorrelation coefficient and a fluid particle velocity autocorrelation coefficient for the shear flow simulations.

Reproduced with permission of the copyright owner. Further reproduction prohibited without permission.

correlation falls off much slower than the fluid particle correlation. This is also qualitatively the same in the isotropic case, mentioned below (see figure 51). However, Shlien's (1971) recent wind tunnel measurements indicate the opposite. For instance, he found that the fluid particle velocity microscales were much larger than the Eulerian velocity microscales. However, in our case, $\gamma_{F_{22}}$ = 0.254, while $\gamma_{E_{22}}$ = 0.525, just the reverse. (The same is true in the isotropic case. See section B.1 below.) Also, some intuitive arguments (e.g. Corrsin 1963) indicate that the velocity following a fluid point would on the average be more persistant than the velocity at a fixed point (in a coordinate system with no mean velocity at that point).

Thus we suspect that the results presented in figure 41 are unrealistic, and are probably due to the neglect of the non-linear terms in the Navier-Stokes equations in the model (since the Fourier modes that make up the Eulerian velocity field are not allowed to interact). This aspect of the Euler-Lagrange problem has, however, not been resolved, and in fact our results are in qualitative agreement with arguments put forth by Kraichnan (1964), Peskin (1965), and others.

Figure 42 is a graph of the fluid particle velocity cross-correlation $\mathcal{R}_{F_{12}}(\tau)$ and the Eulerian cross-correlation $\frac{\langle u_1'(\xi,t)\, u_2'(\xi,t+\tau)\rangle}{\langle u_1'(\xi,t)\, u_2'(\xi,t)\rangle}$. Integral scales were found to be $\mathcal{T}_{F_{12}}$ = 0.627 ($\tau > 0$) and $\mathcal{T}_{F_{21}}$ = 0.808 ($\tau < 0$). Note that the fluid material velocity cross-correlation has basically the same symmetry properties near the origin as does

Reproduced with permission of the copyright owner. Further reproduction prohibited without permission.

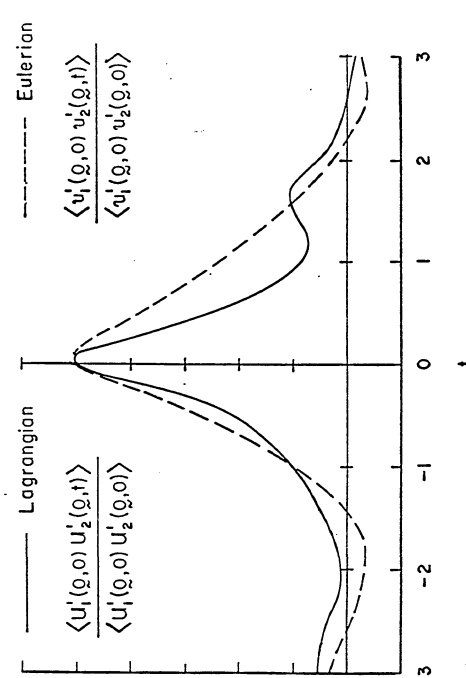

Figure 42. A comparison of the normalized one-point Eulerian time cross-correlation and the normalized fluid particle velocity cross-correlation for the shear flow simulations.

Reproduced with permission of the copyright owner. Further reproduction prohibited without permission.

the Eulerian cross-correlation -- they both peak at $\tau > 0$.

5. Turbulent Diffusivities

It is both interesting and instructive to compute the turbulent diffusivities for the case of a homogeneous, stationary shear flow. It is well known (e.g., Hinze 1959, chapter 5) that, in many cases, the use of turbulent diffusivities gives good predictions of, for example, mean temperature in problems of heat diffusion in turbulent flows (although several adjustable parameters are usually involved). However it has also been pointed out (Batchelor 1950), perhaps not often enough, that the use of turbulent diffusivities is wrong in principle.

Turbulent diffusivities, say $\mathcal{K}_{ij}(t)$ (assuming they are a function of time t alone for this homogeneous flow), are usually defined in the following manner. Assume that $\theta(\underline{x},t)$ (for example temperature or chemical concentration) satisfies the following conservation equation:

$$\frac{\partial}{\partial t}\theta + (\underline{u}\cdot\nabla)\theta = 0 , \tag{31}$$

where the usual molecular diffusivity term has been neglected. Decomposing $\theta(\underline{x},t)$ and $\underline{u}(\underline{x},t)$ into mean and fluctuating parts,

$$\theta(\underline{x},t) = \langle\theta(\underline{x},t)\rangle + \theta'(\underline{x},t) \tag{32}$$

$$\underline{u}(\underline{x},t) = \langle\underline{u}(\underline{x},t)\rangle + \underline{u}'(\underline{x},t) , \tag{33}$$

Reproduced with permission of the copyright owner. Further reproduction prohibited without permission.

substituting (32) and (33) into (31) and averaging gives (with $\nabla \cdot \underline{u}' = 0$):

$$\left\{\frac{\partial}{\partial t} + \langle \underline{u}(\underline{x},t)\rangle \cdot \nabla \right\} \langle \theta(\underline{x},t)\rangle = -\nabla \cdot \left\{ \langle \underline{u}'(\underline{x},t)\theta'(\underline{x},t)\rangle \right\} . \quad (34)$$

In attempting to close this equation, it is sometimes assumed that

$$-\langle u_i'(\underline{x},t)\theta'(\underline{x},t)\rangle = \mathcal{K}_{ij}(\underline{x},t) \frac{\partial}{\partial x_j} \langle \theta(\underline{x},t)\rangle \quad (35)$$

(although one set of unknowns, $\langle u_i'\theta\rangle$, has been traded for another, $\mathcal{K}_{ij}$).

Note that gradient transport assumptions of this type are valid in principle only when the characteristic length scale of $\langle \theta(\underline{x},t)\rangle$, say L_θ , is much greater than the characteristic length scale of the transporting mechanism, which in this case can be taken to be an Eulerian integral length scale, say L_f . In most problems of interest,

$$L_f \simeq O(L_\theta) ,$$

so that equation (35) is wrong in principle.

It can also be shown that, in general, the equation for $\langle \theta(\underline{x},t)\rangle$ must be a functional differential equation (e.g., Roberts 1959).

At any rate, substituting (35) into (34) gives, for a statistically homogeneous flow,

Reproduced with permission of the copyright owner. Further reproduction prohibited without permission.

$$\left\{\frac{\partial}{\partial t} + \langle \underline{u}(\underline{x},t)\rangle \cdot \nabla\right\} \langle \theta(\underline{x},t)\rangle = \kappa_{ij}(t) \frac{\partial^2}{\partial x_i \partial x_j} \langle \theta(\underline{x},t)\rangle . \qquad (36)$$

This is the so-called diffusion equation for $\langle \theta(\underline{x},t)\rangle$, which has been investigated extensively from all points of view, and for various forms for $\langle \underline{u}(\underline{x},t)\rangle$, $\kappa_{ij}(t)$, and the initial and boundary conditions satisfied by $\langle \theta(\underline{x},t)\rangle$. (See, for example, Jost 1952, Lauwerier 1953, Crank 1956, Novikov 1958, and Elrich 1962.)

To compute $\kappa_{ij}(t)$ in the present case, we recall that

$$\langle \theta(\underline{x},t)\rangle = p_{\underline{X}}(\underline{x};t) ,$$

the displacement probability density. Therefore the dispersion tensor $\langle X_i(\underline{a},t) X_j(\underline{a},t)\rangle$ can be computed as the second moment,

$$\sigma_{ij}(t) = \int_{\underline{x}} \langle \theta(\underline{x},t)\rangle x_i x_j \, d\underline{x} , \qquad (37)$$

where $\langle \theta(\underline{x},t)\rangle$ is the analytical solution of equation (36). But we have already computed directly the dispersion tensor (section A.2). Thus, to evaluate $\kappa_{ij}(t)$, we equate $\sigma_{ij}(t)$ and $\langle X_i(\underline{a},t) X_j(\underline{a},t)\rangle$.

Instead of equating the actual mean (temperature) solution of (36) to the probability density of displacement, we equate only their respective second moments. If $\langle \theta(\underline{x},t)\rangle$ and $p_{\underline{X}}(\underline{x};t)$ were Gaussian, our approach would of course be

Reproduced with permission of the copyright owner. Further reproduction prohibited without permission.

equivalent to equating $\langle \theta(\underline{x},t)\rangle$ and $\bar{\theta}(\underline{x},t)$. In any case, if $\langle \theta(\underline{x},t)\rangle = \bar{\theta}(\underline{x},t)$, then $\sigma_{ij}(t) = \langle \Sigma_i(\underline{\rho},t)\Sigma_j(\underline{\rho},t)\rangle$.

In our case, $\langle u(\underline{x},t)\rangle = \left(\frac{dU_1}{dx_2}\right) x_2 \hat{i}_1$. Multiplying equation (36) by x_1^2, and integrating over all space gives, with (37),

$$\frac{d}{dt}\sigma_{11} - 2\left(\frac{dU_1}{dx_2}\right)\sigma_{12} = 2\varkappa_{11} \tag{38}$$

The same procedure with x_1x_2, x_2^2, and x_3^2 gives

$$\frac{d}{dt}\sigma_{12} - \left(\frac{dU_1}{dx_2}\right)\sigma_{22} = \varkappa_{21} + \varkappa_{12} \tag{39}$$

$$\frac{d}{dt}\sigma_{22} = 2\varkappa_{22} \tag{40}$$

$$\frac{d}{dt}\sigma_{33} = 2\varkappa_{33}. \tag{41}$$

With the identifications made above, these expressions imply

$$\frac{d}{dt}\langle \Sigma_1^2(\underline{\rho},t)\rangle - 2\left(\frac{dU_1}{dx_2}\right)\langle \Sigma_1(\underline{\rho},t)\Sigma_2(\underline{\rho},t)\rangle = 2\varkappa_{11} \tag{42}$$

$$\frac{d}{dt}\langle \Sigma_1(\underline{\rho},t)\Sigma_2(\underline{\rho},t)\rangle = \left(\frac{dU_1}{dx_2}\right)\langle \Sigma_2^2(\underline{\rho},t)\rangle + \varkappa_{12} + \varkappa_{21} \tag{43}$$

$$\frac{d}{dt}\langle \Sigma_2^2(\underline{\rho},t)\rangle = 2\varkappa_{22} \tag{44}$$

$$\frac{d}{dt}\langle \Sigma_3^2(\underline{\rho},t)\rangle = 2\varkappa_{33}. \tag{45}$$

Reproduced with permission of the copyright owner. Further reproduction prohibited without permission.

Note that when $\left(\frac{dU_1}{dx_2}\right) = 0$, the case without shear, these expressions reduce to

$$\frac{d}{dt}\langle X_i X_j \rangle = K_{ij} + K_{ji} \quad ,$$

as presented by Batchelor (1949).

The fluid particle position vector equations,

$$\frac{\partial}{\partial t}\underline{X}(\underline{a},t) = \left(\frac{dU_1}{dx_2}\right) X_2(\underline{a},t)\, \underline{i}_1 + \underline{U}'(\underline{a},t) \qquad (46)$$

has x_1-component

$$\frac{\partial}{\partial t} X_1(\underline{a},t) = \left(\frac{dU_1}{dx_2}\right) X_2(\underline{a},t) + U_1'(\underline{a},t),$$

so that (42) reduces to

$$K_{11}(t) = \langle U_1'(\underline{a},t) X_1(\underline{a},t) \rangle. \qquad (47)$$

Similarly

$$K_{12}(t) + K_{21}(t) = \langle U_1'(\underline{a},t) X_2(\underline{a},t) \rangle + \langle U_2'(\underline{a},t) X_1(\underline{a},t) \rangle, \qquad (48)$$

$$K_{22}(t) = \langle U_2'(\underline{a},t) X_2(\underline{a},t) \rangle, \qquad (49)$$

and

$$K_{33}(t) = \langle U_3'(\underline{a},t) X_3(\underline{a},t) \rangle. \qquad (50)$$

Substituting appropriate components of (46) into (47) to (50), integrating by parts, and using the fluid particle velocity correlation

Reproduced with permission of the copyright owner. Further reproduction prohibited without permission.

coefficients defined by equation (3), we find

$$\mathcal{K}_{11}(t) = \langle U_1'^2(\varrho,t)\rangle \int_0^t R_{F_{11}}(\tau)\,d\tau + \left(\frac{dU_1}{dx_2}\right)\langle U_1'(\varrho,t)U_2'(\varrho,t)\rangle \int_0^t \tau R_{F_{12}}(\tau)\,d\tau \tag{51}$$

$$\mathcal{K}_{12}(t) + \mathcal{K}_{21}(t) = \langle U_1'(\varrho,t)U_2'(\varrho,t)\rangle \int_0^t [R_{F_{12}}(\tau) + R_{F_{21}}(\tau)]\,d\tau + \left(\frac{dU_1}{dx_2}\right)\langle U_2'^2(\varrho,t)\rangle \int_0^t \tau R_{F_{22}}(\tau)\,d\tau \tag{52}$$

$$\mathcal{K}_{22}(t) = \langle U_2'^2(\varrho,t)\rangle \int_0^t R_{F_{22}}(\tau)\,d\tau \tag{53}$$

$$\mathcal{K}_{33}(t) = \langle U_3'^2(\varrho,t)\rangle \int_0^t R_{F_{33}}(\tau)\,d\tau. \tag{54}$$

These expressions are time dependent and tend to constants only for large times. Also, the usual (unsheared) homogeneous flow expressions for $\mathcal{K}_{ij}(t)$ are modified by the presence of the $\left(\frac{dU}{dx_2}\right)$ terms.

Figures 43, 44, and 45 are plots of the diffusivities measured in the simulations, actually using expressions (47) to (50) in the computations. Unfortunately there is a large degree of scatter in the results.

This scatter can be explained, using the error analysis in Appendix B. In Appendix B, it is shown that, in a computation of the mean value of a random function $\phi(t)$, the resulting error bound E_N is approximately

$$E_N = \sigma_\phi(t)\sqrt{\frac{10}{N}} \tag{55}$$

Reproduced with permission of the copyright owner. Further reproduction prohibited without permission.

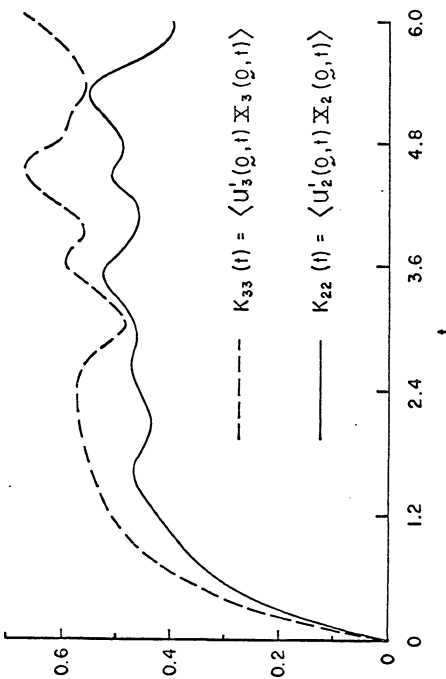

Figure 43. The turbulent diffusivities $\mathcal{K}_{22}(t)$ and $\mathcal{K}_{33}(t)$ computed from the shear flow simulations using equations (49) and (50).

Reproduced with permission of the copyright owner. Further reproduction prohibited without permission.

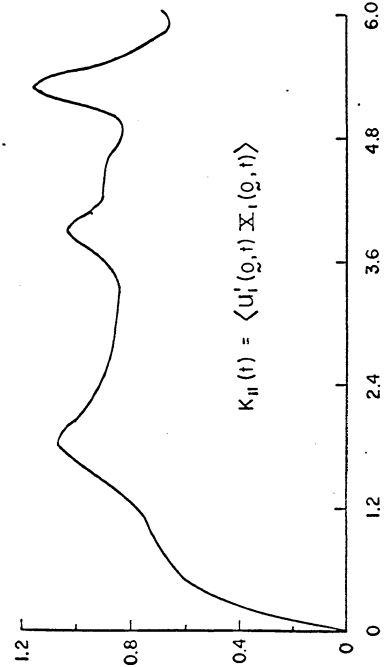

Figure 44. The turbulent diffusivity $\mathcal{K}_{11}(t)$ computed from the shear flow simulations using equation (47).

Reproduced with permission of the copyright owner. Further reproduction prohibited without permission.

Reproduced with permission of the copyright owner. Further reproduction prohibited without permission.

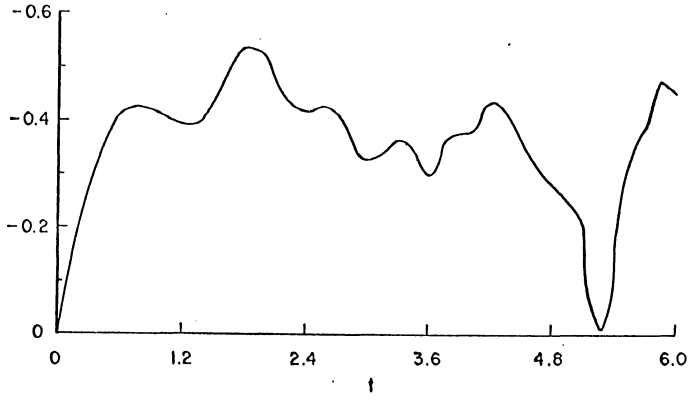

Figure 45. The turbulent diffusivity $K_{12}(t) + K_{21}(t)$ computed from the simulations using equation (48).

where $\sigma_\phi(t)$ is the standard deviation of $\phi(t)$, and N the sample size.

Consider the random variable

$$\phi(t) = u(t)\,\chi(t) \quad \text{, where} \tag{56}$$

$$\chi(t) = \int_0^t u(t_1)\,dt_1 . \tag{57}$$

Now $$\langle \phi(t) \rangle = \langle u(t)\chi(t) \rangle = \langle u^2(t) \rangle \int_0^t R(\tau)\,d\tau , \tag{58}$$

where $R(\tau)$ is the autocorrelation coefficient of $u(t)$ (which is assumed stationary). So

$$\langle \phi(t) \rangle \longrightarrow \langle u^2(t) \rangle\, T \quad \text{as} \quad t \to \infty , \tag{59}$$

where T is the integral scale of $u(t)$. Also

$$\langle \phi^2(t) \rangle = \langle u^2(t)\chi^2(t) \rangle = \int_0^t \int_0^t \langle u^2(t)u(t_1)u(t_2) \rangle\, dt_1\, dt_2 . \tag{60}$$

Making the "quasi-normal" hypothesis

$$\langle u^2(t)u(t_1)u(t_2) \rangle = \langle u^2(t) \rangle^2 \left\{ R(t_2 - t_1) + 2R(t - t_1)R(t - t_2) \right\}, \tag{61}$$

and using integration by parts gives:

$$\langle \phi^2(t) \rangle = 2\langle u^2(t) \rangle^2 \left\{ \int_0^t (t - \tau)R(\tau)\,d\tau + \left[\int_0^t R(\tau)\,d\tau \right]^2 \right\} \tag{62}$$

Reproduced with permission of the copyright owner. Further reproduction prohibited without permission.

Thus $\langle \phi'^2(t) \rangle \longrightarrow 2\langle u^2(t) \rangle^2 T t \quad as \quad t \to \infty.$ (63)

So the standard deviation of $\phi(t)$, defined by

$$\sigma_\phi(t) = \left\{ \langle \phi^2(t) \rangle - \langle \phi(t) \rangle^2 \right\}^{1/2} \tag{64}$$

goes as $\sigma_\phi(t) \longrightarrow \langle u^2(t) \rangle (2tT)^{1/2} = \langle u^2(t) \rangle T \left(\frac{2t}{T}\right)^{1/2}$ as $t \to \infty$. (65)

From (55), the error bound E_N goes as

$$E_N \longrightarrow \langle u^2(t) \rangle T \left(\frac{2t}{T} \frac{10}{N}\right)^{1/2}, \tag{66}$$

and the relative error bound, $E_R = \dfrac{E_N}{\langle \phi(t) \rangle}$, as [using (59)]

$$E_R \longrightarrow \left(\frac{20\,t}{NT}\right)^{1/2}. \tag{67}$$

Thus the relative error in a measurement of $\langle u(t) u(t) \rangle$ diverges as $t \to \infty$. And so the scatter in computing the values of $K_{ij}(t)$ [see equations (47) to (50)].

Crude estimates of $K_{ij}(t)$ for "large" t (say K_{ij}^{∞}) were obtained from the plots. They were

$$K_{ij}^{\infty} + K_{ji}^{\infty} \doteq \begin{pmatrix} 1.80 & -0.40 & 0 \\ -0.40 & 0.94 & 0 \\ 0 & 0 & 1.10 \end{pmatrix} \tag{68}$$

Reproduced with permission of the copyright owner. Further reproduction prohibited without permission.

The principal axes of ($\kappa_{ij}^{\infty} + \kappa_{ji}^{\infty}$) in the x_1x_2 plane are thus:

$$\alpha_{\kappa} \equiv \frac{1}{2}\tan^{-1}\left\{\frac{2(\kappa_{12}+\kappa_{21})}{2\kappa_{11}-2\kappa_{22}}\right\} \doteq -43°, 47°. \qquad (69)$$

6. Simulation of Plume Dispersion Experiments

In a typical wind tunnel measurement of turbulent dispersion, a heated wire is stretched normal to the direction of the mean velocity (say the x_1 direction), and mean temperature measurements are taken in the heated air plume, along an axis (say the x_2

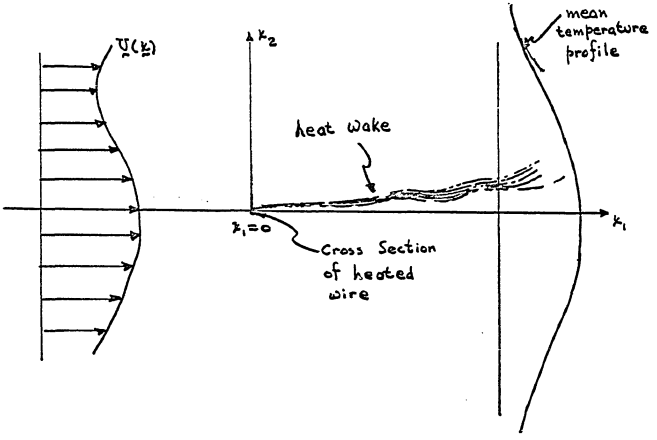

Figure 46.

Reproduced with permission of the copyright owner. Further reproduction prohibited without permission.

axis) normal to the mean flow, at various distances x_1 = D downstream from the heated wire. (See figure 46.) If possible, the wire is usually positioned so that the flow field is statistically homogeneous in the direction of the axis of the wire (x_3).

The result of the measurement is not $f_{I_2}(x_2;t)$, the probability density of displacement in the x_2 direction as a function of time, but $f_{I_2}(x_2/x_1=D)$, the probability density of $I_2(\varrho,t)$, conditional on x_1 = D. Only in special cases, for instance for homogeneous flows (with uniform mean velocity U say) at low turbulence levels, are these two densities approximately the same (with t = D/U). (See, for example, Frenkiel 1953.)

This type of measurement is easily simulated by (i) adding the effect of a constant mean velocity (U_0) to the results for each realization, (ii) recording $I_2(\varrho,t)$ and $U_2'(\varrho,t)$ for each particle when it reaches the plane x_1 = D, and (iii) having completed (i) and (ii) for various values of D, computing statistics from this newly created ensemble. Thus various statistics for $I_2(\varrho,t)$ and $U_2'(\varrho,t)$ were obtained, conditional on x_1 = D.

This allowed comparison of the statistics of $I_2(\varrho,t)$ and $U_2'(\varrho,t)$ conditional on x_1 = D, with those of $I_2(\varrho,t)$ and $U_2'(\varrho,t)$ when $t = D/U_0$. It also allowed comparisons of simulation results with laboratory measurements. For example, Hinze and van der Hegge Zijnen (1951) measured mean temperature downstream of a heated wire in the shear turbulence of a free jet. Their results (and theoretical analysis) indicated that, for "short" times,

Reproduced with permission of the copyright owner. Further reproduction prohibited without permission.

(i) the centroid of the mean temperature profile was displaced slightly in the direction of greater mean velocity, and (ii) the skewness factor was such that the spread of the mean temperature was also greatest in this direction. Corrsin (1953) has also suggested that, for "long" times, the skewness factor will be such that the spread of the mean temperature will be greater in the direction opposite that of greater mean velocity.

For notational convenience, let $Y(D)$ and $V(D)$ represent the position $X_2(\underline{0},t)$ and velocity $U_2'(\underline{0},t)$ of a fluid particle as it passes through the plane $x_1 = D$. It is the joint statistics of $Y(D)$ and $V(D)$ that are obtained in the conditional measurements mentioned above. For example, $f_Y(x_2;D)$, the probability density of $Y(D)$, equals $f_{X_2}(x_2/x_1=D)$.

Figures 47, 48, and 49 show typical plots of the probability densities $f_Y(x_2;D)$ and $f_{X_2}(x_2;D/U_0)$ for $U_0 = 10.0$ (and hence "turbulence level" $\langle u_1'^2\rangle^{1/2}/U_0 \doteq 13.5\%$), and for D = 6.0, 12.0, and 18.0 respectively. In each plot, the two density functions are quite close, and the two skewness effects mentioned above are not noticeable. For "short" times, the effect observed by Hinze and van der Hegge Zijnen is below the "noise level" of our measurements. The "long" time effect suggested by Corrsin depends on the non-dimensional parameter $\frac{\langle u_2'^2\rangle T_{F_{22}}^2}{U_0^2}\left(\frac{dU_1}{dx_2}\right)^2 \frac{x_1}{U_0 T_{F_{22}}}$ (Lauwerier 1951). It was not possible to increase this parameter so that the suggested skewness was appreciable.

Table 2 compares moments of $Y(D)$ and $V(D)$ with the

Reproduced with permission of the copyright owner. Further reproduction prohibited without permission.

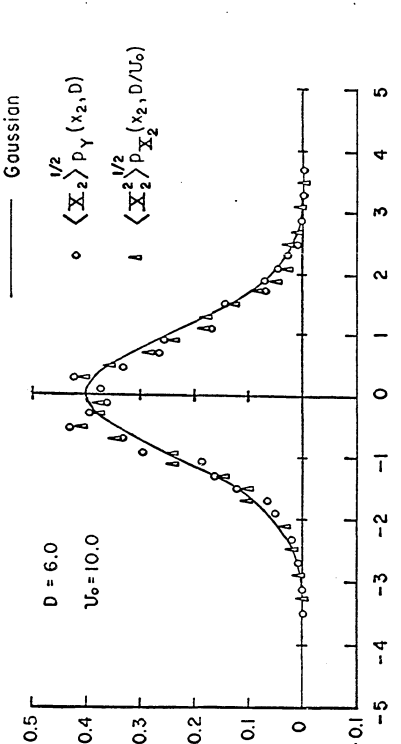

Figure 47. The displacement probability densities $P_Y(x_2; D)$ and $P_{X_2}(x_2; \frac{D}{U_0})$ for U_0 = 10.0 and D = 6.0.

Reproduced with permission of the copyright owner. Further reproduction prohibited without permission.

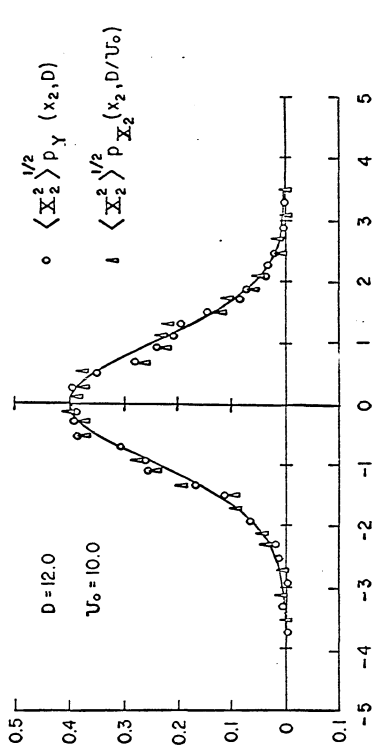

Figure 48. The displacement probability densities $f_\beta(x_2; D)$ and $f_{\Sigma_t}(x_2; \frac{D}{U_0})$ for U_0 = 10.0 and D = 12.0.

Reproduced with permission of the copyright owner. Further reproduction prohibited without permission.

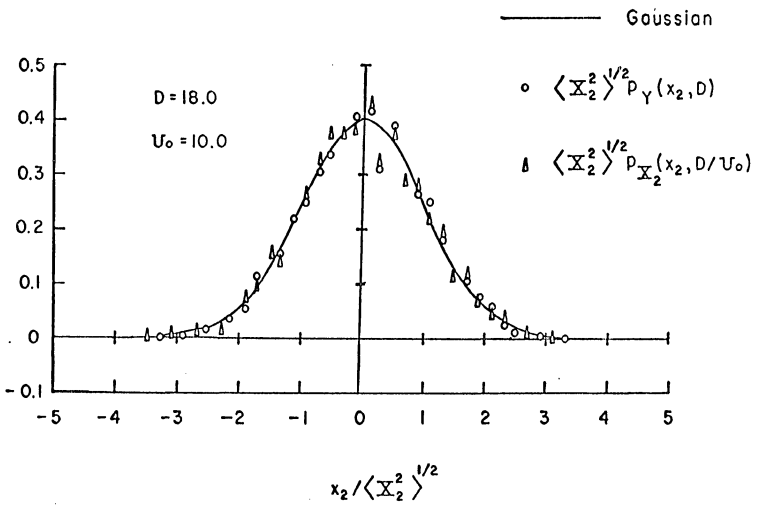

Figure 49. The displacement probability densities $p_Y(x_2; D)$ and $p_{X_2}(x_2; \frac{D}{U_0})$ for U_0 = 10.0 and D = 18.0.

Reproduced with permission of the copyright owner. Further reproduction prohibited without permission.

D	$\langle Y(D)\rangle$	$\langle Y^2(D)\rangle$	$\langle Y^3(D)\rangle$	$\frac{\langle Y^3(D)\rangle}{\langle Y^2(D)\rangle^{3/2}}$	$\langle V(o)V(D)\rangle$	$\langle \Sigma_2(o,\frac{D}{U_o})\rangle$	$\langle \Sigma_2^2(o,\frac{D}{U_o})\rangle$	$\langle \Sigma_2^3(o,\frac{D}{U_o})\rangle$	$\frac{\langle \Sigma_2^3(o,\frac{D}{U_o})\rangle}{\langle \Sigma_2^2(o,\frac{D}{U_o})\rangle^{3/2}}$	$\langle U_2'(o,\varepsilon)U_2'(o,\frac{D}{U_o})\rangle$
0.6	0.00242	0.00323	0.0000945	0.515	0.802	-0.000975	0.00305	-.0000197	-0.1171	0.809
6.0	0.00613	0.229	0.0229	0.210	0.239	-0.0107	0.229	-.00813	-0.0743	0.240
12.0	0.00169	0.679	0.00215	0.00385	0.0984	-0.0115	0.675	-.0483	-0.0870	0.1031
18.0	0.0296	1.222	0.0727	0.0538	0.0314	0.00935	1.218	0.0207	0.0155	0.0522
24.0	0.0356	1.752	-.120	-.0516	0.0301	0.0248	1.753	-.0581	-0.0251	0.0461
30.0	0.0250	2.350	-.689	-.1916	0.0135	0.0219	2.317	-.167	-0.0475	0.0190

Table 2.

Reproduced with permission of the copyright owner. Further reproduction prohibited without permission.

corresponding moments of $\mathcal{I}_2(\varrho, \frac{D}{U_0})$ and $U_2'(\varrho, \frac{D}{U_0})$.

Hinze and van der Hegge Zijnen (1951) have shown that for "small" times, the displacement of the centroid of $f_y(x_2; D)$ is given by

$$\langle Y(D) \rangle \doteq -\frac{\gamma \langle U_1'(\varrho;t) U_2'(\varrho;t) \rangle}{U_0^2} D. \tag{70}$$

For the values D = 0.6 (which corresponds here to t = 0.06), using $\langle U_1'(\varrho;t) U_2'(\varrho;t) \rangle = -0.520$, and $U_0 = 10.0$, (70) yields

$$\langle Y(D) \rangle \doteq \frac{0.520}{100} \cdot 0.6 \doteq 0.0031,$$

which is close to the value of 0.00242 measured in the simulations.

Furthermore, there is a noticeable trend in the skewness $\frac{\langle Y^3(D) \rangle}{\langle Y^2(D) \rangle^{3/2}}$. The skewness begins positive, goes through zero, and becomes increasingly negative. This fact agrees with both the skewness effects mentioned above.

Finally, note that the computed values of $\langle Y^2(D) \rangle$ and $\langle V(D)V(D) \rangle$ agree very well with the computed values of $\langle \mathcal{I}_2^2(\varrho, \frac{D}{U_0}) \rangle$ and $\langle U_2'(0,0) U_2'(0, \frac{D}{U_0}) \rangle$.

Simulations for "alien" particle diffusion on the homogeneous, stationary shear flow have not been performed.

Reproduced with permission of the copyright owner. Further reproduction prohibited without permission.

B. Simulation Results for Fluid Particle and "Alien" Particle Dispersion on a Stationary, Isotropic Field

1. Fluid Particle Results

Simulations were completed for fluid particle and "alien" particle dispersion on the isotropic field. Note that the velocity field was defined (Chapter III) in a coordinate system moving with the mean velocity, so that in the simulations the Eulerian mean velocity was zero.

In the fluid particle case, an ensemble of 2000 realizations was computed, using the equations

$$\frac{\partial}{\partial t}\underset{\sim}{X}(\underset{\sim}{a},t) = \underset{\sim}{u}\left[\underset{\sim}{X}(\underset{\sim}{a},t),t\right] \;,\; \underset{\sim}{X}(\underset{\sim}{a},t_0) = \underset{\sim}{a} \qquad (71)$$

to track the particles, where $\underset{\sim}{u}(\underset{\sim}{x},t)$ denotes the Eulerian velocity field. The position $\underset{\sim}{X}(\underset{\sim}{a},t)$ and the velocity $\underset{\sim}{U}(\underset{\sim}{a},t)$ of the fluid particle (which was at $\underset{\sim}{a}$ at time t_0) were recorded as functions of (discrete) time for each realization, and ensemble averages were computed.

Autocorrelation coefficients of the Eulerian velocity and the (Lagrangian) fluid particle velocity are defined by

$$R_{E_{ij}}(\underset{\sim}{r},\tau) = \frac{\langle u_i(\underset{\sim}{x},t)\,u_j(\underset{\sim}{x}+\underset{\sim}{r},t+\tau)\rangle}{\langle u_i(\underset{\sim}{x},t)\,u_j(\underset{\sim}{x},t)\rangle} \qquad (72)$$

$$R_{\underset{\sim}{E}_{ij}}(\tau) = \frac{\langle U_i(\underset{\sim}{a},t)\,U_j(\underset{\sim}{a},t+\tau)\rangle}{\langle U_i(\underset{\sim}{a},t)\,U_j(\underset{\sim}{a},t)\rangle} \qquad (73)$$

Reproduced with permission of the copyright owner. Further reproduction prohibited without permission.

It was found that the mean position $\langle \underset{\sim}{X}(\underset{\sim}{a},t) \rangle$ and mean velocity $\langle \underset{\sim}{U}(\underset{\sim}{a},t) \rangle$ were $\underset{\sim}{0}$ to within the accuracy of the measurements. Thus in all the results discussed for this case, it will be assumed that

$$\langle \underset{\sim}{X}(\underset{\sim}{a},t) \rangle = \langle \underset{\sim}{U}(\underset{\sim}{a},t) \rangle = \underset{\sim}{0}. \tag{74}$$

Figure 50 is a plot of the fluid particle velocity autocorrelation coefficients $\mathcal{R}_{F_{11}}(\tau)$, $\mathcal{R}_{F_{22}}(\tau)$, and $\mathcal{R}_{F_{33}}(\tau)$. They should be identical, and are equal to within the accuracy of the measurements (± 0.07). The microscales, defined by

$$\tau_{F_{ij}} = \sqrt{\frac{-2}{\mathcal{R}_{F_{ij}}''(0)}} \tag{75}$$

were found to be $\tau_{F_{11}} = 0.379$, $\tau_{F_{22}} = 0.346$, and $\tau_{F_{33}} = 0.341$, while the integral scales, defined by

$$T_{F_{ij}} = \int_0^\infty \mathcal{R}_{F_{ij}}(\tau)\, d\tau \tag{76}$$

turned out to be approximately $T_{F_{11}} = 0.584$, $T_{F_{22}} = 0.618$, and $T_{F_{33}} = 0.565$.

Figure 51 compares the Eulerian velocity autocorrelation coefficient $\mathcal{R}_{\xi_{11}}(\underset{\sim}{a},t)$ with its fluid particle velocity counterpart $\mathcal{R}_{F_{11}}(\tau)$. Here again, as in the case of the homogeneous shear flow, the Eulerian correlation falls off slower than the fluid particle

Reproduced with permission of the copyright owner. Further reproduction prohibited without permission.

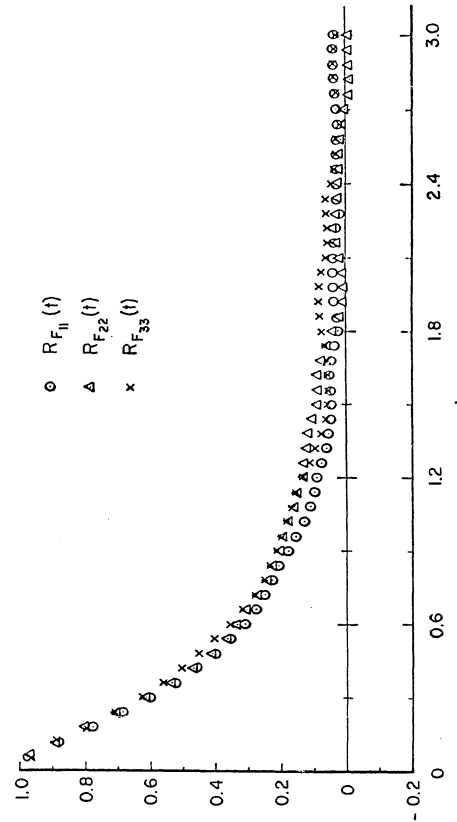

Figure 50. Fluid particle velocity autocorrelation coefficients for the isotropic flow simulations.

Reproduced with permission of the copyright owner. Further reproduction prohibited without permission.

Reproduced with permission of the copyright owner. Further reproduction prohibited without permission.

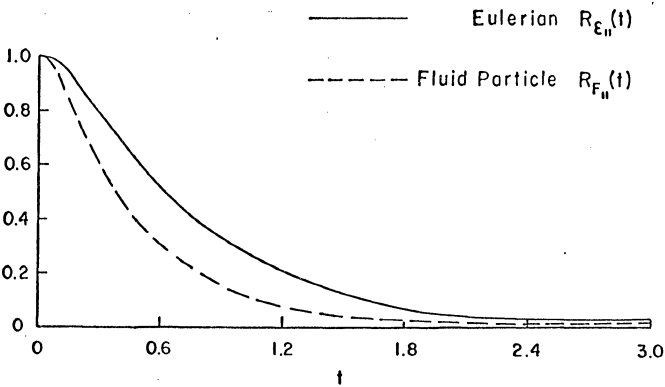

Figure 51. A comparison of the one-point Eulerian time autocorrelation coefficient $\mathcal{R}_{\varepsilon_{11}}(\varrho, t)$ and the fluid particle velocity autocorrelation coefficient $\mathcal{R}_{F_{11}}(t)$ for the isotropic flow simulations.

correlation. (See the discussion following figure 41.)

Figure 52 is a plot of the mean square displacements $\langle X_i^2(a,t)\rangle$ (no sum on i) along the three coordinate axes versus time. (Since the functions were almost identical, only one curve is shown.) With the values of $\langle U_1^2(a,0)\rangle = 0.771$, $\langle U_2^2(a,0)\rangle = 0.729$, and $\langle U_3^2(a,0)\rangle = 0.771$ measured in the simualtions (the differences in these values are do to statistical scatter), and $T_{E_{ij}}$ mentioned above, the simulation results exhibited the proper "short" time

$$\langle X_i^2(a,t)\rangle = \langle U_i^2(a,0)\rangle t^2 + O(t^3) \quad \text{(no sum on i)} \qquad (77)$$

and the "long" time

$$\langle X_i^2(a,t)\rangle \longrightarrow 2\langle U_i^2(a,0)\rangle T_{E_{ii}}\, t \quad \text{(no sum on i)} \qquad (78)$$

asymptotic behaviors (Taylor 1921).

2. "Alien" Particle Results

a. Introduction

In the "alien" particle case, the equations (see Chapter IV)

$$\frac{\partial}{\partial t}\underline{V}(b,t) + \alpha\left\{\underline{V}(b,t) - \underline{u}\left[\underline{Y}(b,t),t\right]\right\} = \frac{g}{\nu} + \alpha\frac{\partial}{\partial t}\underline{u}\left[\underline{Y}(b,t),t\right] \qquad (79)$$

$$\frac{\partial}{\partial t}\underline{Y}(b,t) = \underline{V}(b,t) \qquad (80)$$

Reproduced with permission of the copyright owner. Further reproduction prohibited without permission.

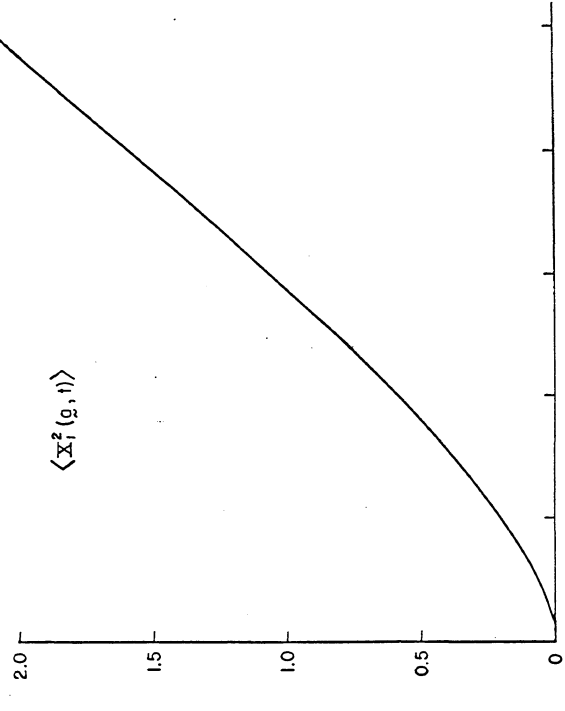

Figure 52. Fluid particle dispersion for the isotropic model flow.

Reproduced with permission of the copyright owner. Further reproduction prohibited without permission.

were used to track the particles. α^{-1} is the "relaxation" time of the particle, and $\underset{\sim}{g}$ the effective (net) gravity force. The parameter κ determines how well the particles react to accelerations in the fluid. In all the realizations performed, the value of κ was taken to be identically zero. This implies [see equation (IV.47) and following] that the ratio of the density of the particle to the density of the fluid is very large. The parameter α was allowed to vary over the range 5.0, 25.0, 50.0, and ∞ (the fluid particle case) with $\underset{\sim}{g} = \underset{\sim}{0}$. With $\underset{\sim}{g} = g\,\underset{\sim}{i}_2$ and $\alpha = 5.0$, the parameter g was allowed to take on the values 0.0, -4.0, and -25.0. The ensemble (sample) size for the case with $\alpha = 25.0$, $g = 0.0$ was 1600. In all the other simulations reported, the sample size was 2000.

A variety of different initial conditions may be physically interesting. Two obvious choices for the initial particle velocity were (i) $\underset{\sim}{0}$, i.e., particles released from rest, and (ii) particles launched with the local instantaneous velocity of the fluid. It was thought that this second choice would speed attainment of the asymptotic stationary state (thus saving computer time), so the initial conditions on the particle were taken to be

$$\underset{\sim}{Y}(\underset{\sim}{b},t_0) = \underset{\sim}{b} \tag{81}$$

$$\underset{\sim}{V}(\underset{\sim}{b},t_0) = \underset{\sim}{v}(\underset{\sim}{b},t_0) \tag{82}$$

All of the statistical data presented below, except the particle

Reproduced with permission of the copyright owner. Further reproduction prohibited without permission.

mean fallout velocities, were computed after the particles had achieved a statistically stationary state.

The position $\underset{\sim}{Y}(\underset{\sim}{b},t)$, the velocity $\underset{\sim}{V}(\underset{\sim}{b},t)$, and the acceleration $\underset{\sim}{A}(\underset{\sim}{b},t)$ of the "alien" particle (which was at $\underset{\sim}{b}$ at time t_0) were recorded for each realization. The relative velocity of the "alien" particle and neighboring fluid $\underset{\sim}{W}(\underset{\sim}{b},t)$, defined by

$$\underset{\sim}{W}(\underset{\sim}{b},t) = \underset{\sim}{V}(\underset{\sim}{b},t) - \underset{\sim}{u}\left[\underset{\sim}{Y}(\underset{\sim}{b},t),t\right], \tag{83}$$

was computed from [see equation (79) with $\kappa = 0$]

$$\underset{\sim}{W}(\underset{\sim}{b},t) = -\frac{1}{\alpha}\left\{\underset{\sim}{A}(\underset{\sim}{b},t) - \underset{\sim}{g}\right\}. \tag{84}$$

The following autocorrelation coefficients will be needed in the discussion below.

$$\mathcal{R}_{V_{ij}}(\tau) = \frac{\langle V_i(\underset{\sim}{b},t)\, V_j(\underset{\sim}{b},t+\tau)\rangle}{\langle V_i(\underset{\sim}{b},t)\, V_j(\underset{\sim}{b},t)\rangle} \tag{85}$$

$$\mathcal{R}_{u_{ij}}(\tau) = \frac{\langle u_i[\underset{\sim}{Y}(\underset{\sim}{b},t),t]\, u_j[\underset{\sim}{Y}(\underset{\sim}{b},t+\tau),t+\tau]\rangle}{\langle u_i[\underset{\sim}{Y}(\underset{\sim}{b},t),t]\, u_j[\underset{\sim}{Y}(\underset{\sim}{b},t),t]\rangle} \tag{86}$$

$$\mathcal{R}_{D_{ij}}(\tau) = \frac{\langle W_i(\underset{\sim}{b},t)\, W_j(\underset{\sim}{b},t+\tau)\rangle}{\langle W_i(\underset{\sim}{b},t)\, W_j(\underset{\sim}{b},t)\rangle} \tag{87}$$

b. A Typical Case

Figure 53 shows, for a typical sluggish particle (in this case $\alpha = 5.0$, $g = 0.0$), values of the autocorrelation

Reproduced with permission of the copyright owner. Further reproduction prohibited without permission.

Reproduced with permission of the copyright owner. Further reproduction prohibited without permission.

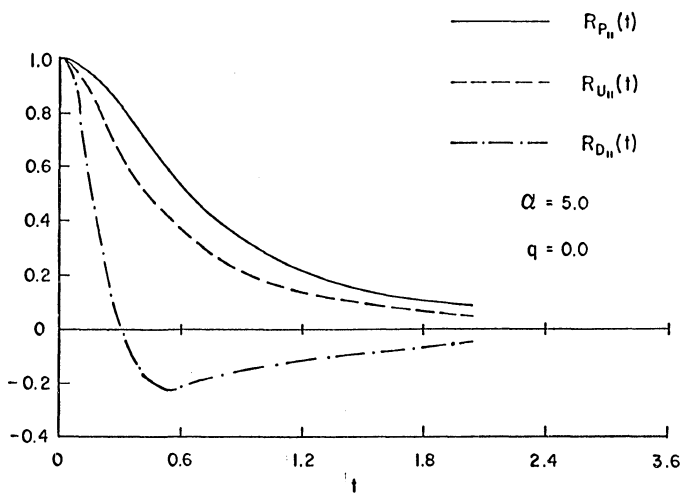

Figure 53. A comparison of the autocorrelation coefficients of the particle velocity, $R_{P_{11}}(t)$, of the velocity of the fluid in the vicinity of the particle, $R_{U_{11}}(t)$, and of the relative velocity, $R_{D_{11}}(t)$, for a typical "sluggish" particle (α = 5.0, q = 0.0, K = 0.0).

coefficients of the particle velocity, $\mathcal{R}_{P_{11}}(\tau)$, of the velocity of the fluid in the vicinity of the particle, $\mathcal{R}_{u_{11}}(\tau)$, and of the relative velocity, $\mathcal{R}_{D_{11}}(\tau)$.

The fluid in the vicinity of the particle acts as a kind of driving force on the particle. The particle does not respond to all the higher frequency oscillations of the fluid (i.e., it acts like a "low pass" filter), so its correlation, $\mathcal{R}_{P_{11}}(\tau)$, drops off slower than that of the surrounding fluid, $\mathcal{R}_{u_{11}}(\tau)$. The qualitative behavior of $\mathcal{R}_{D_{11}}(\tau)$ is discussed in the following.

Assume that $f(t)$ is a stationary, random process. Then, in particular,

$$\langle f(t)\, f(t+\tau)\rangle = \mathcal{R}(\tau) = \mathcal{R}(-\tau), \tag{88}$$

say, independent of t. Also, assume that the random process $g(t)$ is defined by

$$\mu\, g(t) = \frac{d}{dt} f(t) \quad ; \quad \mu \neq 0. \tag{89}$$

Then $$\mu^2 \langle g(t_1) g(t_2)\rangle = \left\langle \frac{d}{dt_1} f(t_1) \frac{d}{dt_2} f(t_2)\right\rangle = \frac{d^2}{dt_1 dt_2} \langle f(t_1) f(t_2)\rangle$$

$$= \frac{d^2}{dt_1 dt_2} \mathcal{R}(t_2 - t_1) = -\mathcal{R}''(t_2 - t_1), \tag{90}$$

where $$\mathcal{R}'(\tau) = \frac{d}{d\tau}\mathcal{R}(\tau). \tag{91}$$

Thus $$\langle g(t)\, g(t+\tau)\rangle = -\frac{1}{\mu^2}\mathcal{R}''(\tau) \equiv \mathcal{S}(\tau), \tag{92}$$

Reproduced with permission of the copyright owner. Further reproduction prohibited without permission.

say. The integral scale of $g(t)$, T_g, is defined by

$$T_g = \frac{1}{S(0)} \int_0^\infty S(\tau)\, d\tau, \tag{93}$$

so that, with (92), [assuming that $R''(0) \neq 0$],

$$T_g = \frac{1}{R''(0)} \int_0^\infty R''(\tau)\, d\tau = \frac{1}{R''(0)} R'(\tau) \Big|_0^\infty$$

$$= \frac{1}{R''(0)} \left[R'(\infty) - R'(0) \right]. \tag{94}$$

Assuming that $R'(0)$ exists, then since $R(\tau) = R(-\tau)$, it follows that $R'(0) = 0$. Furthermore, assuming that $R(\tau)$ falls off fast enough as $\tau \to \infty$, then $R'(\infty) = 0$, so that, from (94),

$$T_g = 0. \tag{95}$$

Also, defining the microscale for f, τ_f, as $\tau_f = \sqrt{\frac{-2\langle f^2(t) \rangle}{R''(0)}}$; then from (90),

$$\langle g^2(t) \rangle = S(0) = \frac{2}{\mu^2} \frac{\langle f^2(t) \rangle}{\tau_f^2}. \tag{96}$$

Now, consider the force balance equation for the particle [equation (79)] with $\underset{\sim}{g} = \underset{\sim}{e}$:

$$\frac{d}{dt} V_i(\underset{\sim}{b},t) + \alpha \left\{ V_i(\underset{\sim}{b},t) - u_i\left[\underset{\sim}{Y}(\underset{\sim}{b},t),t\right] \right\} = K \frac{d}{dt} u_i\left[\underset{\sim}{Y}(\underset{\sim}{b},t),t\right]$$

Reproduced with permission of the copyright owner. Further reproduction prohibited without permission.

where $\frac{\partial}{\partial t}$ is the time derivative holding $\underline{b}$ fixed, that is, the time derivative following the particle. This can be rearranged as [using (83)],

$$\frac{\partial}{\partial t}\left\{ V_i(\underline{b},t) - \kappa U_i[\underline{Y}(\underline{b},t),t] \right\} = -\alpha W_i(\underline{b},t). \qquad (97)$$

Identifying $V_i - \kappa U_i$ with f, W_i with g, and $-\alpha$ with μ, and assuming that V_i and U_i are stationary, random functions of t, then equation (95) implies that

(I) The integral scale of the velocity difference is zero, i.e.,

$$T_{D_{ii}} \equiv \int_0^\infty R_{D_{ii}}(r)\,dr = 0 \qquad \text{(no sum on i)} \quad (98)$$

and equation (96) implies that, with $\kappa = 0$,

$$\text{(II)} \quad \langle W_i^2(\underline{b},t)\rangle = \frac{2}{\alpha^2}\,\frac{\langle V_i^2(\underline{b},t)\rangle}{r_{D_{ii}}^2} \qquad \text{(no sum on i)} \quad (99)$$

where $r_{D_{ij}} = \sqrt{\frac{-2}{R_{D_{ij}}''(0)}}$.[1]

Returning to the discussion of figure 53, the foregoing predicts that, with $\underline{g} = \underline{g}$, the integral scale of $R_{D_{11}}(r)$ is zero. This

---

1. An equation similar to (99) was obtained independently by Lumley (1957) and Friedlander (1957) for the case α "very large". (98) was obtained by Lumley (1957), also for α "very large".

Reproduced with permission of the copyright owner. Further reproduction prohibited without permission.

was found to be approximately valid in all the applicable cases. Also, from equation (84) with $\underset{\sim}{g} = \underset{\sim}{0}$, the relative velocity is proportional to the particle acceleration. Thus $R_{D_{ij}}(\tau)$ is also the correlation coefficient for the particle acceleration when $\underset{\sim}{g} = \underset{\sim}{0}$.

Figure 54 is a typical plot of the cross-correlation coefficient between particle velocity and velocity of surrounding fluid,

$$\frac{\langle u_i[\underset{\sim}{Y}(\underset{\sim}{b},t),t]V_i(\underset{\sim}{b},t+\tau)\rangle}{\langle u_i[\underset{\sim}{Y}(\underset{\sim}{b},t),t]V_i(\underset{\sim}{b},t)\rangle}.$$

(In this case, $\alpha = 5.0$, $\underset{\sim}{g} = 0.0$.) Notice that the correlation peaks not at the origin ($\tau = 0$) but at a positive value of τ, approximately α^{-1}. This peak shift is due to the fact that whenever a velocity difference exists between the particle and surrounding fluid it takes the particle a finite amount of time (approximately α^{-1}) to respond to this difference.

c. The Effect of Varying the Particle Inverse Relaxation Time α

Figure 55 shows plots of the particle velocity autocorrelation coefficient $R_{P_{ii}}(\tau)$ for different values of α.[1] As

1. It was found that the statistical results for the fluid particle case ($\alpha \to \infty$) and for the alien particle case with $\alpha = 50.0$ differed very little. The alien particle with $\alpha = 50.0$ statistically behaved almost as a fluid particle. Thus, in the results presented below, there will often be no distinction made between the fluid

Reproduced with permission of the copyright owner. Further reproduction prohibited without permission.

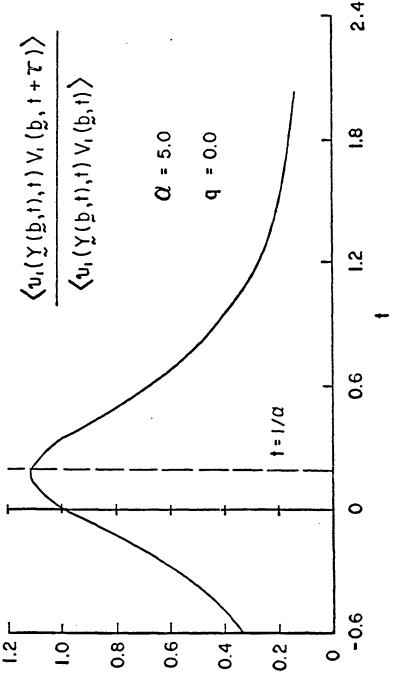

Figure 54. A typical plot (α = 5.0, β = 0.0, K = 0.0) of the cross-correlation coefficient between the particle velocity and the velocity of surrounding fluid.

Reproduced with permission of the copyright owner. Further reproduction prohibited without permission.

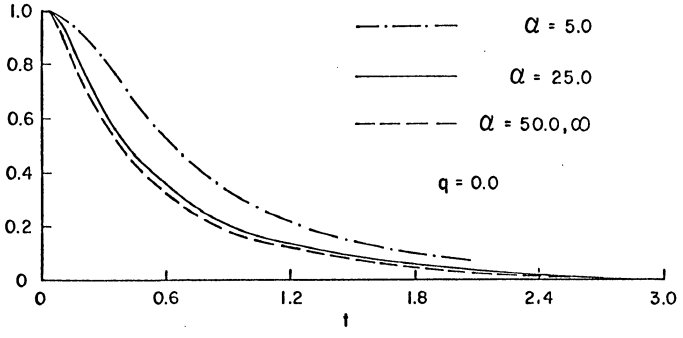

Figure 55. The "alien" particle velocity autocorrelation coefficient, $R_{\rho_{\parallel}}(t)$, for various values of α (with q = 0.0, α = 0.0).

Reproduced with permission of the copyright owner. Further reproduction prohibited without permission.

α decreases, (i.e. the particle relaxation time increases; the particles become more sluggish), the velocity correlations fall off less rapidly.

Part of the reason for this can be seen if we first examine the autocorrelation coefficient of the velocity of the fluid surrounding the particle, for the three different values of α (figure 56). It is seen that these correlations are almost identical for the different values of α. Thus the different particles experience approximately the same random driving force. The more sluggish particles react less rapidly to it, causing their correlations to drop off slower.

We might not have guessed ahead of time that the $u[\underline{Y}(b,t),t]$ autocorrelations would be so insensitive to changes in α. It might be expected that the more sluggish particles follow the fluid particle paths less accurately, and they cross the trajectories of fluid particles more often and more rapidly. This suggests that the record of the fluid velocity surrounding the more sluggish particles should show more high frequency content than the fluid velocity surrounding the less sluggish particles. This would imply that the correlations would fall off more rapidly as α is decreased. For the α-range studied, they do not. This result could be due to the neglect of the turbulent-turbulent non-linear terms in the Navier-Stokes equations. For this intuitive notion is consistent

---

particle case ($\alpha \to \infty$) and the case $\alpha = 50.0$.

Reproduced with permission of the copyright owner. Further reproduction prohibited without permission.

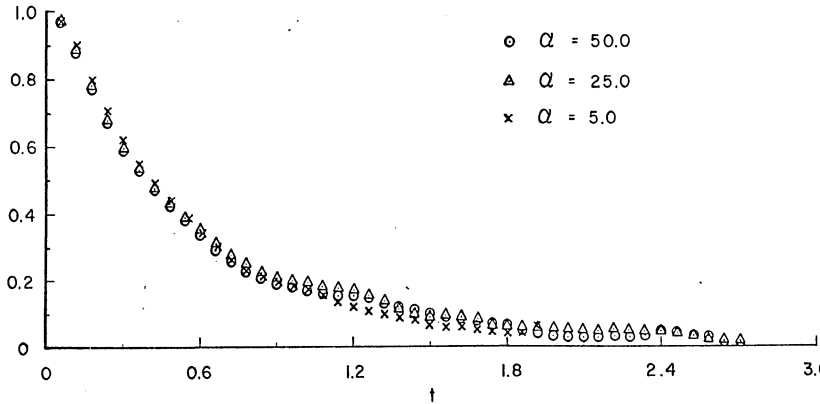

Figure 56. The autocorrelation coefficient of the velocity of the fluid surrounding the "alien" particle, $R_{u_{\parallel}}(t)$, for various values of α (with q = 0.0, κ = 0.0).

Reproduced with permission of the copyright owner. Further reproduction prohibited without permission.

with the notion that in general fluid particle velocities persist longer in time than one-point Eulerian velocities.

Figure 57 is a plot of the relative velocity autocorrelation coefficients $R_{D_{ij}}(r)$ for the various α. The high frequency content of the relative velocity, as in the case of the "alien" particle velocity, also appears to decrease as α decreases. This is to be expected since the relative velocity $W_i(\underline{b},t)$ is proportional to the particle acceleration $A_i(\underline{b},t)$ [equation (84)].

Table 3 is a list of some important averages computed from the simulations for α = 5.0, 25.0, 50.0, and ∞ and ζ = 0.0. Note that the values of $\langle \alpha^2 W_i^2(\underline{b},t) \rangle$ agree approximately with those of $2\,\frac{\langle V_i^2(\underline{b},t)\rangle}{\gamma_{ii}^2}$, thus giving a check of equation (99). Also note that the values of $\langle V_i^2(\underline{b},t)\rangle$ tend to decrease and $\langle W_i^2(\underline{b},t)\rangle$ increase as α decreases, while the $\langle v_i^2[\underline{y}(\underline{b},t),t]\rangle$ are approximately constant for the various values of α.

d. The Effect of Varying the Effective Gravity Force: The "Fallout Problem"

Next, the simulation results for "alien" spherical particle "fallout" speed and diffusion in gravitational fields are presented. Figure 58 is a plot of the mean fallout velocities $\langle V_2(\underline{b},t)\rangle$ as functions of time for the cases with ζ = -4.0, α = 5.0, and g = -25.0, α = 5.0 ($\underline{g} = g\underline{i}_2$). (The ratio of the rms turbulent velocity ($\langle v_1^2 \rangle^{1/2}$) to the mean terminal velocity ($\simeq g/\alpha$) was approximately 1.10 for the case with g = -4.0, and 0.18 for the case with g = -25.0.) The particles were released

Reproduced with permission of the copyright owner. Further reproduction prohibited without permission.

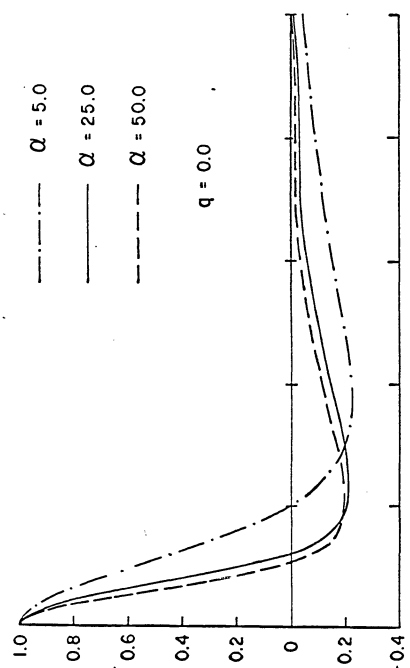

Figure 57. The autocorrelation coefficient of the relative velocity of the "alien" particle and the surrounding fluid, $R_{\alpha_n}(t)$, for various values of α (with $\beta = 0.0, \chi = 0.0$).

Reproduced with permission of the copyright owner. Further reproduction prohibited without permission.

α	5.0			25.0			50.0			∞		
Component (i)	1	2	3	1	2	3	1	2	3	1	2	3
$\langle V_i^2(\underline{b},t)\rangle$	0.546	0.551	0.566	0.701	0.730	0.744	0.733	0.740	0.772	0.771	0.729	0.771
$\langle u_i^2[\underline{Y}(\underline{b},t),t]\rangle$	0.696	0.698	0.702	0.723	0.743	0.755	0.741	0.743	0.775	0.771	0.729	0.771
$\langle \alpha^2 W_i^2(\underline{b},t)\rangle$	3.702	3.647	3.638	11.516	11.701	11.285	13.080	13.948	13.048	–	–	–
$\langle V_i u_i\rangle$	0.547	0.552	0.561	0.703	0.727	0.740	0.735	0.739	0.771	0.771	0.729	0.771
$\frac{\langle V_i u_i\rangle}{\langle V_i^2\rangle^{1/2}\langle u_i^2\rangle^{1/2}}$	0.888	0.890	0.889	0.987	0.987	0.987	0.997	0.997	0.997	1.000	1.000	1.000
η_{p_i}	0.598	0.570	0.596	0.363	0.352	0.355	0.321	0.329	0.339	0.379	0.346	0.341
$2\frac{\langle V_i^2\rangle}{\eta_{p_i}^2}$	3.054	3.390	3.187	10.650	11.80	11.825	14.250	13.70	13.45	10.750	12.200	13.28
$\langle W_i^2(\underline{b},t)\rangle$	0.1480	0.1457	0.1454	0.01843	0.01872	0.01805	0.00523	0.00558	0.00521	0.0	0.0	0.0

Table 3.

Reproduced with permission of the copyright owner. Further reproduction prohibited without permission.

Reproduced with permission of the copyright owner. Further reproduction prohibited without permission.

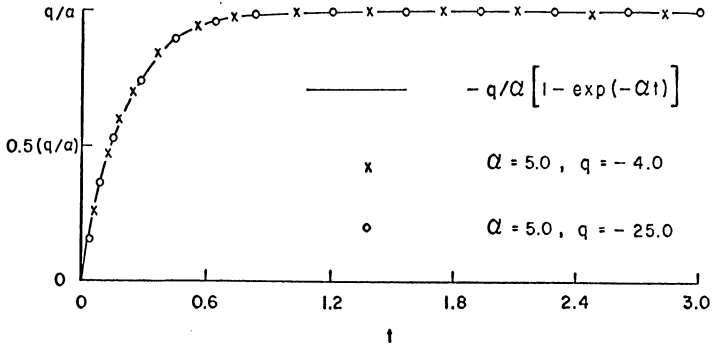

Figure 58. The mean fallout velocity of "alien" particles for the cases $\alpha = 5.0$, $\beta = -4.0$ and $\alpha = 5.0$, $\beta = -25.0$. The continuous line is the quiescent fallout velocity (equation (110)).

with velocities initially equal to those of the surrounding fluid [see equation (81) and (82)], and thus initially have zero mean velocity. The continuous line in the figure is the fallout velocity of a particle released with zero velocity in a fluid at rest, the quiescent fallout velocity,

$$\underset{\sim}{V}_f = +\underset{\sim}{i}_2 \frac{g}{\alpha}\left\{1 - \exp(-\alpha t)\right\}. \qquad (100)$$

Some theoretical and computational results (Corrsin and Patterson 1970) using hypothetical binary Eulerian fields indicated that the mean fallout velocities of the alien particles $\langle V_2(\underset{\sim}{b},t)\rangle$ would be less than their quiescent fallout velocities. However, they were found to be approximately equal for values of the effective body force (g) used in these simulations.

The particles released with gravitational fields were allowed to reach a statistically stationary state, and then the following correlation functions were computed. (Note, in particular, that in these results their mean velocities $\langle \underset{\sim}{V}(\underset{\sim}{b},t)\rangle$ are nearly equal to the asymptotic quiescent fallout velocity $+\frac{g}{\alpha}\underset{\sim}{i}_2$.)

Figure 59 is a comparison of the autocorrelation coefficient of the velocity of the fluid in the vicinity of the particles, $\hat{R}_{u_n}(r)$, for the cases $\alpha = 5.0$, $g = 0.0$; $\alpha = 5.0$, $g = -4.0$; and $\alpha = 5.0$, $g = -25.0$. These results describe the "lateral driving force" experienced by the particles for each case. The results indicate that, as the effective gravity force is increased, the high frequency

Reproduced with permission of the copyright owner. Further reproduction prohibited without permission.

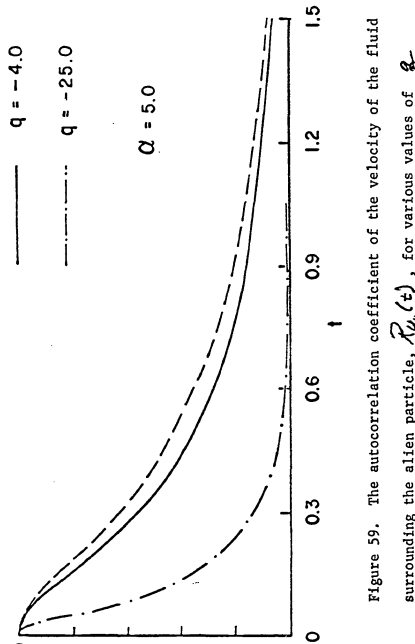

Figure 59. The autocorrelation coefficient of the velocity of the fluid surrounding the alien particle, $R_{u_n}(t)$, for various values of β with $\alpha = 5.0$.

Reproduced with permission of the copyright owner. Further reproduction prohibited without permission.

content of the "driving force" increases, i.e., its correlation falls off faster. This is simply due to the fact that, as the effective gravity force is increased, the particles fall through the fluid faster, and thus "see" higher frequency fluctuations.

Figure 60 displays the effect of fallout on the sluggish particle velocity correlation coefficient, $R_{P_{ii}}(\tau)$. The result is that, as the effective gravity force is increased, the correlations fall off faster. This is expected from the results observed in figure 59. For an increase in the high frequency content of the driving force causes an increase in the high frequency content of the particle velocity. This result has been predicted by various authors (e.g., Yudine 1959, Csanady 1963, Katz 1966). Since the dispersion $\langle V_i^2(\underline{b},t)\rangle$ behaves asymptotically like $2\langle V_i^2(\underline{b},t)\rangle T_{P_{ii}}\, t$ for large t [where $T_{P_{ii}}$ is the integral time scale of $V_i(\underline{b},t)$], these results indicate, in conjunction with the values of $\langle V_i^2(\underline{b},t)\rangle$ given below, that the fallout tends to inhibit the turbulent diffusion process, at least in this model.

It has often been conjectured (e.g., Yudine 1959, Csanady 1963) that for particles falling out fast enough a hypothesis analogous to Taylor's approximation (Lin 1953, Uberoi and Corrsin 1953), often used experimentally to equate fixed point Eulerian velocity autocorrelations in flowing turbulence with Eulerian spatial correlations, might give good estimates of the autocorrelation of the velocity of the fluid in the vicinity of the alien particle, $R_{u_{ij}}(\tau)$. If the particle trajectory is nearly a straight line, this is

Reproduced with permission of the copyright owner. Further reproduction prohibited without permission.

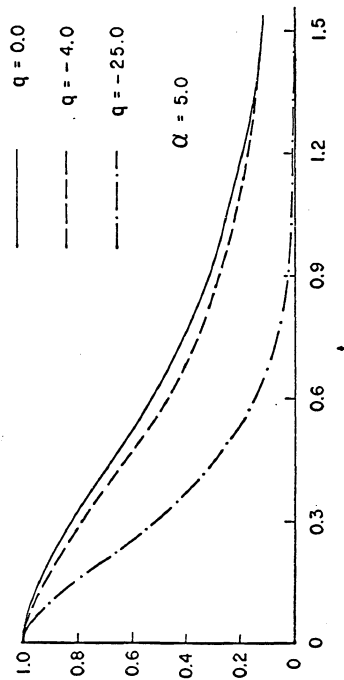

Figure 60. The "alien" particle velocity autocorrelation coefficient, $R_{\beta_1}(t)$, for various values of β with $\alpha = 5.0$.

Reproduced with permission of the copyright owner. Further reproduction prohibited without permission.

certainly plausible.

Assume that $\mathcal{R}_{ij}(\underline{r},t)$ is the (Eulerian) space-time velocity correlation of a homogeneous, turbulent fluid in a coordinate system (I) which is moving with the mean velocity of the fluid $\underline{U}$ in a fixed coordinate system (I'). If a velocity measuring device is placed at a fixed point in coordinate system (I'), and temporal correlations, $\mathcal{R}'_{ij}(\tau)$, are measured, then the resultant measurement in terms of the space-time correlation $\mathcal{R}_{ij}(\underline{r},\tau)$ is

$$\mathcal{R}'_{ij}(\tau) = \mathcal{R}_{ij}(\underline{U}\tau,\tau). \tag{101}$$

Taylor suggested that for large enough $\frac{\underline{U}}{\sqrt{\langle u^2 \rangle}}$ this relation is

$$\mathcal{R}'_{ij}(\tau) \doteq \mathcal{R}_{ij}(\underline{U}\tau,0). \tag{102}$$

Thus, assuming that this is correct, the temporal measurements $\mathcal{R}'_{ij}(\tau)$ approximately give the spatial correlation $\mathcal{R}_{ij}(\underline{r},0)$, where $\underline{r}$ is parallel to the mean velocity $\underline{U}$.

In the fallout problem, assume that the position $\underline{Y}(\underline{b},t)$ and velocity $\underline{V}(\underline{b},t)$ of the alien particle are decomposed into a mean and fluctuating parts, i.e., let

$$\underline{Y}(\underline{b},t) = \langle \underline{Y}(\underline{b},t) \rangle + \underline{Y}'(\underline{b},t) \tag{103}$$

$$\underline{V}(\underline{b},t) = \langle \underline{V}(\underline{b},t) \rangle + \underline{V}'(\underline{b},t) \tag{104}$$

Reproduced with permission of the copyright owner. Further reproduction prohibited without permission.

where $\langle \underset{\sim}{y}'(\underset{\sim}{b},t)\rangle = \langle \underset{\sim}{v}'(\underset{\sim}{b},t)\rangle = \underset{\sim}{0}$ by definition. From the discussion above (after figure 58) it is known that, in these simulations, the asymptotic mean fallout velocity and position are approximately [equation (100)]

$$\langle \underset{\sim}{v}(\underset{\sim}{b},t)\rangle = \frac{g}{\alpha} = \frac{g}{\alpha}\,\underset{\sim}{i}_z \tag{105}$$

$$\langle \underset{\sim}{y}(\underset{\sim}{b},t)\rangle = \underset{\sim}{b} + \frac{g}{\alpha}(t-t_0)\,\underset{\sim}{i}_z . \tag{106}$$

Thus the autocorrelation of the fluid in the vicinity of the particle is

$$\langle u_i(\underset{\sim}{b},t_0)\, u_j[\underset{\sim}{y}(\underset{\sim}{b},t),t]\rangle = \langle u_i(\underset{\sim}{b},t_0)\, u_j[\underset{\sim}{b} + \tfrac{g}{\alpha}(t-t_0)\underset{\sim}{i}_z + \underset{\sim}{y}'(\underset{\sim}{b},t),t]\rangle \tag{107}$$

The conjecture is that for $\dfrac{|\underset{\sim}{y}'(\underset{\sim}{b},t)|}{\frac{g}{\alpha}(t-t_0)}$ "small" in some sense, then

$$\langle u_i(\underset{\sim}{b},t_0)\, u_j[\underset{\sim}{y}(\underset{\sim}{b},t),t]\rangle \doteq \langle u_i(\underset{\sim}{b},t_0)\, u_j[\underset{\sim}{b} + \tfrac{g}{\alpha}(t-t_0),t]\rangle \tag{108}$$

In terms of autocorrelation coefficients,

$$\mathcal{R}_{ij}(\tau) \doteq \mathcal{R}_{ij}\left(\frac{g}{\alpha}\tau\,\underset{\sim}{i}_z, \tau\right) \qquad \text{with} \quad \tau = t-t_0 . \tag{109}$$

Furthermore, if $\frac{g}{\alpha}$ is large enough that Taylor's hypothesis be valid, then finally

Reproduced with permission of the copyright owner. Further reproduction prohibited without permission.

$$R_{u_{ij}}(r) \doteq R_{\varepsilon_{ij}}\left(\frac{g}{\alpha} r \hat{i}_2, 0\right). \tag{110}$$

In the present problem, using the fact that the velocity field is statistically isotropic, (110) implies that

$$R_{u_{11}}(r) \doteq g\left(\frac{g}{\alpha} r\right) \tag{111}$$

$$R_{u_{22}}(r) \doteq f\left(\frac{g}{\alpha} r\right) \tag{112}$$

$$R_{u_{33}}(r) \doteq g\left(\frac{g}{\alpha} r\right), \tag{113}$$

where f and g are the usual Kármán-Howarth velocity correlation coefficients of the Eulerian field (Hinze 1959, page 147).

Figure 61 shows plots of $R_{u_{11}}(r)$, $R_{u_{22}}(r)$, and $R_{u_{33}}(r)$ computed from the simulations (for the case $\alpha = 5.0$ and $\frac{g}{\alpha} = -25.0$), compared with $g\left(\frac{g}{\alpha} r\right)$, $f\left(\frac{g}{\alpha} r\right)$, and $g\left(\frac{g}{\alpha} r\right)$ respectively, measured from Eulerian field simulations. The ratio of the rms turbulent velocity $\langle u_i^2 \rangle^{1/2}$ to the asymptotic mean fallout velocity $\frac{g}{\alpha}$, the turbulence level for this case, was approximately 18%. The results agree well with the conjecture.

Figure 62 is a plot of the particle velocity autocorrelation coefficients for the case $\alpha = 5.0$, $\frac{g}{\alpha} = -25.0$. Note that the correlation $R_{p_{22}}(r)$ falls off slower than $R_{p_{11}}(r)$ and $R_{p_{33}}(r)$, an effect which would be expected from the discussion immediately above. This implies that the integral time scale of $V_2(\underline{b}, t)$ is larger

Reproduced with permission of the copyright owner. Further reproduction prohibited without permission.

Reproduced with permission of the copyright owner. Further reproduction prohibited without permission.

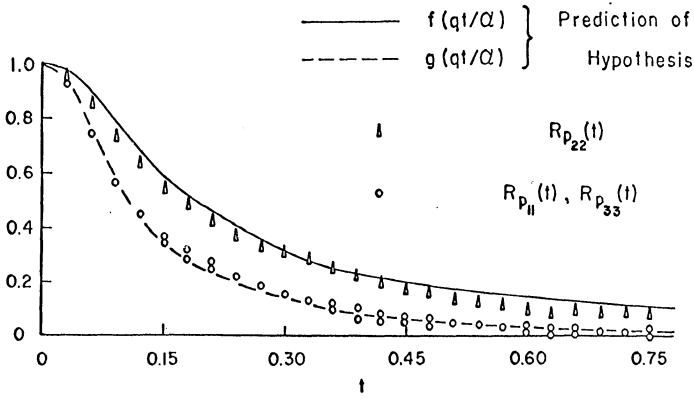

Figure 61. A comparison of the simulation results for $\hat{R}_{u_{11}}(t)$, $\hat{R}_{u_{22}}(t)$, and $\hat{R}_{u_{33}}(t)$ (for the case α = 5.0, $\frac{q}{\beta}$ = -25.0) with the hypothesis expressed by equations (111), (112), and (113).

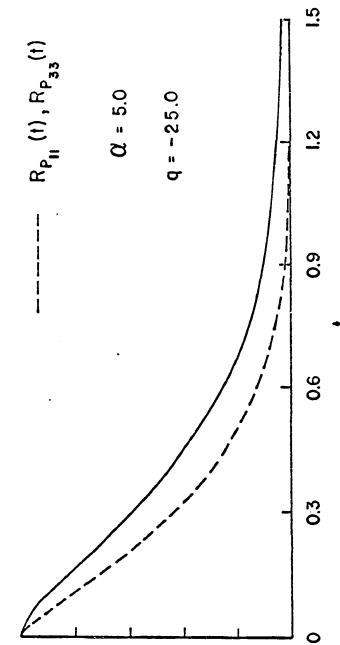

Figure 62. The "alien" particle velocity autocorrelation coefficients $R_{P_{11}}(t)$, $R_{P_{22}}(t)$, and $R_{P_{33}}(t)$ for the case $\alpha = 5.0$ and $q = -25.0$.

Reproduced with permission of the copyright owner. Further reproduction prohibited without permission.

than that of $V_1(\underline{b},t)$ or $V_3(\underline{b},t)$, i.e., $T_{P_{22}} > T_{P_{11}}, T_{P_{33}}$. It was also found (see Table 4 below) that $\langle V_2^2(\underline{b},t)\rangle > \langle V_1^2(\underline{b},t)\rangle$, $\langle V_3^2(\underline{b},t)\rangle$. Thus the diffusion (e.g., expressed in terms of $\langle Y_i(\underline{b},t)\, Y_j(\underline{b},t)\rangle$) will be greater in the x_2 direction than in the x_1 or x_3 directions, an effect which was predicted by Csanady (1963).

Table 4 is a list of some averages computed from the simulations for the cases $\alpha = 5.0$, $\frac{g}{\beta} = 0.0$; $\alpha = 5.0$, $\frac{g}{\beta} = -4.0$; and $\alpha = 5.0$, $\frac{g}{\beta} = -25.0$. Note that $\langle V_i^2(\underline{b},t)\rangle$ tends to decrease as $|\frac{z}{b}|$ increases.

Reproduced with permission of the copyright owner. Further reproduction prohibited without permission.

α, β	5.0, 0.0			5.0, -4.0			5.0, -25.0		
Component (i)	1	2	3	1	2	3	1	2	3
$\langle V_i^2(\underline{x},t)\rangle$	0.546	0.551	0.566	0.543	0.591	0.590	0.328	0.441	0.336
$\langle u_i^2[\underline{Y}(\underline{x},t),t]\rangle$	0.696	0.698	0.702	0.759	0.753	0.799	0.746	0.730	0.726
$\langle \alpha^2 W_i^2(\underline{x},t)\rangle$	3.702	3.647	3.638	4.531	4.055	4.135	10.37	7.66	9.46
$\langle V_i u_i\rangle$	0.547	0.552	0.561	0.555	0.593	0.606	0.330	0.433	0.342
$\frac{\langle V_i u_i\rangle}{\langle V_i^2\rangle^{1/2}\langle u_i^2\rangle^{1/2}}$	0.888	0.890	0.889	0.865	0.888	0.883	0.666	0.763	0.692
$\gamma_{\beta_{ii}}$	0.598	0.570	0.596	0.495	0.520	0.520	0.278	0.329	0.248
$2\frac{\langle V_i^2\rangle}{\beta_{ii}^2}$	3.054	3.390	3.187	4.435	4.375	4.370	8.48	8.15	10.92
$\langle W_i^2(\underline{x},t)\rangle$	0.1480	0.1457	0.1454	0.1812	0.1621	0.1654	0.415	0.306	0.378

Table 4.

Reproduced with permission of the copyright owner. Further reproduction prohibited without permission.

VII. SUMMARY AND SOME CONCLUSIONS

The present study was undertaken to investigate the feasibility and the results of numerically simulating turbulent diffusion without catastrophic cost in computer time. The following was taken as the definition of the problem: given the random Eulerian velocity field $\{\underset{\sim}{u}(\underset{\sim}{x},t)\}$ defined in some statistical sense and satisfying the Navier-Stokes equations and appropriate initial and boundary conditions, compute the joint statistical properties of

$$\left\{ \underset{\sim}{Y}(\underset{\sim}{b},t),\ \frac{\partial}{\partial t}\underset{\sim}{Y}(\underset{\sim}{b},t),\ \underset{\sim}{u}\left[\underset{\sim}{Y}(\underset{\sim}{b},t),t\right] \right\}$$

satisfying

$$\frac{\partial^2}{\partial t^2}\underset{\sim}{Y}(\underset{\sim}{b},t) + \alpha\left\{\frac{\partial}{\partial t}\underset{\sim}{Y}(\underset{\sim}{b},t) - \underset{\sim}{u}\left[\underset{\sim}{Y}(\underset{\sim}{b},t),t\right]\right\} = \frac{g}{\rho} + \nu\frac{\partial}{\partial t}\underset{\sim}{u}\left[\underset{\sim}{Y}(\underset{\sim}{b},t),t\right] \qquad (1)$$

$$\underset{\sim}{Y}(\underset{\sim}{b},t_0) = \underset{\sim}{b} \qquad (2)$$

$$\frac{\partial}{\partial t}\underset{\sim}{Y}(\underset{\sim}{b},t)\Big|_{t=t_0} = \underset{\sim}{u}(\underset{\sim}{b},t) \qquad (3)$$

The method of solution was to first set up a mathematical model of the random velocity field. Then an "ensemble" of realizations of this field was generated digitally. In each realization, the governing equations were integrated numerically for various values of α and $\frac{g}{\rho}$ with $\nu = 0$, and the output was stored on magnetic tape. After a large enough number of realizations had been completed so that meaningful statistical results could be obtained,

Reproduced with permission of the copyright owner. Further reproduction prohibited without permission.

various statistical quantities of interest were computed. In this manner a solution to the problem was obtained. Its validity depends mainly on the characteristics of the mathematical model of the original Eulerian velocity field.

Two Eulerian flow fields were modeled, a homogeneous turbulent shear flow and a turbulent isotropic flow, both in three dimensions[1]. Among the shear flow Lagrangian diffusion results were the following:

(i) Agreement with Corrsin's (1953) kinematic predictions.

(ii) Extensive results on the spatial development of the diffusion process, and in particular, results concerning the time history of $\langle Y_i(b,t)\, Y_j(b,t) \rangle$ and the joint probability density $p_{Y_1 Y_2}(x_1, x_2; t)$.

(iii) The fluid particle velocity time correlation fell off faster than the one-point Eulerian time correlation (a result which we tend to believe is unrealistic).

(iv) Turbulent diffusivities.

(v) Simulation of "wind tunnel" plume dispersion experiments.

Among the results in the isotropic case were:

(i) Agreement with Taylor's (1921) kinematic predictions for fluid particle (Lagrangian) diffusion.

---

1. Attempts made to simulate the shear flow turbulence in two dimensions led to Eulerian properities qualitatively different from those measured in homogeneous, turbulent shear flow (Champagne, Harris, and Corrsin 1970), and so the three dimensional simulation was preferred.

Reproduced with permission of the copyright owner. Further reproduction prohibited without permission.

(ii) The fluid particle velocity time correlation again fell off faster than the Eulerian one-point time correlation (again possibly unrealistic).

(iii) Holding $\frac{g}{\delta} = \underline{\alpha}$ and decreasing α tended to increase the alien particle velocity time correlation.

(iv) With α constant, increasing $|\frac{g}{\delta}|$ tended to inhibit the alien particle diffusion.

(v) For alien particles "rapidly" falling out, a hypothesis similar to Taylor's (Yudine 1959, Csanady 1963) gave accurate estimates of the autocorrelation of the velocity of the fluid in the vicinity of the particles.

It is hoped that in the near future this investigation will be extended to include (i) the effects of varying K, especially for $K > 1$ (the "bubble" case), and (ii) the effects of the shear on "alien" particle diffusion.

This method of investigation appears to be useful when qualitative kinematic effects are sought (e.g., the time development of $\langle Y_i Y_j \rangle$ in the shear flow problem). It also appears reliable when the Eulerian spatial field is the determining factor in the process (e.g., in "rapid" fallout problems), since the Eulerian spatial statistics can be modeled very precisely, especially in the isotropic case. However, when the results depend crucially on the time development of the flow field (e.g., in the comparison of the Eulerian and the fluid particle velocity time correlations), the method appears to exhibit unrealistic results.

Reproduced with permission of the copyright owner. Further reproduction prohibited without permission.

It does have the advantage that almost all the important quantities involved in the process -- the particle position, velocity, and acceleration, the velocity of the fluid in the vicinity of the particles, and the relative velocity of the fluid and particle -- can be easily measured, and their statistical properites computed. Thus an in depth study of an individual process (for a given α, $\frac{g}{\delta}$, and K) can be made. Furthermore, the various parameters involved -- α, $\frac{g}{\delta}$, and K -- can be easily varied, and so the effects of the different terms in the governing equations can be investigated in great detail.

Numerical simulation of turbulent diffusion may prove to be of even more value when numerically integrated turbulent flow fields are realized[1]. For in this case, the time development of the flow field would also be well modeled, eliminating the main drawback in the present model, and all the advantages of the method could be utilized.

---

1. In fact, this has been done for fluid particle diffusion on a numerically integrated turbulent shear flow (where the smaller scales were simulated by eddy coefficients proportional to the local velocity deformation) by Deardorff and Peskin (1970), as has already been mentioned in Chapter II, and for fluid particle diffusion on a numerically integrated, two-dimensional isotropic field by Peskin, Lilly, and Fulker (1971).

Reproduced with permission of the copyright owner. Further reproduction prohibited without permission.

Appendix A. Random Number Generation

To produce random variates digitally, "pseudo-random" methods were used. Sequences of variates produced in this manner are not strictly random, since they are generated by some deterministic algorithm. However, they do seem to possess the essential characteristics of truly random sequences in the present context.

All of the methods used depend on the existence of a sequence of random variates, uniformly distributed over the interval (0, 1). The uniform sequences were produced by the so-called "power residue method", where the $(j+1)^{th}$ variate (R_{j+1}) is determined from the jth (R_j) by the formula

$$R_{j+1} = K R_j \pmod{m} \qquad (1)$$

(This gives variates uniformily distributed over (0, m). Dividing R_{j+1} by m gives variates uniformily distributed over (0, 1).) The generation of uniformly distributed variates in this manner has been investigated extensively (see, for example, IBM 1959 and Moshman 1960) and found to satisfy most tests of randomness.

In the simulations performed at the JHU Computing Center, on an IBM 7094 (a 35 bit binary machine), the values $K = 2^{18} + 3$ and $m = 2^{35}$ were used, as suggested by Greenberger (1961). In the simulations computed at NCAR, the NCAR library routine RANF was used, which has $K = 2^{24} - 3$ and $m = 2^{48}$. In both cases, R_0 was chosen to be 2003.

Reproduced with permission of the copyright owner. Further reproduction prohibited without permission.

To generate normally distributed variates with mean M and standard deviation σ, the "direct approach" of Muller and Box (1958) was used. Starting with a pair of independent, uniformly distributed numbers (U_1, U_2), two independent, normally distributed numbers (X_1, X_2) were produced by the transformation

$$X_1 = M + \sigma\left(-\tfrac{1}{2}\ln U_1\right)^{1/2}\cos(2\pi U_2)$$
$$X_2 = M + \sigma\left(-\tfrac{1}{2}\ln U_1\right)^{1/2}\sin(2\pi U_2) \qquad (2)$$

This method has the desirable characteristics that (i) the transformation for going from uniform deviates to normal deviates is exact, (ii) the accuracy obtainable depends only on the precision of the function subroutines used, and (iii) the method gives higher accuracy than other methods of comparable speed.

In several instances, the "inverse transform" method was employed to generate deviates of a required distribution. This method relies on the fact that, if X is a random variable with probability distribution $P_X(s)$ and U a random variable uniformly distributed over (0, 1), then the random variable $P_X^{-1}(U)$ is statistically identical to X. Here $P_X^{-1}(\cdot)$ is defined by the relation

$$P_X[P_X^{-1}(s)] \equiv s. \qquad (3)$$

To see this, consider the random variable $Y = P_X^{-1}(U)$. Now since

Reproduced with permission of the copyright owner. Further reproduction prohibited without permission.

$F_X(\xi)$ is a monotonic, non-decreasing function of ξ, then $F_X^{-1}(\eta)$ is a monotonic, non-decreasing function of η. Thus,

$$Y = F^{-1}(U) \leq \xi$$

if and only if

$$F_X[F_X^{-1}(U)] = U \leq F_X(\xi)$$

so that

$$Prob\{Y \leq \xi\} = Prob\{U \leq F_X(\xi)\} \tag{4}$$

(where $Prob(A)$ is the probability of A). However, since U is uniformly distributed over (0, 1),

$$Prob\{U \leq u^*\} = u^*$$

for u^* defined on (0, 1), so that (4) gives

$$Prob\{Y \leq \xi\} = F_X(\xi). \tag{5}$$

Thus $Y = F_X^{-1}(U)$ is statistically identical to X.

This method is useful only when an algorithm to compute the function $F_X^{-1}(\cdot)$ (fairly rapidly) is available. Thus, in most cases, for example normally distributed variables, the method is not used.

For random variables defined over a finite interval (a, b) and of such a statistical nature that the previous methods could not be used, the "von Neumann rejection method" was used (von Neumann

Reproduced with permission of the copyright owner. Further reproduction prohibited without permission.

1951). This technique procedes as follows. Suppose one wants to generate random variates from a distribution defined by the probability density $f_x(x)$, and has a sequence of independent, uniformly distributed variates over (0, 1) available. Then

I. choose M such that $M f_x(x) \geq 1$ for all x;

II. generate two uniform variates, say u_i, u_{i+1};

III. Let $y = a + (b-a) u_i$

IV. If $u_{i+1} \leq M f_x(y)$, then accept y as a variate with density $f_x(x)$. If $u_{i+1} > M f_x(y)$, reject y, return to step II, and repeat the process until the inequality is finally satisfied.

The justification for this method is as follows. The probability density $f_y(x)$ of the random variable y generated by this process is

$$f_y(x) = \lim_{\Delta x \to 0} \frac{Prob\{x \leq y < x + \Delta x\}}{\Delta x}$$

$$= \lim_{\Delta x \to 0} \frac{Prob\{x \leq a + (b-a)u_i < x + \Delta x \,/\, u_{i+1} \leq M f_x[a + (b-a)u_i]\}}{\Delta x} \quad (6)$$

where the vertical bar denotes that the probability of the statement preceding the bar is condition to the statement following the bar. But

$$Prob\{x \leq a + (b-a)u_i < x + \Delta x \,/\, u_{i+1} \leq M f_x[a + (b-a)u_i]\}$$

$$= \frac{Prob\{x \leq a + (b-a)u_i < x + \Delta x;\ u_{i+1} \leq M f_x[a + (b-a)u_i]\}}{Prob\{u_{i+1} \leq M f_x[a + (b-a)u_i]\}} \quad (7)$$

Now

$$Prob\{u_{i+1} \leq M f_x[a + (b-a)u_i]\} = \int_a^b Prob\{u_{i+1} \leq M f_x(x);\ x \leq a + (b-a)u_i < x + dx\}$$

Reproduced with permission of the copyright owner. Further reproduction prohibited without permission.

$$= \int_a^b M f_X(x) \frac{dx}{b-a} = \frac{M}{b-a} \tag{8}$$

using the fact that u_i, u_{i+1} are independent and uniformly distributed. Also, $Prob\{x \le a+(b-a)u_i < x+\Delta x;\ u_{i+1} \le M f_X[a+(b-a)u_i]\}$

$$= Prob\{x \le a+(b-a)u_i < x+\Delta x;\ u_i \le M f_X(x)\} + O[(\Delta x)^2]$$

$$= \frac{\Delta x}{b-a} M f_X(x) + O[(\Delta x)^2], \tag{9}$$

again using the fact that u_i, u_{i+1} are independent and uniformly distributed. Using (7), (8), and (9) in (6) gives

$$f_y(x) = \lim_{\Delta x \to 0} \frac{1}{\Delta x} \left\{ \frac{\frac{\Delta x}{b-a} M f_X(x)}{\frac{M}{b-a}} + O[(\Delta x)^2] \right\}$$

$$= \lim_{\Delta x \to 0} \{f_X(x) + O(\Delta x)\} = f_X(x). \tag{10}$$

Thus y is statistically identical to X.

This method is useful when all others fail, for if (i) the variable can be defined over a finite interval, and (ii) an algorithm for $f_X(\cdot)$ is available, then variates with the distribution $f_X(\cdot)$ can be generated.

Note that the probability of rejection is given by

$$Prob\{rejection\} = Prob\{u_{i+1} > M f_X[a+(b-a)u_i]\}$$

Reproduced with permission of the copyright owner. Further reproduction prohibited without permission.

$$= 1 - \text{Prob}\left\{ u_{i+1} \le M f_Y[a + (b-a)u_i] \right\}. \qquad (11)$$

Using (8),

$$\text{Prob}\{\text{rejection}\} = 1 - \frac{M}{b-a}.$$

Reproduced with permission of the copyright owner. Further reproduction prohibited without permission.

Appendix B. Random Sampling and Error Analysis

1. Introduction

Suppose there exists a random process $\phi(t)$ whose mean value m we want to compute. Assume the existence of a Gibbsian ensemble, or universe, of events, say $\{\phi_i(t)\}$, which statistically defines the random process $\phi(t)$. Then "by a random sample we mean a subset of variates (events) in which each individual from the universe has an equal and independent chance to be included".[1] We denote a random sample of N events from the universe $\{\phi_i(t)\}$ by $\{\lambda_i(t), i = 1, 2, \ldots N\}$. Note that (with $\langle x \rangle$ denoting a probability, or (∞) ensemble average of x)

$$\langle \lambda_i(t) \rangle = \langle \phi(t) \rangle = m \tag{1}$$

$$\langle [\lambda_i(t) - m]^2 \rangle = \langle [\phi(t) - m]^2 \rangle = \sigma^2 \tag{2}$$

where σ is the standard deviation of $\phi(t)$, and

$$\langle [\lambda_i(t) - m][\lambda_j(t) - m] \rangle = 0 \quad \text{for } i \neq j, \tag{3}$$

using the independence of the events in the sample.

2. Computation of an Average

Using the random sample $\{\lambda_i(t), i = 1, 2, \ldots N\}$ of the ensemble $\{\phi_i(t)\}$, let the average $\overline{\phi}_N(t)$ be defined by

$$\overline{\phi}_N(t) = \frac{1}{N} \sum_{i=1}^{N} \lambda_i(t). \tag{4}$$

1. Kenney, John F. Mathematics of Statistics, Part II.

Reproduced with permission of the copyright owner. Further reproduction prohibited without permission.

Note that $\bar{\phi}_N(t)$, the sum of a finite number (N) of random functions, is itself a random function. Its mean, m_N , is given by

$$m_N = \langle \bar{\phi}_N(t) \rangle = \left\langle \frac{1}{N} \sum_{i=1}^{N} \lambda_i(t) \right\rangle = m, \tag{5}$$

while its standard deviation, σ_N , is

$$\sigma_N^2 = \left\langle (\bar{\phi}_N - m)^2 \right\rangle = \left\langle \left[\left(\frac{1}{N} \sum_{i=1}^{N} \lambda_i(t) \right) - m \right] \left[\left(\frac{1}{N} \sum_{j=1}^{N} \lambda_j(t) \right) - m \right] \right\rangle$$

$$= \frac{1}{N^2} \sum_{i,j=1}^{N} \left\langle [\lambda_i(t) - m][\lambda_j(t) - m] \right\rangle = \sigma^2/N . \tag{6}$$

Since $\bar{\phi}_N(t)$ is the sum of independent, identically distributed variates, then according to De Moivre's version of the Central Limit Theorem, the probability density of $\bar{\phi}_N(t)$ tends to a normal density as N tends to infinity. That is, for large N,

$$p_{\bar{\phi}_N}(u;t) \sim \frac{1}{\sqrt{2\pi}\,\sigma_N} \exp\left\{ - \frac{(u-m)^2}{2\sigma_N^2} \right\} . \tag{7}$$

The average $\bar{\phi}_N(t)$ will be used to approximate m. So the random error involved, $\epsilon_N = \bar{\phi}_N(t) - m$, is approximately normally distributed with standard deviation $\sigma/\sqrt{N}$. Since ϵ_N is approximately normally distributed with standard deviation $\sigma/\sqrt{N}$, the probability that $|\epsilon_N|$ is greater than $\sqrt{10\,\frac{\sigma^2}{N}}$ is about 0.0018. Thus $\sqrt{10\,\frac{\sigma^2}{N}}$ will be arbitrarily chosen as the error bound E_N for ϵ_N . That is

$$E_N \equiv \sqrt{\frac{10}{N}}\,\sigma . \tag{8}$$

Reproduced with permission of the copyright owner. Further reproduction prohibited without permission.

Note that with N = 2000, $E_N \doteq 0.07\sigma$.

3. Computation of an Autocorrelation

Consider the stationary random process $\{u(t), -\infty < t < \infty\}$ where

$$\langle u(t) \rangle = 0 \tag{9}$$

$$\langle u(t)\, u(t+\tau) \rangle = R(\tau). \tag{10}$$

Identifying $u(t)\,u(t+\tau)$ (for fixed τ) with $\phi(t)$ above, then the autocorrelation $R(t)$ will be approximated by

$$\bar{R}_N(t,\tau) = \frac{1}{N}\sum_{i=1}^{N} u_i(t)\, u_i(t+\tau), \tag{11}$$

where $\{u_i(t), i = 1, 2, \cdots N\}$ is a random sample from the universe defining $u(t)$. Note that

$$\langle \bar{R}_N(t,\tau) \rangle = \left\langle \frac{1}{N}\sum_{i=1}^{N} u_i(t)\, u_i(t+\tau) \right\rangle = R(\tau). \tag{12}$$

In order to find the error bound E_N (see equation (8)), we need the standard deviation of $u(t)\,u(t+\tau)$, i.e.,

$$\sigma_{uu}^2 = \langle [u(t)\,u(t+\tau) - R(t)]^2 \rangle = \langle u^2(t)\, u^2(t+\tau) \rangle - R^2(\tau). \tag{13}$$

Assuming that $u(t)$ satisfies the quasi-normal condition

Reproduced with permission of the copyright owner. Further reproduction prohibited without permission.

$$\langle u^2(t)\,u^2(t+\tau)\rangle = \langle u^2(t)\rangle\langle u^2(t+\tau)\rangle + 2\langle u(t)u(t+\tau)\rangle^2, \qquad (14)$$

and defining the rms and autocorrelation coefficient by

$$v = \langle u^2(t)\rangle^{1/2} \qquad (15)$$

and

$$\rho(\tau) = \frac{R(\tau)}{v^2}, \qquad (16)$$

then

$$\sigma_{uu}^2 = v^4\,[\,1 + \rho(\tau)\,]. \qquad (17)$$

Thus the error bound E_N (see equation (8)) for this case will be

$$E_N = v^2\sqrt{\frac{10\,[1+\rho(\tau)]}{N}}. \qquad (18)$$

Note that for $\tau = 0$ (the case of a mean square), and N = 2000,

$$E_N \doteq v^2 \cdot 0.10_3$$

while for large τ, and N = 2000, $E_N \doteq v^2\,0.07$.

4. Computation of a Probability Density

Again consider the random process $\{u(t); -\infty < t < \infty\}$ whose probability density $f_u(x;t)$ we wish to determine. Another random process $\pi(\cdot,\cdot,\cdot)$ can be defined by

$$\pi(x,\Delta x,t) = \begin{cases} 1 & \text{if } x \le u(t) < x+\Delta x \\ 0 & \text{otherwise} \end{cases} \qquad (19)$$

Reproduced with permission of the copyright owner. Further reproduction prohibited without permission.

Thus

$$\langle \pi(x, \Delta x, t) \rangle = 1 \cdot P\{x = u(t) < x + \Delta x\}$$

$$= p_u(x; t)\, \Delta x + O[(\Delta x)^2] \tag{20}$$

for small Δx. Also

$$\langle [\pi(x, \Delta x, t) - \langle \pi(x, \Delta x, t) \rangle]^2 \rangle = \langle \pi^2(x, \Delta x, t) \rangle - \langle \pi(x, \Delta x, t) \rangle^2$$

$$= p_u(x; t)\, \Delta x + O[(\Delta x)^2]. \tag{21}$$

Identifying $\dfrac{\pi(x, \Delta x, t)}{\Delta x}$ with $\phi(t)$ above, the probability density can be approximated by

$$\bar{p}_N(x, \Delta x, t) = \frac{1}{N} \sum_{i=1}^{N} \frac{\pi_i(x, \Delta x, t)}{\Delta x} \tag{22}$$

where $\{\pi_i(x, \Delta x, t), i = 1, \ldots, N\}$ is a random sample from the ensemble defining $\pi(x, \Delta x, t)$. Note that

$$\langle \bar{p}_N(x, \Delta x, t) \rangle = \frac{1}{N} \sum_{i=1}^{N} \frac{\langle \pi_i(x, \Delta x, t) \rangle}{\Delta x} = p_u(x; t) + O(\Delta x). \tag{23}$$

The error bound ε_N (using (8) and (21)) will be

$$\varepsilon_N = \sqrt{\frac{10\, p_u(x; t)}{N \Delta x}} \tag{24}$$

Reproduced with permission of the copyright owner. Further reproduction prohibited without permission.

$\Delta\kappa$ should by chosen with two constraints in mind: (i) to minimize the error involved in approximating $\langle \pi(\kappa, \Delta\kappa, t) \rangle$ by $p_u(\kappa; t)\,\Delta\kappa$, which implies selecting $\Delta\kappa$ as small as possible, and (ii) to minimize the error bound ε_N, which implies selecting $\Delta\kappa$ as large as possible.

In all the plots shown in this paper, $\frac{\Delta\kappa}{\sigma_u}$ was selected to be 1/5, where σ_u is the standard deviation of $u(t)$. Thus, since in all cases $p_u(\kappa; t)$ was approximately normal, then the relative error bound near the origin ($\kappa = 0$) is, with N = 2000

$$\frac{\varepsilon_N}{p_u(0;t)} = \sqrt{\frac{10}{N\Delta\kappa\, p_u(0;t)}} \doteq \sqrt{\frac{10\pi \cdot 5}{2000}} \doteq 0.25.$$

5. Computation of a Joint Probability Density

Following the discussion in section 4, consider the random processes $\{u(t), v(t), -\infty < t < \infty\}$ whose joint probability density $p_{uv}(x, y; t)$ we wish to determine. Define $\pi(\cdot, \cdot, \cdot, \cdot, \cdot)$ by

$$\pi(x, y, \Delta\kappa, \Delta\gamma; t) = \begin{cases} 1 \text{ if } \kappa \le u(t) < \kappa + \Delta\kappa,\ \gamma \le v(t) < \gamma + \Delta\gamma \\ 0 \text{ otherwise} \end{cases} \quad (25)$$

so that $$\langle \pi(x, y, \Delta\kappa, \Delta\gamma; t) \rangle = p_{uv}(x, y; t)\,\Delta\kappa\Delta\gamma + O[\Delta^3] \quad (26)$$

$$\langle [\pi(x, y; \Delta\kappa, \Delta\gamma; t) - \langle \pi(x, y, \Delta\kappa, \Delta\gamma; t) \rangle]^2 \rangle = p_{uv}(x, y; t)\,\Delta\kappa\Delta\gamma + O[\Delta^3]. \quad (27)$$

Reproduced with permission of the copyright owner. Further reproduction prohibited without permission.

$\rho_{uv}(x,y;t)$ is approximated by

$$\overline{\rho}_N(x,y,\Delta x,\Delta y;t) = \frac{1}{N}\sum_{i=1}^{N}\frac{\pi_i(x,y,\Delta x,\Delta y;t)}{\Delta x\,\Delta y} \qquad (28)$$

where $\{\pi_i(x,y,\Delta x,\Delta y;t),\ i=1,2,\ldots N\}$ is a random sample from the ensemble defining π.

With (8), (27), and (28), the error bound is

$$E_N \doteq \sqrt{\frac{10\,\rho_{uv}(x,y;t)}{N\,\Delta x\,\Delta y}}\,. \qquad (29)$$

With ρ_{uv} of normal form, $\frac{\Delta y}{\sigma_v} = \frac{\Delta x}{\sigma_u}$ = 1/5, and N = 2000, then the relative error bound is:

$$\frac{E_N}{\rho_{uv}(0,0,t)} \doteq \sqrt{\frac{2\pi\cdot 10\cdot 25}{2000}} \doteq 0.87,$$

which is extremely large.

Reproduced with permission of the copyright owner. Further reproduction prohibited without permission.

Appendix C. Numerical Integration Procedure

The method chosen to integrate numerically the ordinary differential equations (equations I.8 or I.12) for the particle trajectories was Hamming's (1959) modified "predictor-corrector" method.

It was chosen because (i) it is a stable method, (ii) it is a fourth-order integration procedure that requires the evaluation of the "right hand side" only twice per step (as opposed to other methods of the same order of accuracy, especially the Range-Kutta method, which requires the evaluation four times per step), and (iii) a well written FORTRAN IV subroutine was available which employs this method.

An algorithm using the method has been presented by Ralston (1960). This algorithm has in turn been used as the basis for the FORTRAN IV subroutine HPCG, described and listed in the IBM System/360 Scientific Subroutine Package (1968). It was this subroutine that was employed in the simulations.

However, it was found that the subroutine did not have all the characteristics claimed in the programmer's manual. In particular, it did not guarrantee outputting at the values of time $t_0 + j\Delta t$ (where $j = 0, 1, \ldots$ and Δt is the integration step size). So the subroutine was modified, first by the author, and then in a much more concise and time saving form by K. Smith of the JHU Computing Center.

Reproduced with permission of the copyright owner. Further reproduction prohibited without permission.

BIBLIOGRAPHY

Batchelor, G. K. (1949). "Diffusion in a Field of Homogeneous Turbulence; (I-Eulerian Analysis)", Austral. J. Sci. Res., vol. 2, pp. 437-450.

Batchelor, G. K. (1950). "Note on Free Turbulent Flows, with Special Reference to the Two-Dimensional Wake", J. Aero. Sci., vol. 17, pp. 441-445.

Batchelor, G. K. (1953). The Theory of Homogeneous Turbulence. Cambridge University Press.

Batchelor, G. K. (1969). "Computation of the Energy Spectrum in Homogeneous Two-Dimensional Turbulence", Phys. Fl. Supplament II, pp. II-233 to II-239.

Batchelor, G. K. and A. A. Townsend. (1956). "Turbulent Diffusion" from Surveys in Mechanics, edited by G. K. Batchelor and R. M. Davies. Cambridge University Press.

Bird, R. B., W. E. Stewart, and E. N. Lightfoot. (1960). Transport Phenomena. John Wiley and Sons, Inc. New York.

Box, G. E. P. and M. E. Muller. (1958). "A Note on the Generation of Normal Deviates", Ann. Math. Stat., vol. 28, pp. 610-611.

Champagne, F. H., V. G. Harris, and S. Corrsin. (1970). "Experiments on Nearly Homogeneous Turbulent Shear Flow", J. Fluid Mech., vol. 41, pp. 81-139.

Comte-Bellot, G. and S. Corrsin. (1971). "Simple Eulerian Time Correlation of Full- and Narrow-Band Velocity Signals in Grid Generated, 'Isotropic' Turbulence", J. Fluid Mech., in press.

Corrsin, S. (1953). "Remarks on Turbulent Heat Transfer" from the Proceedings of the Iowa Thermodynamics Symposium.

Corrsin, S. (1959a). "Progress Report on Some Turbulent Diffusion Research" from Proc. Int. Symp. on Atm. Diff. and Air Poll., Advances in Geophysics, vol. 6, pp. 161-164.

Corrsin, S. (1959b). "Lagrangian Correlation and Some Difficulties in Turbulent Diffusion Experiments", from Proc. Int. Symp. on Atm. Diff. and Air Poll., Advances in Geophysics, vol. 6, pp. 441-446.

Reproduced with permission of the copyright owner. Further reproduction prohibited without permission.

Corrsin, S. (1961). "Theories of Turbulent Dispersion," from Mechanique de la Turbulence. Colloques Internationaux du Centre National de la Recherche Scientifique, no. 108, Editions du C. N. R. S., Paris, pp. 27-52.

Corrsin, S. (1962). "Turbulence: Experimental Methods" from the Encyclopedia of Physics, vol. VIII/2, edited by S. Flugge and C. Truesdell. Springer-Verlag. Berlin.

Corrsin, S. (1963). "Estimates of the Relations between Eulerian and Lagrangian Scales in Large Reynolds Number Turbulence", J. Atm. Sci., vol. 20, pp. 115-119.

Corrsin, S. and J. Lumley. (1956). "On the Equation of Motion for a Fluid Particle in Turbulent Fluid", Appl. Sci. Res., vol. 6, pp. 114-116.

Corrsin, S. and G. S. Patterson. (1970). Private Communication.

Courant, R. and D. Hilbert. (1953). Methods of Mathematical Physics. Vol. II. Interscience Publishers, Inc. New York.

Crank, J. (1956). The Mathematics of Diffusion. Clarendon Press. Oxford.

Csanady, G. T. (1963). "Turbulent Diffusion of Heavy Particles in the Atmosphere", J. Atm. Sci., vol. 20, pp. 201-208.

Deardorff, J. W. (1970). "A Numerical Study of Three-Dimensional Turbulent Channel Flow at Large Reynolds Numbers", J. Fluid. Mech., vol. 41, pp. 453-480.

Deardorff, J. W. and R. L. Peskin. (1970). "Lagrangian Statistics from a Numerically Integrated Turbulent Shear Flow", Phys. Fl., vol. 13, pp. 584-595.

Elrick, D. E. (1962). "Source Functions for Diffusion in Uniform Shear Flow", Austral. J. Phys., vol. 15, pp. 283-288.

Faxen, H. (1927). "Simplified Representation of the Generalized Green's Equations for the Constant Motion of Translation of a Rigid Body in a Viscous Fluid", Arkiv. Mat. Astr. Fysik, vol. 20, section A, no. 8.

Fjörtoft, R. (1953). "On the Changes in the Spectral Distribution of Kinetic Energy for Two-Dimensional, Nondivergent Flow", Tellus, vol. 5, pp. 225-230.

Reproduced with permission of the copyright owner. Further reproduction prohibited without permission.

Frenkiel, F. N. (1953). "Turbulent Diffusion: Mean Concentration Distribution in a Flow Field of Homogeneous Turbulence", Adv. In Appl. Mech., vol. 3, pp. 61-107.

Friedlander, S. K. (1957). "Behavior of Suspended Particles in a Turbulent Fluid", A. I. Ch. E. Journal, vol. 3, pp. 381-385.

Graham, J. A. H., V. G. Harris, and S. Corrsin. (1971). "Advances in Nearly Homogeneous Turbulent Shear Flow", submitted to the J. Fluid Mech.

Grant, H. L., R. W. Stewart, and A Moilliet. (1962). "Turbulence Spectra from a Tidal Channel", J. Fluid Mech., vol. 12, pp. 241-263.

Greenberger, M. (1961). "Notes on a New Pseudo-Random Number Generator", J. Assoc. Comp. Mach., vol. 8, pp. 177-179.

Hamming, R. W. (1959). "Stable Predictor-Corrector Methods for Ordinary Differential Equations", J. Assoc. Comp. Mach., vol. 6, pp. 37-47.

Harper, E. Y. and I-Dee Chang. (1968). "Maximum Dissipation Resulting from Lift in a Slow Viscous Fluid", J. Fluid Mech., vol. 33, pp. 209-225.

Hinze, J. O. (1959). Turbulence. McGraw-Hill. New York.

Hinze, J. O. and B. G. van der Hegge Zijnen. (1951). "General Discussion on Heat Transfer". Inst. of Mech. Eng., London, pp. 188-191.

Inoue, E. (1951). "On the Lagrangian Correlation Coefficient for the Turbulent Diffusion and its Application to the Atmospheric Diffusion Phenomena". Unpublished Report, Geophys. Inst., Univ. of Tokyo.

International Business Machines Corporation. (1959). Random Number Generation and Testing. IBM Manual C20-8011-0.

International Business Machines Corporation. (1968). System/360 Scientific Subroutine Package. IBM Manual H20-0205-3.

Jost, W. (1952). Diffusion. Academic Press, Inc. New York.

Kampe de Feriet, J. (1939). "Les Fonctions Aleatoires Stationnaires et la Theorie Statistique de la Turbulence Homogene", Ann. Soc. Sci. de Brux., vol. 59, pp. 145-194.

Reproduced with permission of the copyright owner. Further reproduction prohibited without permission.

Kaplun, S. and P. A. Lagerstrom. (1957). "Asymptotic Expansions of Navier-Stokes Solutions for Small Reynolds Numbers", J. Math. and Mech., vol. 6, pp. 585-593.

Katz, E. J. (1966). "Atmospheric Diffusion and Settling of Particles with Sluggish Response", J. Atmos. Sci., vol. 23, pp. 159-166.

Kennedy, D. A. (1965). Some Measurements of the Dispersion of Spheres in a Turbulent Flow. Ph. D. Dissertation. The Johns Hopkins University.

Kenney, John F. (1954). Mathematics of Statistics. Part II. D. Van Nostrum Co., Inc. New York.

Kraichnan, R. H. (1959). "The Structure of Isotropic Turbulence at Very High Reynolds Numbers", J. Fluid Mech., vol. 5, pp. 497-543.

Kraichnan, R. H. (1964). "Relation Between Lagrangian and Eulerian Correlation Times of a Turbulent Velocity Field", Phys. Fl., vol. 7, pp. 142-143.

Kraichnan, R. H. (1967). "Inertial Ranges in Two-Dimensional Turbulence", Phys. Fl., vol. 10, pp. 1417-1423.

Kraichnan, R. H. (1970). "Diffusion by a Random Velocity Field", Phys. Fl., vol. 13, pp. 22-31.

Lauwerier, H. A. (1954). "Diffusion from a Source in a Skew Velocity Field", Appl. Sci. Res., vol. 4, section A, pp. 153-156.

Lilly, D. K. (1969). "Numerical Simulation of Two-Dimensional Turbulence", Phys. Fl. Supplement II, pp. II-240 to II-248.

Lin, C. C. (1953). "On Taylor's Hypothesis and the Acceleration Terms in the Navier-Stokes Equations", Quart. Appl. Math., vol. 10, pp. 295-306.

Lumley, J. L. (1957). Some Problems Connected with the Motion of Small Particles in Turbulent Fluid. Ph. D. Dissertation. The Johns Hopkins University.

Lumley, J. L. (1961). "The Mathematical Nature of the Problem of Relating Lagrangian and Eulerian Statistical Functions in Turbulence" from Mechanique de la Turbulence. Colloques Internationaux du Centre National de la Recherche Scientifique, No. 108, Editions du C. N. R. S., Paris, pp. 17-26.

Lumley, J.L. (1970). "Towards a Turbulent Constitutive Relation", J. Fluid Mech., vol. 41, pp. 413-434.

Reproduced with permission of the copyright owner. Further reproduction prohibited without permission.

Lumley, J. L. and S. Corrsin. (1959). "A Random Walk with Both Lagrangian and Eulerian Statistics" from the Proc. Int. Symp. on Atm. Diff. and Air Poll., Advances in Geophysics, vol. 6, pp. 179-183.

Mickelsen, W. R. (1955). "An Experimental Comparison of the Lagrangian and Eulerian Correlation Coefficients in Homogeneous Isotropic Turbulence". NACA TN 3570.

Moshman, J. (1960). "Random Number Generation" from Mathematical Methods for Digital Computers, vol. 1, edited by A. Ralston and H. S. Wilf. John Wiley and Sons, Inc. New York.

Naylor, T. H., J. L. Balintfy, D. S. Burdick, and K. Chu. (1966). Computer Simulation Techniques. John Wiley and Sons, Inc. New York.

Novikov, E. A. (1958). "Concerning a Turbulent Diffusion in a Stream with a Transverse Gradient of Velocity", PMM, vol. 22, pp. 576-579.

Oseen, C. W. (1927). Hydrodynamik. Ak. Verlagsges. Leipzig.

Patterson, G. S. and S. Corrsin. (1966). "Computer Experiments on Random Walks with Both Eulerian and Lagrangian Statistics" from Dynamics of Fluids and Plasmas, edited by S. I. Pai and others. Academic Press Inc. New York. pp. 275-307.

Peskin, R. L. (1965). "Short Time Eulerian-Lagrangian Independence", Phys. Fl., vol. 8, pp. 993-994.

Peskin, R. L., D. K. Lilly, and D. Fulker. (1970). "Numerical Modeling of Two-Dimensional Turbulent Diffusion", Bulletin of The American Physical Society, series 2, vol. 15, no. 11, p. 1537.

Proudman, I. and J. R. A. Pearson. (1957). "Expansions at Small Reynolds Numbers for the Flow Past a Sphere and a Circular Cylinder", J. Fluid Mech., vol. 2, pp. 237-262.

Ralston, A. (1960). "Numerical Integration Methods for the Solution of Ordinary Differential Equations" from Mathematical Methods for Digital Computers, vol. 1, edited by A. Ralston and H. S. Wilf. John Wiley and Sons, Inc. New York.

Roberts, P. H. (1961). "Analytic Theories of Turbulent Diffusion", J. Fluid Mech., vol. 11, pp. 257-283.

Rose, W. G. (1966). "Results of an Attempt to Generate a Homogeneous Turbulent Shear Flow", J. Fluid Mech., vol. 25, pp. 97-120.

Reproduced with permission of the copyright owner. Further reproduction prohibited without permission.

Rubinow, S. I. and J. B. Keller. (1961). "The Transverse Force on a Spinning Sphere Moving in a Viscous Fluid", J. Fluid Mech., vol. 11, pp. 447-459.

Saffman, P. G. (1961). "Some Aspects of the Effects of the Molecular Diffusivity in Turbulent Diffusion" from Mechanique de la Turbulence. Colloques Internationaux du Centre National de la Recherche Scientifique, No. 108, Editions du C. N. R. S., Paris, pp. 53-62.

Saffman, P. G. (1965). "The Lift on a Small Sphere in a Slow Shear Flow", J. Fluid Mech., vol. 22, pp. 385-400.

Schubauer, G. B. (1935). "A Turbulence Indicator Utilizing the Diffusion of Heat". NACA Rep. 524.

Shlien, D. J. (1971). Private Communication.

Skramstad, H. K. and G. B. Schubauer. (1938). "The Application of Thermal Diffusion to the Study of Turbulent Air Flow", Phys. Rev., vol. 53, p. 927.

Snyder, W. H. (1969). Some Measurements of Particle Velocity Autocorrelations in a Turbulent Flow. Ph. D. Dissertation. The Pennsylvania State University.

Taylor, G. I. (1921). "Diffusion by Continuous Movements", Proc. Lond. Math. Soc., series A, vol. 20, pp. 196-211.

Taylor, G. I. (1935). "Statistical Theory of Turbulence", Proc. Roy. Soc. (London), series A, vol. 151, pp. 421-478.

Tchen Chan-Mou. (1947). Mean Value and Correlation Problems Connected with the Motion of Small Particles Suspended in a Turbulent Fluid. (Dissertation-Delft). Martinus Nijhoff. The Hague.

Townsend, A. A. (1954). "The Diffusion Behind a Line Source in Homogeneous Turbulence", Proc. Roy. Soc. (London), series A, vol. 224, pp. 487-512.

Uberoi, M. S. and S. Corrsin. (1953). "Diffusion of Heat from a Line Source in Isotropic Turbulence". NACA Rep. 1142.

von Neumann, J. (1951). "Various Techniques Used in Connection with Random Digits" from Monte Carlo Methods, National Bureau of Standards, Applied Mathematics Series 12, pp. 36-38.

Yudine, M. I. (1959). "Physical Considerations on Heavy-Particle Diffusion" from Proc. Int. Symp. on Atm. Diff. and Air Poll., Advances in Geophysics, vol. 6, pp. 185-191.

Reproduced with permission of the copyright owner. Further reproduction prohibited without permission.

VITA

James Joseph Riley, Jr., was born in Kansas City, Missouri on February 25, 1944, and was raised in the Kansas City metropolitan area. He attended Rockhurst College, majoring in Physics, and received the AB degree from there in 1965.

He came to the Johns Hopkins University in 1965 on an NDEA Fellowship. There he tutored an undergraduate course and worked on several research projects before beginning formal work on his thesis. He presented a paper entitled "Simulation and Computation of Dispersion in Turbulent Shear Flow" (with S. Corrsin) at the Conference on Air Pollution Meteorology of the American Meteorological Society (in cooperation with the Air Pollution Control Association) in April, 1971.

Reproduced with permission of the copyright owner. Further reproduction prohibited without permission.